



**Ana Margarida Correia Rafael**

Bachelor's degree in Biomedical Sciences

**Development of substrates for reconstructed human dermis  
based on polyhydroxyalkanoates (PHAs) and FucoPol**

Dissertation for the degree of Master's in Biotechnology

Supervisor: Doctor Filomena Freitas, Assistant Professor,  
UCIBIO, FCT-UNL

Co-supervisor: Doctor Abel Oliva, Senior Researcher,  
ITQB-UNL



**December 2020**



**Ana Margarida Correia Rafael**

Bachelor's degree in Biomedical Sciences

**Development of substrates for reconstructed human dermis  
based on polyhydroxyalkanoates (PHAs) and FucoPol**

Dissertation for the degree of Master's in Biotechnology

Supervisor: Doctor Filomena Freitas, Assistant Professor,  
UCIBIO, FCT-UNL

Co-supervisor: Doctor Abel Oliva, Senior Researcher,  
ITQB-UNL

**December 2020**



## **Development of substrates for reconstructed human dermis based on polyhydroxyalkanoates (PHAs) and FucoPol**

Copyright © Ana Margarida Correia Rafael, Faculdade de Ciências e Tecnologia, Universidade Nova de Lisboa

A Faculdade de Ciências e Tecnologia e a Universidade Nova de Lisboa têm o direito, perpétuo e sem limites geográficos, de arquivar e publicar esta dissertação através de exemplares impressos reproduzidos em papel ou de forma digital, ou por qualquer outro meio conhecido ou que venha a ser inventado, e de a divulgar através de repositórios científicos e de admitir a sua cópia e distribuição com objetivos educacionais ou de investigação, não comerciais, desde que seja dado crédito ao autor e editor.



## Acknowledgements

First of all, I would like to thank my supervisors, Filomena Freitas and Abel Oliva, for trusting me with this project, receiving me in their labs and always being there to teach, guide and support me.

This work would not be feasible without all the people that collaborated in it, Prof. Elvira Fortunato (CENIMAT, FCT/NOVA), for allowing me to use CENIMAT installations, Carolina Marques for helping with SEM analysis, Prof. Madalena Dionísio (REQUIMTE, FCT/NOVA) for receiving me and helping with the DSC analysis, Prof. Christian Grandfils (CEIB, Univ. Liège) for the determination of  $M_w$  and PDI, Fernando Silva and Mariana Matos for the MMC biomass, Patrícia Reis and Diana Araújo for the FucoPol.

I would also like to thank everyone in the BIOENG group that hosted and helped me, Ana Teresa, Rita, Patrícia, Sílvia and Diana. A special thank you to João and Asiyah for the patience and guidance whenever needed, and to my colleagues, Marta, Cristiana, Thomas and Kleyde, for the comradery and company throughout this journey. To Patrícia, Sara and Mafalda from the Biomolecular Diagnostics Lab, thank you for all the help with the dermal constructs and for the patience and advice.

Lastly, I want to thank to all my friends, the ones that always have been with me, the ones that joined me in the way, the ones that still remain, Ana, Catarina, Rita and Maria, thank you for all the friendship and love. A special thank you to Catarina and Joana, for the extra patience and all the help. To Jessica, thank you for accompanying me. To Luís, thank you for all the unconditional love, patience and for never leaving my side. To my parents and sister, thank you for supporting me wherever I decide to go. A special mention to my mother, for putting up with me through it all, for being my right arm and always having a word of wisdom to give.

Thank you all, for making this journey lighter on me.





## Abstract

Skin tissue engineering represents an important tool in various fields such as cosmetic testing and regenerative medicine. The possibility of reproducing *in vitro* the fundamental properties of *in vivo* skin introduces new opportunities for creating knowledge. One of the techniques employed is the production of scaffolds to harbor cells, allowing for their proliferation and differentiation into functional tissues. These scaffolds must have certain characteristics, such as biocompatibility, biodegradability, appropriate physico-chemical and mechanical properties, ease of production and cost-effectiveness, all dependent on the material chosen. Thus, polyhydroxyalkanoates (PHAs) represent a potential scaffold material due to all of their relevant characteristics for biomedical applications. Also, the exopolysaccharide FucoPol can be incorporated with PHA as a blend or coating, possibly introducing bioactivity to the scaffolds. Therefore, the aim of this work was the production of scaffolds for reconstruction of human dermis, through the emulsion templating method, resulting in porous constructs that were tested with human dermal fibroblasts (HDFn).

The scaffolds obtained in this work were based on P(HBVHHx), a PHA composed of 51 wt% 3-hydroxybutyrate, 18 wt% 3-hydroxyvalerate and 31 wt% 3-hydroxyhexanoate, and had a porous structure with some interconnected pores. The scaffolds produced through emulsion with water had mechanical, thermal and physical properties comparable with the scaffolds produced through emulsion with FucoPol solution, both of them suitable for skin tissue engineering.

These scaffolds were tested with HDFn to assess their bioactivity. In both the cells were able to adhere, proliferate and differentiate, showing possible extracellular matrix (ECM) deposition. The eight-day assay revealed increased cellular growth and organized ECM deposition in the scaffolds with FucoPol compared to the ones without. The fourteen-day assay confirmed pore geometry as the limiting factor for the full invasion of the scaffolds. This work demonstrated the potential of naturally derived P(HBVHHx)/FucoPol scaffolds for the reconstruction of human dermis.

**Keywords:** skin tissue engineering; PHA-based scaffolds; short chain length-medium chain length polyhydroxyalkanoates (scl-mcl-PHAs); poly (3-hydroxybutyrate-co-3-hydroxyvalerate-co-3-hydroxyhexanoate) (P(HBVHHx)); FucoPol



## Resumo

A engenharia de tecidos da pele representa uma ferramenta importante em várias áreas, como a cosmética e a medicina regenerativa. A possibilidade de reproduzir *in vitro* as propriedades fundamentais da pele *in vivo*, introduz oportunidades para criar conhecimento. Uma das técnicas aplicada é o desenvolvimento de *scaffolds* para cultura celular, permitindo a sua proliferação e diferenciação em tecidos funcionais. Estes *scaffolds* devem possuir certas características, tais como biocompatibilidade, biodegradabilidade, propriedades físico-químicas e mecânicas apropriadas, facilidade de produção e custo-eficácia, todas dependentes do material escolhido. Assim, os polihidroxialcanoatos (PHAs) representam um potencial material para este efeito, devido a todas as suas características relevantes para aplicações biomédicas. Adicionalmente, o exopolissacárido FucoPol pode ser incorporado como uma mistura ou revestimento do *scaffold* de PHA, possivelmente introduzindo bioatividade. O objetivo deste trabalho foi produzir *scaffolds* para reconstrução da derme humana, através da técnica de emulsão, resultando em estruturas porosas que foram testadas *in vitro* com fibroblastos humanos (HDFn).

Os *scaffolds* de PHA produzidos, com composição monomérica 51 wt% 3-hidroxiobutirato, 18 wt% 3-hidroxi valerato e 31 wt% 3-hidroxi hexanoato, resultaram numa estrutura porosa com alguns poros interconectados. A emulsão com água resultou em *scaffolds* com propriedades mecânicas, térmicas e físicas comparáveis aos obtidos através de emulsão com solução aquosa de FucoPol, sendo ambos adequados para a aplicação pretendida.

Estes *scaffolds* foram testados com HDFn para avaliar a bioatividade. Em ambos as células conseguiram aderir, proliferar e diferenciar, com possível deposição de matriz extracelular (ECM). O ensaio de oito dias revelou um aumento no crescimento celular e deposição organizada de ECM nos *scaffolds* com FucoPol em detrimento dos *scaffolds* sem FucoPol. O ensaio de catorze dias confirmou a geometria dos poros como sendo o fator limitante para a invasão completa dos *scaffolds*. Este trabalho demonstrou o potencial de *scaffolds* P(HBVHx)/FucoPol para a reconstrução de derme humana.

**Palavras-chave:** engenharia de tecidos da pele; *scaffolds* baseados em PHA; polihidroxialcanoatos de cadeia curta-cadeia média (*scI-mcl*-PHA); poli (3-hidroxiobutirato-co-3-hidroxi valerato-co-3-hidroxi hexanoato) (P(HBVHx)); FucoPol



# List of Contents

---

Acknowledgements .....	vii
Abstract .....	ix
Resumo .....	xi
List of Figures .....	xvii
List of Tables .....	xix
List of Abbreviations .....	xxi
Chapter One – Introduction and Motivation .....	1
1.1    Introduction .....	2
1.1.1    Three-Dimensional (3D) Human Skin Equivalents .....	2
1.1.1.1    Human Skin Structure .....	2
1.1.1.2    From 2D to 3D cell culture: overview .....	4
1.1.1.3    3D human skin constructs .....	7
1.1.1.4    Reconstructed Human Dermis: Scaffold material .....	9
1.1.2    Biopolymers .....	10
1.1.2.1    PHAs .....	12
1.1.2.2    Polysaccharides .....	14
1.2    Motivation .....	15
Chapter Two – Biopolymers for scaffolds development .....	17
2.1    Introduction .....	18
2.1.1    PHAs .....	18
2.1.1.1    P(HBVHx) .....	20
2.1.2    FucoPol .....	21
2.2    Materials and Methods .....	22
2.2.1    Biopolymers production and extraction .....	22
2.2.2    Characterization of the PHA .....	23
2.2.2.1    Composition .....	23
2.2.2.2    Molecular Mass Distribution .....	23

2.2.2.3	X-Ray Diffraction .....	24
2.2.2.4	Thermal Properties.....	24
2.3	Results and Discussion .....	25
2.3.1	P(HBVHx).....	25
2.3.1.1	Composition .....	25
2.3.1.2	Molecular Mass Distribution .....	26
2.3.1.3	X-Ray Diffraction .....	26
2.3.1.4	Thermal Properties.....	27
2.3.2	FucoPol .....	28
2.4	Conclusions .....	29
Chapter Three – Production and characterization of biopolymer-based scaffolds .....		31
3.1	Introduction .....	32
3.1.1	Scaffold-based techniques .....	32
3.1.2	Emulsion Templating .....	34
3.1.3	Desired scaffolds specifications .....	37
3.2	Materials and Methods .....	38
3.2.1	Scaffolds fabrication .....	38
3.2.1.1	Non-porous scaffolds .....	38
3.2.1.2	Porous scaffolds by water emulsion .....	38
3.2.1.3	Porous scaffolds by aqueous FucoPol-solution emulsion .....	38
3.2.1.4	Porous scaffolds by water emulsion and FucoPol coating .....	38
3.2.2	Scaffolds characterization .....	39
3.2.2.1	Morphology.....	39
3.2.2.2	Thermal Properties and XRD .....	39
3.2.2.3	Swelling in Water .....	39
3.2.2.4	Porosity.....	39
3.2.2.5	Mechanical Properties .....	40
3.3	Results and Discussion .....	41
3.3.1	Non-porous film by solvent evaporation .....	41
3.3.1.1	Morphology .....	41

3.3.1.2	Thermal properties and XRD .....	42
3.3.1.3	Mechanical properties .....	43
3.3.2	Porous scaffolds by water emulsion templating .....	44
3.3.2.1	Morphology .....	44
3.3.2.2	Thermal properties and XRD .....	46
3.3.2.3	Porosity.....	46
3.3.2.4	Swelling in water .....	47
3.3.2.5	Mechanical properties .....	47
3.3.3	Porous scaffolds by FucoPol-water emulsion templating.....	48
3.3.3.1	Morphology .....	48
3.3.3.2	Thermal properties and XRD .....	50
3.3.3.3	Porosity.....	51
3.3.3.4	Swelling in water .....	51
3.3.3.5	Mechanical properties .....	52
3.3.4	Porous scaffolds by water emulsion templating and FucoPol coating .....	54
3.3.4.1	Morphology.....	54
3.4	Conclusions .....	56
Chapter Four – Biopolymer-based scaffolds for reconstructed human dermis.....		58
4.1	Introduction .....	59
4.1.1	Desired Dermal Construct Specifications .....	59
4.2	Materials and Methods .....	60
4.2.1	Dermal Construct.....	60
4.2.1.1	Fibroblasts Defrosting and Subculture .....	60
4.2.1.2	Cell Seeding and Dermal Construct.....	60
4.2.2	Histological Processing .....	61
4.2.2.1	Paraffin embedded sections.....	61
4.2.2.2	Cryo-sections.....	61
4.2.3	Microscopic evaluation .....	61
4.3	Results and Discussion .....	62
4.3.1	Eight-day assays .....	62

4.3.1.1	Non-porous film and porous scaffold by water emulsion templating .....	62
4.3.1.2	FucoPol-water emulsion templating porous scaffolds.....	63
4.3.1.3	FucoPol-coated water emulsion templated scaffolds.....	64
4.3.2	Fourteen-day assay.....	67
4.3.2.1	Water emulsion templated and FucoPol-water emulsion templated porous scaffolds .....	67
4.4	Conclusions .....	70
Chapter Five – Conclusions and Future Perspectives .....		72
5.1	Conclusions and Future Perspectives.....	73
References .....		76
Appendices.....		88



## List of Figures

<b>Figure 1.1.</b> Healthy Skin Structure. ....	3
<b>Figure 1.2.</b> Number of publications per year (1975-2020) on 3D cell cultures .....	5
<b>Figure 1.3.</b> Hanging drop plate technique .....	7
<b>Figure 2.1.</b> PHAs granular inclusions. ....	18
<b>Figure 2.2.</b> General structure of PHA polymer family .....	19
<b>Figure 2.3.</b> P(HBHVHHx) polymer (raw) diffractogram .....	27
<b>Figure 3.1.</b> Non-porous scaffold images;. ....	41
<b>Figure 3.2.</b> Images of porous scaffold by water emulsion templating. ....	45
<b>Figure 3.3.</b> Images of porous scaffold by FucoPol-water emulsion templating. ....	49
<b>Figure 3.4.</b> Images of porous scaffolds by water emulsion templating and FucoPol coating .....	54
<b>Figure 4.1.</b> Microscopic images of the eight-day dermal constructs with porous scaffolds by water emulsion templating. ....	62
<b>Figure 4.2.</b> Microscopic images of the eight-day dermal constructs with porous scaffolds by FucoPol-water emulsion templating. ....	64
<b>Figure 4.3.</b> Microscopic images of the eight-day dermal constructs with porous scaffolds by water emulsion templating with 2 % (w/v) FucoPol coating. ....	65
<b>Figure 4.4.</b> Microscopic images of the eight-day dermal constructs with porous scaffolds by water emulsion templating with 1.5 % (w/v) FucoPol coating .....	66
<b>Figure 4.5.</b> Microscopic images of the fourteen-day dermal constructs with porous scaffolds by water emulsion templating. ....	68
<b>Figure 4.6.</b> Microscopic images of the fourteen-day dermal constructs with porous scaffolds by FucoPol-water emulsion templating (0.1 % (w/v) of FucoPol) .....	69
<b>Figure A.</b> SEC analysis of the extracted P(HBHVHHx). ....	89
<b>Figure B.</b> TGA curve of the extracted P(HBHVHHx). ....	90



## List of Tables

<b>Table 1.1.1.</b> Comparison between 2D and 3D cell cultures..	6
<b>Table 1.2.</b> Examples of biopolymeric scaffolds employed in skin tissue engineering	12
<b>Table 2.1.</b> Thermo-mechanical properties of some PHAs and most common petroleum-based plastics.....	20
<b>Table 2.2.</b> Different P(HBHVHHx) thermo-mechanical properties in literature.....	21
<b>Table 2.3.</b> Composition (wt%), Molecular weight ( $M_w$ ), Molecular number ( $M_n$ ) and polydispersity index (PDI) of P(HBHVHHx) used in this work with comparison to other terpolyesters found in the literature.....	25
<b>Table 2.4.</b> Thermal properties of the P(HBHVHHx) extracted in this study, compared to other PHAs found in the literature.....	28
<b>Table 3.1.</b> Commonly used methods to produce porous scaffolds, with their advantages and limitations.....	33
<b>Table 3.2.</b> Examples of emulsion templated scaffolds.....	35
<b>Table 3.3.</b> Comparison of thermal properties and crystallinity between raw P(HBHVHHx) and the non-porous film produced with that polymer. ....	42
<b>Table 3.4.</b> Comparison of mechanical properties between the non-porous film obtained in this work and others found in the literature.....	43
<b>Table 3.5.</b> Comparison of thermal properties and crystallinity between raw P(HBHVHHx), non-porous film and water emulsion templated porous scaffold produced with that polymer.....	46
<b>Table 3.6.</b> Comparison of mechanical properties between the non-porous film and water emulsion templated porous scaffold obtained in this work .....	47
<b>Table 3.7.</b> Comparison of thermal properties and crystallinity between raw P(HBHVHHx), non-porous film, water emulsion templated and FucoPol-water emulsion templated porous scaffolds produced with that polymer .....	50
<b>Table 3.8.</b> Comparison of mechanical properties between the non-porous film, water emulsion templated and FucoPol-water emulsion templated porous scaffolds obtained in this work and others found in the literature.....	52



## List of Abbreviations

<b>3HB</b>	3-hydroxybutyrate
<b>3HHx</b>	3-hydroxyhexanoate
<b>3HV</b>	3-hydroxyvalerate
<b>DSC</b>	Differential scanning calorimetry
<b>ECM</b>	Extracellular matrix
<b>EPS</b>	Exopolysaccharide
<b>FBs</b>	Fibroblasts
<b>FBS</b>	Fetal bovine serum
<b>GC</b>	Gas chromatography
<b>HA</b>	Hydroxyalcanoates
<b>HDFn</b>	Human dermal fibroblasts, neonatal
<b>HSE</b>	Human skin equivalent
<b>mcl</b>	Medium chain length
<b>MMC</b>	Mixed microbial culture
<b>M<sub>n</sub></b>	Number-average molecular weight
<b>M<sub>w</sub></b>	Molecular weight
<b>n.a.</b>	Data not available
<b>n.d.</b>	Data not detected
<b>PCL</b>	Poly( $\epsilon$ -caprolactone)
<b>PDI</b>	Polydispersity index
<b>PHA</b>	Polyhydroxyalkanoates
<b>PHB</b>	Poly (hydroxybutyrate)
<b>P(HBHHx)</b>	Poly (hydroxybutyrate – co – hydroxyhexanoate)
<b>P(HBHV)</b>	Poly (hydroxybutyrate – co – hydroxyvalerate)
<b>P(HBHVHHx)</b>	Poly (hydroxybutyrate – co – hydroxyvalerate – co - hydroxyhexanoate )
<b>PHV</b>	Poly (hydroxyvalerate)
<b>PLA</b>	Poly(lactic acid)
<b>PLGA</b>	Poly(lactic-co-glycolic acid)
<b>PS</b>	Polystyrene
<b>rpm</b>	Rotation per minute
<b>scl</b>	Short chain length
<b>SCPL</b>	Solvent-casting particulate leaching
<b>SEC</b>	Size exclusion chromatography

<b>SEM</b>	Scanning electron microscopy
<b>T<sub>deg</sub></b>	Degradation temperature
<b>T<sub>g</sub></b>	Glass transition temperature
<b>TGA</b>	Thermogravimetric analysis
<b>TIPS</b>	Thermally induced phase separation
<b>T<sub>m</sub></b>	Melting temperature
<b>X<sub>c</sub></b>	Crystallinity fraction
<b>XRD</b>	X-ray diffraction



## **Chapter One – Introduction and Motivation**

---

## 1.1 Introduction

### 1.1.1 Three-Dimensional (3D) Human Skin Equivalents

The search for a physiologically relevant *in vitro* three-dimensional (3D) Human Skin Equivalent (HSE) has been an endeavour of the past century. Since 2013, with new EU regulations (Regulation (EC) N° 1223/2009), cosmetic products (or any component in the formulation, ingredient combination and final product) that have been subjected to animal testing cannot be placed on the EU market (Derr *et al.*, 2019). With these new restrictions, studies for *in vitro* HSEs have seen a relevant increase in the past decade. Adding to the cosmetic testing (e.g. safety and toxicity studies), pharmaceutical testing and tissue engineering (e.g. regenerative medicine) are also using *in vitro* human skin models. A full-thickness *in vitro* HSE can also be considered an important tool for the fundamental study of the biology and pathology of the human skin (Kinikoglu, 2017).

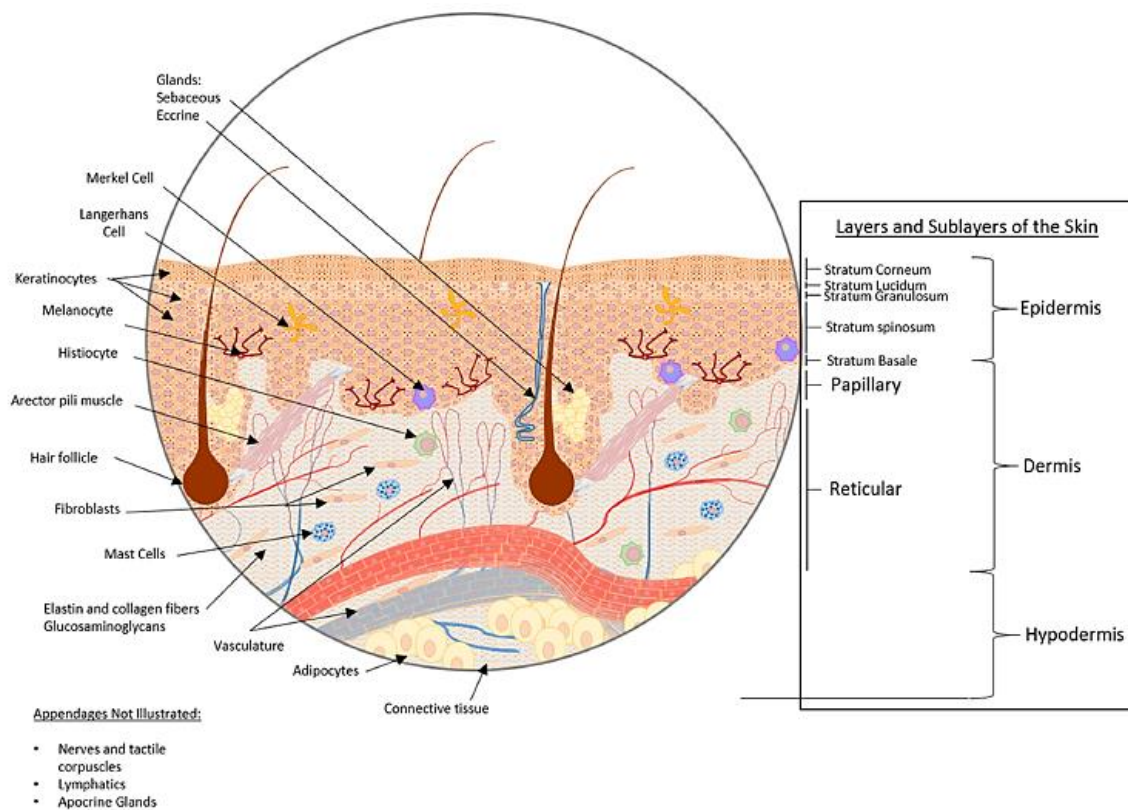
Three-dimensional HSEs, when achieved by the classic tissue engineering approach, are constructed with a 3D scaffold analogue to the extracellular matrix (ECM), aiming to guide adhesion, growth and differentiation of the human skin seeded cells, resulting in a 3D construct that resembles *in vivo* tissue properties: structural, mechanical and functional (Kinikoglu, 2017; Randall, Jüngel, Rimann, & Wuertz-Kozak, 2018a).

#### 1.1.1.1 Human Skin Structure

Being the largest human organ, reaching 1.7 m<sup>2</sup> of covering area and approximately 15 % of bodyweight, skin acts as the first protective barrier at the interface between the human body and the surrounding environment (Lanigan & Zaidi, 2010). Structurally it can be divided in three layers, from the most internal to the external facing: hypodermis, dermis and epidermis, as depicted in Figure 1.1. Hypodermis, also known as the subcutaneous layer, is comprised of tiers of fat-storing cells, called adipocytes, runned through by loose connective tissue, both being intersected by blood vessels and nerves, functioning as an insulator, shock absorbant and source of nourishment. Immediately above there is the dermis, a thick fibrous layer consisting of heterogenous cells (fibroblasts, dermal dendrocytes, mast cells and histiocytes), collagen and elastic fibers, ground substance (glycosaminoglycans – GAGs), blood and lymphatic vessels, nerves and appendages (hair follicles, sebaceous, apocrine and eccrine glands and nails). Approximately 75 % of the skin mass is attributed to collagen fibers that confer its elasticity, making the dermis the source for skin's flexibility and tensile strength. Additionally, functions of the dermis include maintenance of hydration, mechanical and thermal protection, sensory signal propagation and immunologic defense (Lanigan & Zaidi, 2010; Randall, Jüngel, Rimann, & Wuertz-Kozak, 2018b).



The outermost layer of the skin is the epidermis, connected to the dermis by the dermo-epidermal junction. Epidermis can be divided in separate strata, increasing in the keratinization (terminal differentiation) degree from the bottom to the surface: *stratum germinatum* (the only dividing cells in this layer), *stratum spinosum* (keratin producing cells), *stratum granulosum* (helps in the aggregation of keratin filaments), *stratum lucidum* (only present in the palms and soles, provides thickness) and *stratum corneum* (composed of anucleated, non-living, keratin filled, flattened corneocytes). About 95 % of the epidermal cells are keratinocytes, the remaining cells are melanocytes (located at the basal layer, providing ultra-violet (UV) protection through the production of melanin), merkel cells (also at the basal layer and responsible for the sense of touch) and Langerhans cells (present in the *stratum spinosum*, being immunologically competent cells) (Lanigan & Zaidi, 2010; Randall *et al.*, 2018a; Suhail *et al.*, 2019).



**Figure 1.1.** Healthy Skin Structure. Retrieved with permission from (Randall *et al.*, 2018)

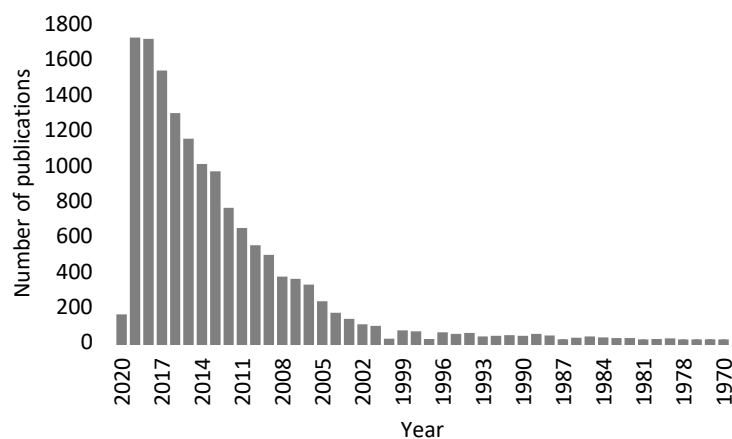
### 1.1.1.2 From 2D to 3D cell culture: overview

The epicenter for the knowledge necessary to generate reconstructed human skin models lies in the middle of the twentieth century, when the first attempts at separating human epidermis from dermis, isolation and cultivation of human keratinocytes were successful (Niehues *et al.*, 2018). Also, in 1948, the cultivation of adult mammalian skin epithelium *in vitro* was accomplished (Medawar, 1948). Later, throughout the next two decades, the development of long-term culture of epithelial-like cells was achieved, although the cells showed more similarities to HeLa cells than to keratinocytes (Wheeler, Canby, & Cawley, 1957). In 1960, the culture of isolated keratinocytes from adult guinea pig skin, with no underlying dermal support, were shown to be able to form colonies when seeded at high densities, however, when subcultured they would differentiate (Cruickshank, Cooper, & Hooper, 1960). Rheinwald & Green, (1975) were able to develop cultures of human keratinocytes that originated from a single keratinocyte, by using a lethally irradiated 3T3 fibroblast layer as a feeder for the single epidermal cell seeded on top. After this, the culture of large quantities of keratinocytes for *in vitro* studies was made possible, making the monolayer culture of human keratinocytes a fundamental tool for the study of skin biology and pathophysiology *in vitro*. This two-dimensional (2D) method allowed for simple, reproducible and high-throughput studies, however, these advantages were outshined by the lack of physiological relevance of this model (Niehues *et al.*, 2018).

The shift from 2D models, that remained the standard method for cell cultures for over a century and still are appealing to some laboratory studies (due to ease and cost-effectiveness), is motivated by the need of creating cellular models that mimic *in vivo* physiological conditions – representing the full-thickness and three-dimensional spatial arrangement of real tissues.

These 2D models consist of a monolayer of cells seeded and grown on a solid flat surface (glass or polystyrene), fed by a medium that contains all the nutrients (amino acids, carbohydrates, vitamins and minerals), growth factors, hormones, pH and osmotic pressure needed, maintained with the right atmosphere (O<sub>2</sub>, CO<sub>2</sub>) and temperature. Despite of the fundamental role that these 2D cell cultures played in furthering the knowledge in cell behaviour and drug discovery, not all results and conclusions can be translated into *in vivo* physiology. Studies of cancer mechanism greatly evolved due to 2D cell culture, however, it also became clear that it is not the right model for drug development, demonstrating its flaws in predicting *in vivo* toxicity and drug efficacy. These models were unrepresentative of three-dimensional arrangements of cells *in vivo*, namely cell-cell, cell-matrix and cell-environment interactions, affecting cellular responses (morphology, migration, proliferation, differentiation, mechanical and biochemical signalling as well as gene and protein expression) (Antoni, Burckel, Josset, & Noel, 2015; Hoarau-Véchet, Rafii, Touboul, & Pasquier, 2018; Randall *et al.*, 2018a).

For all these limitations, the development of 3D constructs became increasingly more relevant and in the late 1970's the first HSE, using a collagen hydrogel, was described (Bell, Ivarsson, & Merrill, 1979). In the past three decades there have been a noticeable expansion in the literature regarding 3D cell cultures (Figure 1.2), with some studies demonstrating that the cellular response in 3D cultures is more physiologically relevant when compared with 2D cultures (Hoarau-Véchet *et al.*, 2018).



**Figure 1.2.**Number of publications per year (1975-2020) on 3D cell cultures (data gathered from PubMed).

One of the advantages of 3D cell cultures is the fact that this method can be highly tunable and adaptable to suit the type of study performed. This allows a variety of applications, such as cancer research, drug discovery, stem cell research and physiological and disease models of tissues (Jensen & Teng, 2020). A comparison between 2D and 3D cell cultures is summarized in Table 1.1, explaining some of the advantages and disadvantages of both models.

HSEs have developed and improved greatly over the past decades, bringing to light many advantages over the use of animal models, being less expensive, less time-consuming and more ethically correct. Additionally, the most frequently used animal model, mice, is not the best suited model to correlate with human skin, especially due to divergencies in its architecture, such as presenting a much thinner epidermis with more densely packed hair follicles, melanocytes located mainly in dermal hair follicles and an extra cutaneous muscle layer that is absent in human dermis. The one approach that can represent almost ideal *in vivo* conditions is the culture of human skin (gold standard) explants obtained from biopsies and donors, achieved by the culturing of the intact skin samples (containing all the resident skin cells). However, this method owes to its complexity, cost, ethical questions, lack of variability and availability, the reasons why it is not suited for most studies (Ali *et al.*, 2015; Randall *et al.*, 2018a).

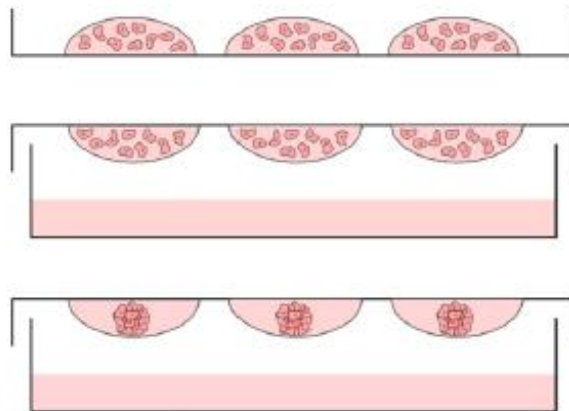
By filling the gaps in both 2D and animal models, 3D cell culture appears to be the way forward. Giving the recent and constantly evolving advances in the field, as well as the ethical questions imposed by the use of animal and explant models, it is possible and justified to develop *in vitro* 3D models that can mimic physiological conditions and more accurately represent tissues *in vivo*.

**Table 1.1.** Comparison between 2D and 3D cell cultures. Adapted with permission from (Jensen & Teng, 2020).

<b>Characteristics</b>	<b>2D cell culture</b>	<b>3D cell culture</b>
<b>Cell shape</b>	<ul style="list-style-type: none"> <li>○ Cell shape is flat and elongated</li> <li>○ Cells grow into a monolayer on the plate</li> </ul>	<ul style="list-style-type: none"> <li>○ Natural cell shape is maintained</li> <li>○ Cells grow into aggregates/spheroids</li> <li>○ Spheroids contain multiple layers</li> </ul>
<b>Cell proliferation</b>	<ul style="list-style-type: none"> <li>○ Proliferation occurs at a unnaturally rapid pace</li> </ul>	<ul style="list-style-type: none"> <li>○ Proliferation rates are realistic and depend on the technique and types of cells being studied</li> </ul>
<b>Cell differentiation</b>	<ul style="list-style-type: none"> <li>○ Differentiation is poor</li> </ul>	<ul style="list-style-type: none"> <li>○ Cells are well differentiated</li> </ul>
<b>Cell junction</b>	<ul style="list-style-type: none"> <li>○ Cell junctions less frequent and unrepresentative of the real junctions</li> </ul>	<ul style="list-style-type: none"> <li>○ Cell junctions are common and allow for cell-cell communication</li> <li>○ Communication through exchange of ions, small molecules and electrical currents</li> </ul>
<b>Cell exposure to medium</b>	<ul style="list-style-type: none"> <li>○ All cells receive the same amount of nutrients and growth factors</li> <li>○ More cells in the same stage of the cell cycle</li> </ul>	<ul style="list-style-type: none"> <li>○ Nutrients do not have to be equally divided for all cells but can be if needed</li> </ul>
<b>Drug sensitivity</b>	<ul style="list-style-type: none"> <li>○ Cells have less resistance to drugs, making it look like the drugs administered were a successful treatment</li> <li>○ Drugs are not well metabolized</li> </ul>	<ul style="list-style-type: none"> <li>○ Cells have better drug resistance</li> <li>○ Drug metabolism is improved</li> <li>○ More accurate representation of the drugs effect</li> </ul>
<b>Response to stimuli</b>	<ul style="list-style-type: none"> <li>○ Inaccurate representation of response to mechanical stimuli</li> <li>○ Cells are not subject to gravity since they are unable to expand three-dimensionally</li> </ul>	<ul style="list-style-type: none"> <li>○ Accurate representation of response to mechanical stimuli</li> <li>○ Cells can expand in 3D, giving a more accurate representation of <i>in vivo</i></li> </ul>
<b>Expression levels</b>	<ul style="list-style-type: none"> <li>○ Gene and protein expression levels are often very different from <i>in vivo</i></li> </ul>	<ul style="list-style-type: none"> <li>○ Levels of gene and protein expression similar to the ones found <i>in vivo</i></li> </ul>
<b>Cost</b>	<ul style="list-style-type: none"> <li>○ It's cheaper than 3D for large scale studies</li> </ul>	<ul style="list-style-type: none"> <li>○ Typically more expensive and time consuming than 2D studies</li> <li>○ Reduces the difference between <i>in vivo</i> and <i>in vitro</i> drug screening, reducing the need to use animal models</li> </ul>
<b>Usage analysis and</b>	<ul style="list-style-type: none"> <li>○ Highly reproducible and easy to interpret</li> <li>○ Better for long-term cultures</li> </ul>	<ul style="list-style-type: none"> <li>○ More difficult to replicate experiments</li> <li>○ More difficult to interpret results</li> </ul>

### 1.1.1.3 3D human skin constructs

3D constructs can be essentially divided in two main categories: scaffold-based and scaffold-free. Scaffold-free systems can be defined as the self-assembly of one or more cell types into non-adherent cell aggregates, producing a spheroid-like structure (hence being called spheroids), grown with no need for a physical support and able to grow their own ECM (Knight & Przyborski, 2014; Randall *et al.*, 2018a). Some examples of these systems are hanging drop microplates, magnetic levitation and spheroid microplates with ultra-low attachment coating. The first is obtained by the force of gravity, when monodispersed cells aggregate due to being immersed in a hanging droplet of medium, adherent to a top plate and without contact to the humidified bottom plate, as pictured in Figure 1.3. When a microplate with ultra-low attachment coating is used to harbour these cell aggregates, the initial media volume is higher allowing the formation of bigger and more complex spheroids. Two of the most valuable applications of this technique are (i) construction of organ spheroids that resemble *in vivo* characteristics, like a cardiac spheroid obtained by co-culture of human primary cardiomyocytes, endothelial cells and fibroblasts that resulted in a 3D model where toxic effects on human heart tissue could be studied (Polonchuk *et al.*, 2017); (ii) 3D models for cancer studies, due to the hypoxic conditions created in some spheroids (Knight & Przyborski, 2014). Magnetic levitation is achieved by loading cells with magnetic nanoparticles, immersing them in a low adhesion plate and forcing them to float at the air-liquid interface with the use of an external magnet. Despite their limitations, these methods can be relevant due to their simplicity, cost and high-throughput (Langhans, 2018; Randall *et al.*, 2018a).



**Figure 1.3.** Hanging drop plate technique. Retrieved with permission from (Knight & Przyborski, 2014).

Scaffold-based methods can be generally defined as systems where cells are seeded in a support scaffold (hydrogel, fibrous or porous material) that allows for their migration, proliferation and differentiation, diverging from scaffold-free methods in their ability to generate a 3D model that mechanically, structurally and functionally resembles real tissues (Randall *et al.*, 2018a). The material used to produce such scaffolds can be classified as natural (e.g. collagen, fibrin, alginate, hyaluronic acid) or synthetic (e.g. titanium, bioactive glass, polystyrene), and the technique applied could result in a hydrogel or a solid scaffold.

Hydrogels are hydrophilic polymeric structures, formed within a highly aqueous environment. They can either be naturally derived or synthetic, being that the polymerization of the chains allows for the production of hybrid hydrogels with different materials combined, resulting in novel physical and biological properties (Chai, Jiao, & Yu, 2017). Therefore, one of the main characteristics is the tunability of properties, permitting better physiological relevance and adaptation to the experiment performed. The process of gelation can occur by different methods, such as electrostatic forces, covalent chemical cross-linking and physical entanglement of polymer chains. When applied to tissue engineering or cell culture, the hydrogel can be designed for encapsulation of the cells or for migration of the cells from the surface to the interior of the gel. The high water content in these scaffolds allows cell-liquid interaction, added to the fact that the hydrogel enables the diffusion (limited to a certain extent) of cytokines and growth factors through the material, counting as some of the advantages of these 3D constructs (Jensen & Teng, 2020; Knight & Przyborski, 2014). However, some drawbacks can be related to their micro-structural complexity that can impair cell shape, mobility, proliferation and consequently matrix production, prolonged cultures in aqueous environment can lead to a structural weakening due to swelling, as well as the use of UV light or other possibly prejudicial components to the cells in the hydrogel production (Duval *et al.*, 2017; Y. S. Zhang & Khademhosseini, 2017). Additionally, conventional hydrogels have limited mechanical strength and their matrix can, under certain conditions, degrade at a faster rate than the formation of new tissue, which leads to a biochemical change and decrease in matrix elasticity (Duval *et al.*, 2017).

Regarding *in vitro* 3D cell cultures, specifically within skin studies, the most widely material used is collagen I, the main constituent of dermal ECM. Due to high water content, collagen I is susceptible to contraction induced by forces exerted by fibroblasts within the matrix (Moulin *et al.*, 1996). Furthermore, enzymatic degradation by some collagenases and gelatinases impairs the long-term use of such scaffolds (Randall *et al.*, 2018a). Some of these 3D scaffolds are commercially available, one of them being Matrigel® (Corning), a 3D culture hydrogel based in the extract of Engelbreth-Holm-Swarm (EHS) mouse sarcoma cells, containing common ECM proteins (e.g. collagen, laminin, fibronectin and entactin) and growth factors. Nonetheless, this model has disadvantages, such as the fact that is derived from tumor cells, its batch-to-batch variability, alterations in cell morphology, migration, proliferation, cell cycle and gene expression patterns (Fontoura *et al.*, 2019; Knight &

Przyborski, 2014). HSEs are 3D cell culture models developed to test pharmaceutical products *in vitro*, research and development studies and that can be used in regenerative medicine as artificial skin grafts. These constructs can represent only the epidermal layer of the skin, the dermal layer or both layers as a full-thickness skin equivalent (Teimouri, Yeung, & Agu, 2019).

Solid scaffolds, as mentioned, can generally be synthesized as a porous matrix or fibrous mesh. The main advantage, when compared to other methods of 3D constructs, is the ability of these scaffolds to reproduce ECM structure, representing an important tool when it comes to study specific interactions, like cell-ECM (Jensen & Teng, 2020).

#### 1.1.1.4 Reconstructed Human Dermis: Scaffold material

One of the most crucial components of HSEs is the scaffold itself that has to fulfill some requirements, in order to achieve a relevant reconstructed human dermis: i) mimic the natural ECM (controlled porosity and interconnectivity of the pores); ii) provide mechanical strength and shape to the reconstructed tissue (stiffness, elastic modulus, etc.); iii) biodegradation at a slow rate; iv) biocompatibility; v) bioactivity required for cell adhesion, proliferation, differentiation and function. Other aspects ought to be considered, such as process of sterilization, availability, ease of production, storage and commercial viability (Kinikoglu, 2017; Nikolova & Chavali, 2019).

As mentioned previously, most of the current HSEs for clinical applications or *in vitro* cell culture studies still make use of collagen as main component. Some are currently commercially available, being the most common examples EpiSkin™ (SkinEthic/L'Oreal, France), EpiDerm™ (MatTek Corp., USA), and SkinEthic RHE™ (EPISKIN Laboratories, France), given that the latter two are constructed by seeding in a polycarbonate filter (Pellevoisin *et al.*, 2018; Suhail *et al.*, 2019). Naturally derived polymers, such as fibronectin, silk, alginate, fibrin, chitosan, elastin or GAGs, being non-cytotoxic and almost immunologically inactive *in vivo*, are considered ideal options for human cell culture. Nonetheless, these polymers are subjected to variability between batches, have weak mechanical properties (due to high water content in some of them) and are prone to enzymatic degradation (Randall *et al.*, 2018a).

For all the above mentioned reasons, attentions started to gravitate towards more tunable materials, that still maintained biocompatibility and biodegradability but granted more control over physicochemical properties and production cost could be reduced. These materials were synthetic polymers, including polyesters like poly( $\epsilon$ -caprolactone) (PCL), polylactic acid (PLA), polyglycolic acid (PGA), polylactic-co-glycolic acid (PLGA) and polyethers such as polyethylene glycol (PEG) and its co-polymers (Randall *et al.*, 2018a). Additionally, synthetic plastics like polystyrene (PS) represent a big portion of the commercially available solid scaffolds for 3D cell culture (e.g. Alvetex®, ReproCell, Glasgow, Scotland), due to being chemically inert, stable and easily mass produced at low-cost, nevertheless the stiff nature and absence of biochemical activity found in soft tissues like the skin

make them less relevant for *in vitro* studies of such tissues (Knight, Murray, Carnachan, & Przyborski, 2011; Knight & Przyborski, 2014). Moreover, PS is synthesized from non-renewable hydrocarbon sources, bearing a heavy impact in environment, health and economy (Muneer *et al.*, 2020). However, synthetic polymers (e.g. PLGA) need an extra step of polymerization for their synthesis making the process elaborate and with the additional disadvantage of lacking bioactive sites that promote cell adhesion, often needing blending with natural polymers to overcome this default (Elmowafy *et al.*, 2019; Knight & Przyborski, 2014). Owing to all the limitations stated and as a sign of the current times, the search for alternative materials that can gather all the requirements for a 3D cell culture scaffold and which synthesis and processing could be achieved through a more sustainable way, led to the study of natural polymers such as polyhydroxyalkanoates (PHAs).

### 1.1.2 Biopolymers

Over the years, biopolymers have been elected as one of the best options for scaffolds material, mainly due to their inherent properties, such as excellent biocompatibility and biodegradability (Ambekar & Kandasubramanian, 2019). In bone tissue engineering spectrum, Chen *et al.* (2016) fabricated poly (L-lactic acid) (PLLA) nanofibrous porous tubular scaffolds by combining thermally induced phase separation (TIPS) and particle leaching, that proved to be biocompatible, cytocompatible and bioactive, revealing the potential for long bone tissue regeneration. Remya *et al.* (2018), through blending PCL with water soluble polyethyleneoxide (PEO) by electrospinning, obtained a PCL scaffold with improved mechanical properties, hydrophilicity and tunable degradation profile, promising for bone tissue engineering applications. For cartilage tissue engineering, Neumann *et al.* (2016) developed a hydrolytically degradable PEG hydrogel that showed promising results for this application. Regarding cardiac tissue engineering, Constantinides *et al.* (2018) demonstrated the applicability of mcl-PHA/PCL porous blends, fabricated as thin films by solvent casting/particulate leaching method, for controlled delivery of cardiovascular progenitor cells (CPCs) and possibly for maximizing myocardial regeneration. Also, Liu *et al.* (2015) used PLLA to produce highly porous nanofibrous scaffolds through phase separation/freeze-drying/particulate leaching method that supported cardiac tissue formation by culturing CPCs. Within neural tissue engineering, Shafei *et al.* (2016) developed a polypyrrole-coated PCL nanofibrous scaffold fabricated by electrospinning followed by vapour phase polymerization, resulting in a promising conducting scaffold for neural tissue engineering applications. Another development was made by Wang *et al.* (2017), for creating a conductive porous scaffold composed of poly(3,4-ethylenedioxythiophene) (PEDOT) nanoparticles on chitosan/gelatine porous hydrogel scaffold, that revealed good biocompatibility, controlled biodegradability and electrical conductivity with potential to be used in neural tissue engineering.



For skin tissue engineering, a great number of studies have been made and published in the last two decades, with a heterogeneity of biomaterials. Han *et al.* (2014) developed a gelatine/chitosan porous scaffold by freeze-drying technique that revealed good fibroblast adhesion and proliferation, but poor regeneration. Later, Lu *et al.* (2016) improved the gelatine/chitosan porous scaffold by blending in ascorbic acid and crosslinking with tannin acid, resulting in a better regeneration capacity that was further improved by loading with platelet-rich plasma. Collagen has been continuously used for tissue engineering, despite some of its drawbacks like poor mechanical properties and fast degradation. Yu *et al.* (2017), developed a collagen hydrogel cross-linked with non-cytotoxic succinimidyl glutarate-PEG (PEG-SC) as the dermal layer, resulting in lower contraction and less enzymatic degradation of this hydrogel. Matsumine *et al.* (2019) obtained very promising results by applying basic fibroblast growth factor impregnated collagen/gelatine sponge (bFGF-CGS) in reconstructive surgery of acute full-thickness skin defects that resulted in wound closure after a short period of time. As mentioned, synthetic polymers commonly need some surface modification or bending with natural polymers in order to improve bioactivity. Accordingly, Gautam *et al.* (2014) modified nanofibrous PCL/gelatine scaffold by grafting with collagen type I after electrospinning of the fibers, resulting in enhanced proliferation of mouse fibroblast cells (L929). Also, Sharif *et al.* (2017) developed an electrospun PCL nanofibrous scaffold grafted with collagen and after seeding with endometrial stem cells (hEnSCs) concluded that this construct was able to stimulate angiogenesis, revealing its potential. A full-thickness scaffold was developed by Halder *et al.* (2019) where the top layer (epidermis) was composed of PCL by casting method, the middle layer (dermis) of PCL nanofibers that were electrospun and the third layer (hypodermis) was a gelatine lyophilized hydrogel, revealing wound-healing efficacy after *in vivo* studies that resembled the structure of native skin.

PLGA is another commonly used biopolymer for skin tissue engineering. Yang *et al.* (2009) prepared a highly porous composite mat of PLGA and collagen obtained by electrospinning that revealed good adhesion, proliferation and ECM secretion of the cultured human dermal fibroblasts, dependent on the quantity of collagen on the composite. Later, Wang *et al.* (2013) fabricated a reinforced hybrid scaffold by integrating PLGA knitted mesh (PLGAm) with a collagen-chitosan (CCS) porous sponge. This PLGAm/CCS revealed improved mechanical properties and ability to induce angiogenesis and *in situ* tissue regeneration, unveiling the potential for skin tissue engineering. More recently, Sobhanian *et al.* (2019) developed an electrospun nanofibrous scaffold composed of poly (vinyl alcohol) (PVA), gelatin and alginate, that was modified by grafting with collagen, revealing better cell viability and proliferation of this scaffold upon comparison with non-modified nanofibrous scaffold. Other biopolymeric scaffolds for skin tissue engineering are listed in Table 1.2.

**Table 1.2.** Examples of biopolymeric scaffolds employed in skin tissue engineering

Material	Method	Result/Properties	Reference
Poly(L-lactic acid)-co-poly( $\epsilon$ -caprolactone) (PLACL)/gelatin	Electrospinning; air plasma treatment	Plasma-treated PLACL/gelatin nanofibrous scaffold showed better overall results, e.g. for proliferation, morphology and secretion of collagen of fibroblasts	Chandrasekaran <i>et al.</i> (2011)
Chitosan/PCL and PLLA	Electrospinning and TIPS	Bi-layer scaffold, upon co-culture of fibroblasts and keratinocytes, rendered a micro-environment similar to native skin	Lou <i>et al.</i> (2014)
PLACL/silk fibroin (SF)/tetracycline hydrochloride (TCH)/ascorbic acid (AA)	Electrospinning	PLACL/SF/TCH/AA scaffolds revealed better microenvironment conditions by collagen secretion, leading to tissue regeneration	Sridhar <i>et al.</i> (2015)
PLGAm/CCS and polyurethane (PU)	TIPS and freeze-drying	Upon transplantation into full-thickness skin defects, the PU-PLGAm/CCS bi-layer dermal substitute revealed favourable regeneration capability	Wang <i>et al.</i> (2016)
Poly( $\epsilon$ -caprolactone)-poly(ethylene glycol)-poly( $\epsilon$ -caprolactone) (PCEC), iron oxide nanoparticles (Fe <sub>3</sub> O <sub>4</sub> NPs)	Electrospinning	Magnetic PCEC/Fe <sub>3</sub> O <sub>4</sub> fibers showed increase in cell adhesion, viability and proliferation with the increase in Fe <sub>3</sub> O <sub>4</sub> NPs concentration	Zhang <i>et al.</i> (2017)
Silk-collagen	Cross-linking hydrogel	The HSE described achieved better resistance to degradation and contraction than collagen-only models	Vidal <i>et al.</i> (2018)

### 1.1.2.1 PHAs

As mentioned previously, the search for more sustainable alternatives to synthetic polymers, especially hydrocarbon sourced, has seen an exponential increase in the last decades. The advent of PHAs as promising biomaterials for tissue engineering is backed by their inherent properties, such as biocompatibility, biodegradability and non-toxicity. Additionally, these natural alternatives do not change their pH value during degradation, allowing for a better interaction with cells and immune system when compared to more commonly used polymers like PLGA, PCL, PGA and PLA. Moreover, the mechanical versatility of these biopolymers, going from thermoplastic to elastomeric, makes them a very promising alternative for tissue engineering, with a great variety of applications, either for hard or soft tissue (Rodriguez-Contreras, 2019).

Early published studies revealed that PHAs can be used to fabricate scaffolds for tissue engineering, being that some of the better known are polyhydroxybutyrate (PHB), polyhydroxyvalerate (PHV) and poly(hydroxybutyrate-co-hydroxyvalerate) (P(HBHV)) (Muneer *et al.*, 2020). Biodegradable PHAs (e.g. PHB and P(HBHV)) possess the ability to support adhesion and growth of cells *in vitro*, which was studied by Shishatskaya and Volova (2004), proposing these biomaterials as a good option for production of matrices for *in vitro* proliferous cells. Zhao *et al.* (2003) developed films and scaffolds of the PHB/P(HBHV) blend that revealed increase in mechanical properties (elongation at break) with the increase in P(HBHV) content, as well as improved growth and proliferation of chondrocytes on the scaffolds, concluding that the constructs allow physiological function and cartilage repair. Santos *et al.* (2004) prepared various blends of PLLA/P(HBHV) and cultured Vero cells on them, obtaining promising results for the maintenance of cell proliferation and production of ECM *in vitro*. A P(HBHV) conduit was constructed by particle leaching method and after one month of implantation in defective sciatic nerve of Sprague-Dawley rats, the disrupted nerves had functionally recovered, indicating a potential application of these conduits for nerve damage repair (Bian, Wang, Aibaidoula, Chen, & Wu, 2009). Recently, in her thesis, Esmail (2019) successfully produced porous/fibrous PHA-based scaffolds with promising results for fibroblast adhesion and proliferation, revealing potential for these 3D scaffolds in skin tissue reconstitution. Over the years, PHAs have been studied, as promising scaffold material, for a variety of applications such as bone tissue engineering (Degli Esposti, Chiellini, Bondioli, Morselli, & Fabbri, 2019), nerve tissue engineering (L. Wang *et al.*, 2010) and skin tissue engineering (Ekaterina I. Shishatskaya, Nikolaeva, Vinogradova, & Volova, 2016; Y. W. Wang *et al.*, 2005).

### 1.1.2.2 Polysaccharides

Polysaccharides are one of the naturally occurring polymers (biopolymers) that can be synthesized by plants, animals, bacteria and fungi. These macromolecules are composed of monosaccharide residues that are coupled to each other by glycosidic bonds (Shi, 2016; F. G. Torres, Troncoso, Pisani, Gatto, & Bardi, 2019). Possessing excellent biocompatibility, polysaccharides have been reported to comprehend complex biological activities and a variety of functions, such as immunoregulatory, anti-tumor, anti-virus, antioxidation and hypoglycaemic activity (Yu *et al.*, 2017). Ferreira *et al.* (2015) reviewed the polysaccharides reported with immunostimulatory activity. Additionally, Khan *et al.* (2019) recently reviewed the promising results of polysaccharides as anticancer agents. Some bacterial exopolysaccharides (EPSs), generally formed intracellularly and transported to the extracellular environment, were able to reach industrial production due to their significant market value (bacterial cellulose and xanthan gum). However, other important applications for these macromolecules include their use in cosmetics, pharmaceuticals and biomedicine, due to high purity and functional properties (Freitas *et al.*, 2010). FucoPol is a newly reported EPS that holds great potential, possessing biological activity related to high fucose content (Freitas, Alves, & Reis, 2011).

The structure of this work was divided in chapters, with an introduction in the beginning, followed by materials and methods, results and discussion and a brief conclusion for each chapter.

## 1.2 Motivation

The skin is the largest organ in humans, representing a barrier between the external environment and the organism and, among various critical functions, prevents the invasion of pathogens, protects against chemical and physical aggressions and limits the loss of water and electrolytes (Ali *et al.*, 2015). Skin tissue engineering is an emerging field that aims to provide efficient alternatives in regenerative medicine as well as in the reconstruction of human skin for drug testing. This reconstructed human skin, as *in vitro* models, could replace the experimentation with animals *in vivo* and at the same time provide a human model that would eliminate the species related differences found in drug testing (Hoarau-Véchet *et al.*, 2018; Kinikoglu, 2017). One common approach to achieve this is based on the use of solid scaffolds that can be defined as 3D porous biomaterials able to guide seeded cells through adherence, proliferation, differentiation and deposition of ECM components, forming a functional and structural analogue of the human skin tissue (R. Hokmabad, Davaran, Ramazani, & Salehi, 2017).

Naturally-derived materials, such as PHAs and polysaccharides, have been studied for biomedical applications, due to their inherently advantageous properties, such as biocompatibility, biodegradability, non-cytotoxicity and bioactivity (Elmowafy *et al.*, 2019; Yu *et al.*, 2017).

In this work a P(HBVHx) terpolyester was used to produce porous scaffolds for dermis reconstruction, by the emulsion templating method. The exopolysaccharide FucoPol was incorporated as a possible emulsion stabilizer and its bioactive functions toward HDFn were studied.

Porous scaffolds were fabricated through water emulsion templating method, later a FucoPol aqueous solution was added as the dispersed phase of the emulsion and lastly a coating method with concentrated FucoPol solution was employed to the water emulsion templated scaffolds, resulting in three different porous scaffolds. These three scaffolds were used for the dermal construct assays with HDFn for eight and fourteen days, assessing their bioactivity.

The aim of this work was the production of porous scaffolds with appropriate properties for application in skin tissue engineering. With P(HBVHx) as a promising biomaterial due to the inherent advantageous properties that possesses and FucoPol an interesting addition with possible improvements in the scaffold production and bioactivity. A naturally-derived porous scaffold, with suitable physical and mechanical properties, that promotes bioactivity towards HDFn was the ultimate goal of the present work.





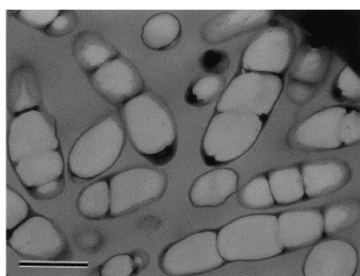
## **Chapter Two – Biopolymers for scaffolds development**

---

## 2.1 Introduction

### 2.1.1 PHAs

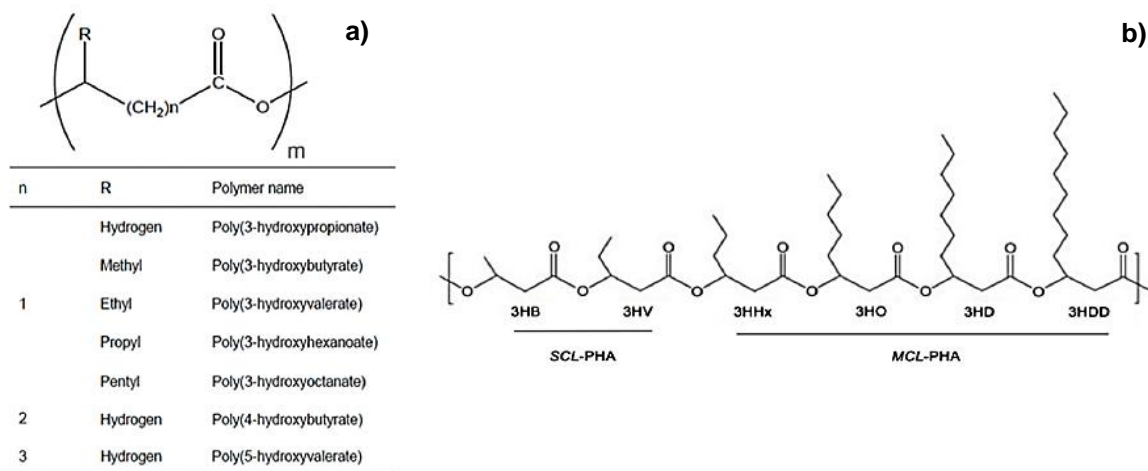
PHAs are a family of biodegradable biopolyesters accumulated intracellularly in prokaryotic organisms such as bacteria, in the form of water insoluble inclusions that mainly act as storage substances in cells subject to stress (Aljuraifani, Berekaa, & Ghazwani, 2018; Lee, 1995; Muneer *et al.*, 2020; Sudesh, Abe, & Doi, 2000). These inclusions, besides acting as sources of carbon and energy for vegetative cells, comprehend complex biological functions, such as protection against intracellular ice formation, UV irradiation, high temperatures and osmotic imbalances (Sedlacek *et al.*, 2018). In 1926, the first PHA was discovered in *Bacillus megaterium* by Lemoigne, reporting that the homopolymer polyhydroxybutyrate (PHB) accumulated intracellularly in this bacteria (Lemoigne, 1926). For several decades PHB was thought to be the only constituent of this reserve polymer, until in 1974 other hydroxyalkanoates (HA) units were observed in chloroform extracts from activated sewage sludge, being this the first report of 3-hydroxyvalerate (3HV) and 3-hydroxyhexanoate (3HHx) units (Wallen & Rohwedder, 1974). PHAs accumulate as granular inclusions (Figure 2.1) in the cells cytoplasm with sizes ranging from 0.2 - 0.5  $\mu\text{m}$  and the molecular weight falls between  $2 \times 10^5$  and  $3 \times 10^6$  Da (Anjum *et al.*, 2016; Khanna & Srivastava, 2005). To date, more than 150 monomers of PHA have been identified. These biopolyesters have different properties depending on the monomer composition, namely, homopolyesters are made up of only one type of monomer while copolyesters are composed of different monomer units (Grigore *et al.*, 2019).



**Figure 2.1.** PHAs granular inclusions. Scale bar at 0.5  $\mu\text{m}$ . Retrieved with permission from Sudesh *et al.*, 2000.

PHAs are linear polymers composed of hydroxyalkanoate units connected by ester bonds (Figure 2.2) (Rodriguez-Contreras, 2019; Sudesh *et al.*, 2000). The bacterial species and carbon source used for PHAs synthesis influence the type of polymer produced in the fermentation process, thus they can be classified as short-chain length PHA (scl-PHA) with 3-5 carbon units, medium-chain length PHA (mcl-PHA) containing 6-14 carbons per monomer and long-chain length PHA (lcl-PHA) with more than 14 carbons (Muneer *et al.*, 2020).





**Figure 2.2.** General structure of PHA polymer family (a); Structure of some common monomers of scl-PHA (HB and HV) and mcl-PHA (3-hydroxyhexanoate: 3HHx, 3-hydroxyoctanoate: 3HO, 3-hydroxydecanoate: 3HD, 3-hydroxydodecanoate: 3HDD) (b). Adapted with permission from Rodriguez-Contreras *et al.*, 2019.

Due to the differences in molecular composition and chain lengths, the physico-chemical, mechanical and thermal properties of PHAs vary greatly. Most of scl-PHAs, such as PHB, are characterized as rigid and brittle biothermoplastics, mainly because of its high crystallinity ranging from 60-80 %, while mcl-PHAs (e.g. poly (hydroxyhexanoate) (PHHx) or poly (hydroxyoctanoate) (PHO)) are considered more elastic and sometimes viscous materials, with lower crystallinity degree, melting and glass transition temperatures (Cruz *et al.*, 2016; Muneer *et al.*, 2020).

PHB is the most comprehensively studied amongst PHA family. It is mainly characterized as being highly crystalline due to its stereo regularity, water insoluble and resistant to hydrolytic degradation to a certain degree. Also, has low O<sub>2</sub> permeability, good thermoplastic properties but poor mechanical properties when compared to some petroleum-based polymers such as polypropylene (PP). This homopolymer is commonly used for bone tissue engineering, as mentioned previously, owing this to being piezoelectric, which helps in the process of osteogenesis (Anjum *et al.*, 2016; Khanna & Srivastava, 2005). The incorporation of other HA monomers in the polymer chain, such as 3HV and 3HHx, improves material properties, including crystallinity, melting temperature, stiffness and toughness. One of this copolymers is P(HBHV) with improved characteristics, namely, relatively lower crystallinity (50-70 %), lower melting point, stiffness, higher flexibility (decrease in Young Modulus) and increased elongation at break, when compared to PHB. The fraction of HV in the copolymer influences the material properties, specifically, the increase in HV content is followed by a decrease in melting temperature and Young Modulus, a increase in elongation at break which makes the copolymer more flexible and thermally processable without thermal degradation (Khanna & Srivastava, 2005). In Table 2.1 a comparison between PHB, other PHAs and petroleum-based plastics is depicted.

**Table 2.1.** Thermo-mechanical properties of some PHAs and most common petroleum-based plastics. Adapted with permission from Khanna *et al.* (2005) and Anjum *et al.* (2016). (n.a – data not available)

Polymer	Composition	Young Modulus (GPa)	Tensile Strength (MPa)	Elongation at Break (%)	Melting temperature (°C)	Glass Transition Temperature (°C)
P(3HB)		3.5 - 4	40	3 - 8	173 - 180	5 - 9
P(3HB-co-HV)	(3 wt% 3HV)	2.9	38	n.a	170	n.a.
	(14 wt% 3HV)	1.5	35	n.a	150	n.a.
	(25 wt% 3HV)	0.7	30	n.a	137	n.a.
P(3HB-co-3HHx)	n.a.	n.a.	20	850	52	-4
PP		1.0 - 1.7	29.3-38.6	400 - 900	170 - 176	-10
PS		3.0 - 3.1	50	3 - 4	80 - 110	21
LDPE		0.05 - 0.2	10 - 78.6	150 - 620	88 - 130	(-30) - (-36)

#### 2.1.1.1 P(HBHVHHx)

Terpolyester P(HBHVHHx), composed of 3-hydroxybutyrate (HB), 3-hydroxyvalerate (HV) and 3-hydroxyhexanoate (HHx) is a random copolyester synthesized by recombinant microorganisms, considered to be one of the most promising additions to PHAs family. Copolymers that have in their composition both scl-HAs and mcl-HAs generally have better material properties when compared to scl-PHAs or mcl-PHAs (W. Zhao & Chen, 2007). Adding to the improvement in thermo-mechanical properties (Ye, Wang, Wang, Chen, & Xu, 2010), P(HBHVHHx) has been also compared with other materials used for biomedical applications, including PLA, P(HBHV), P(HBHx) and tissue culture plates (TCP), revealing better biocompatibility and potential for cell culture, being one of the few PHAs that achieved better results than TCP (plasma-treated PS - tissue culture plates) for cell growth (Hu, Wei, Zhao, Liu, & Chen, 2009). In one of this studies, P(HBHVHHx) revealed promising thermo-mechanical properties for skin tissue engineering, demonstrating a superior ability for epidermal HaCaT cells growth (Y. Ji, Li, & Chen, 2008). Additionally, this terpolyester was also studied for its biocompatibility towards fibroblast cell line L929 and osteoblast cell line MC3T3, proving to be a better substrate for cell attachment and proliferation when compared with PLA, PHB, P(HBHV) and P(HBHx) (Liang, Zhao, & Chen, 2008). Table 2.2 summarizes thermo-mechanical properties of P(HBHVHHx) found in the literature.

**Table 2.2.** Different P(HBHVHHx) thermo-mechanical properties in literature. (n.a – data not available)

P(HBHVHHx) composition	Young Modulus (MPa)	Tensile Strength (MPa)	Elongation at Break (%)	Melting temperature (°C)	Glass Transition Temperature (°C)	Reference
84 mol % HB, 3 mol % HV, 13 mol % HHx	109.8	8	481.1	114	-2.2	Zhao and Chen (2007)
88 mol % HB, 1 mol % HV, 11 mol % HHx	318.9	10.1	276.9	n.a	n.a	Zhao and Chen (2007)
83 mol % HB, 5 mol % HV, 12 mol % HHx	290.5	15.7	340.1	n.a	n.a	Zhao and Chen (2007)
89 mol % HB 3 mol % HV, 8 mol % HHx	n.a	n.a	n.a	148	-1.2	Zhao and Chen (2007)
83 mol % HB 4 mol % HV, 13 mol % HHx	284.6	5.1	263.7	113.2	n.a	Hu <i>et al.</i> (2009)

### 2.1.2 FucoPol

As previously referred, FucoPol is a new fucose-rich extracellular heteropolysaccharide synthesized by *Enterobacter A47*. It has a high molecular weight ( $4.19 \times 10^6 - 5.8 \times 10^6$  Da) and its repeating unit (hexamer) is composed of two fucose, two galactose, one glucose and one glucuronic acid residues (Concórdio-Reis *et al.*, 2020; A. R. V. Ferreira *et al.*, 2014).

Amongst various properties, FucoPol has demonstrated good flocculating capability (Freitas *et al.*, 2011), film-forming (A. R. V. Ferreira *et al.*, 2014, 2016) and emulsifying ability (Freitas *et al.*, 2013, 2011). Additionally, as with many polysaccharides, FucoPol's hydrophilicity, non-toxicity and biodegradability translates its suitability for biomedical applications. Moreover, biological properties such as modulation of cell-cell and cell-matrix interactions, makes these polysaccharides interesting for various applications (Péterszegi, Fodil-Bourahla, Robert, & Robert, 2003; Yu *et al.*, 2017). Recently, Concórdio-Reis *et al.* (2020) demonstrated that FucoPol was not cytotoxic towards human skin keratinocytes and mouse fibroblasts, additionally it was found to promote *in vitro* migration of keratinocytes, revealing promising biocompatibility and possibly regenerative capacity. Additionally, Guerreiro *et al.* (2020) reported the non-cytotoxicity of FucoPol up to 0.25 % (w/v) and corresponding cryoprotective capability towards various cell lines.

## 2.2 Materials and Methods

### 2.2.1 Biopolymers production and extraction

PHA production was performed under the scope of the ResUrbis Project, at the pilot scale facilities of BIOENG (*Faculdade de Ciências e Tecnologia – Universidade Nova de Lisboa*). The biopolymer was produced by cultivation of a mixed microbial consortium in a three-stage bioprocess, as described by Albuquerque *et al.* (2010) using fruit waste as feedstock. The first stage, the acidogenic fermentation phase, was performed in a 100 L bioreactor, where the fruit waste was converted into a mixture of fermentation products (FP). The produced FP were used in the second stage of the bioprocess for the selection of a microbial population enriched in PHA-storing bacteria. This stage was performed in a 100 L bioreactor operated with an alternate feast and famine periods. Finally, in the PHA production stage, performed in a 60 L bioreactor, the selected microorganisms were fed with the FP produced in the acidogenic fermentation for PHA accumulation up to the culture's maximum capacity.

The resulting cultivation broth recovered from the production bioreactor was centrifuged (8000 rpm, 15 minutes at 4 ° C) and the pellets obtained were lyophilized and weighted. PHA was obtained by Soxhlet extraction of the biomass using chloroform (250 mL) (Honeywell) at 80 ° C for 48h. PHA was resolubilized in chloroform and precipitated in ice-cold ethanol (chloroform/ethanol 1:10 v/v) (Fisher Chemical), from which the precipitate was recovered in a previously weighted flask and left in a fume hood, at room temperature, for solvent evaporation.

FucoPol was supplied by BIOENG. It had been previously produced by cultivation of *Enterobacter* A47 (DSM 23139) in a 2 L bioreactor (BioStat B-plus, Sartorius, Germany) under a fed-batch mode, using glycerol as the carbon source, as described by Torres *et al.* (2011), and extracted from the cultivation broth by diafiltration and ultrafiltration, as described by Ferreira *et al.*, (2014). The extracted polymer was composed of fucose (35 wt%), glucose (31 wt%), galactose (24 wt%) and glucuronic acid (10 wt%), and with an additional content of acyl groups (pyruvyl, acetyl and succinyl residues) totalizing 12.3 wt% of the polymer's dry mass (Concórdio-Reis *et al.*, 2020).

## 2.2.2 Characterization of the PHA

### 2.2.2.1 Composition

The polymer composition was determined by gas chromatography (GC), as described by Pereira *et al.* (2019). Briefly, a polymer sample (1.5 mg) was mixed with 2 mL benzoic acid (SIGMA-ALDRICH) in chloroform (Honeywell) (1 g/L) and 2 mL 20 % (v/v) sulphuric acid (Honeywell) in methanol (Fisher Chemical), and heated at 100 °C on a digester (DryBlockHeater, OHAUS), for 4 h. After cooling, 1 mL of deionized water was added and after phase separation, the organic phase was recovered and analysed by GC (430-GC, Bruker) with a Restek column of 60m, 0.53 mmID, 1 µM df, Crossbond, Stabilwax. The injection volume was 2.0 µL, with a running time of 32 min, constant pressure of 14.50 psi and helium as carrier gas. The heating ramp followed a 20 °C/min rate until 100 °C, 3 °C/min until 155 °C and again 20 °C/min until 220 °C. The standards used for this analysis were P(HBV) (SIGMA-ALDRICH) 86 wt% of 3HB and 14 wt% of 3HV, with concentrations ranging between 0.062 and 1.235 g/L and P(HHx) (SIGMA-ALDRICH) with concentrations between 0.05 and 1.0 g/L.

### 2.2.2.2 Molecular Mass Distribution

Size exclusion chromatography (SEC) was performed to determine the molar mass distribution of the PHA in this study. For this characterization, 15 mg of the polymer were weighted and dissolved in 3 mL of chloroform, for 18 h at room temperature. This solution was filtered using a glass fibre filter 47 mm (PALL) and analysed in the SEC System (Waters Millenium) with SEC Support: PLgel 5 µm Guard (Polymer Laboratories), 50 x 7.5 mm; PLgel 5 µm 10 Å (Polymer Laboratories), 300 x 7.5 mm; PLgel 5 µm 500 Å (Polymer Laboratories), 300 x 7.5 mm. Temperature of equilibration at 30 °C, flow rate of 1 mL/min, chloroform as the mobile phase and volume of the sample injected of 100 µL. For the detection of the polymer was used a RI detector (Waters 2410) with a collection duration of 25 min and sensitivity of 512.

### 2.2.2.3 X-Ray Diffraction

X-Ray Diffraction (XRD) was performed in a Benchtop X-Ray Diffractometer (RIGAKU, model MiniFlex II), with copper X-Ray tube (30 KV/15 mA). The  $2\theta$  scans were performed with a scanning range from  $10^\circ$  to  $60^\circ$  and a sampling width of  $0.02^\circ$ . The diffractograms were used to determine the crystallinity fraction ( $X_c$ ) of the samples following the gaussian peak fitting with a linear background method, described elsewhere (Ahvenainen, Kontro, & Svedström, 2016). Briefly, the crystallinity fraction was determined by finding the area below the curve corresponding to the crystalline peaks and dividing the sum of the crystalline area with the total area below the curve, with an added baseline.

### 2.2.2.4 Thermal Properties

Two analysis were performed to determine the thermal properties of this polymer – Differential Scanning Calorimetry (DSC) and Thermogravimetric Analysis (TGA), as described by Zhao and Chen (2007) and Levine *et al.* (2016).

DSC was performed in a DSC 25 (Discover Series, TA instruments, USA), with a Cooling System 90 (TA instruments, USA), by placing the samples in aluminium hermetic pans and analysing them with a heating and cooling speed of  $10^\circ\text{C}/\text{min}$  within a temperature range of  $-80$  and  $200^\circ\text{C}$ . To determine the melting ( $T_m$ ) and glass transition ( $T_g$ ) temperatures of this polymer, the endotherms of the DSC were analysed.

Another DSC equipment was used for the last half of the samples. Those were performed in a DSC 131 (Setaram, France), by placing the samples in aluminium hermetic pans and analysing them with a heating and cooling speed of  $10^\circ\text{C}/\text{min}$  within a temperature range of  $-130$  and  $400^\circ\text{C}$ . The melting ( $T_m$ ) and glass transition ( $T_g$ ) temperatures were also determined by analysing the endotherms of the DSC.

TGA was performed in a Thermogravimetric Analyzer Setaram Labsys EVO with a weighing precision of  $\pm 0.01\%$ , using aluminium crucibles to place the samples (8.6 - 16.3 mg) and analysing them with a temperature range between  $25^\circ\text{C}$  and  $500^\circ\text{C}$ , at  $10^\circ\text{C}/\text{min}$ , in Argon atmosphere. To determine the degradation temperature ( $T_{\text{deg}}$ ) the endotherm peak of the TGA was analysed.

## 2.3 Results and Discussion

### 2.3.1 P(HBHVHHx)

#### 2.3.1.1 Composition

To identify the monomeric composition of the PHA extracted, GC analysis was performed. Results revealed that this polymer is mainly composed of 3HB (51 wt%), 3HHx (31 wt%) and 3HV (18 wt%) (Table 2.3). Most of the P(HBHVHHx) polymers described in the literature have the same monomeric ponderation, with different proportions. This scl-mcl-PHA has an interesting monomeric percentual composition, where 3HB is still the major component but with a lower percentage, whereas 3HV and 3HHx are present with a higher percentage than usually observed with this terpolyester. However, some studies revealed that similar P(HBHVHHx) compositions of those found in this study were achievable, e.g Zhang *et al.* (2009) produced this terpolyester with 3HV contents ranging from 9 to 32 % and 3HHx percentage also flexible from 12 to 34 %, depending on the valerate concentration that was fed to wild-type and recombinants of *Aeromonas hydrophila* cultures. However, this was achieved by fermentation using a pure culture, whereas the scl-mcl-PHA extracted in this study was produced by a mixed microbial culture (MMC).

**Table 2.3.** Composition (wt%), Molecular weight ( $M_w$ ), Molecular number ( $M_n$ ) and polydispersity index (PDI) of P(HBHVHHx) used in this work with comparison to other terpolyesters found in the literature. (n.a – data not available)

Composition (wt%)			Type of production strain	$M_w$ ( $\times 10^4$ Da)	$M_n$ ( $\times 10^4$ Da)	PDI	Reference
3HB	3HV	3HHx					
51	18	31	MMC	22	5.80	4.10	This study
83	4	13	<i>Aeromonas hydrophila</i> 4AK4	30.3	16.7	1.81	Hu <i>et al.</i> (2009)
87	2	11	Recombinant <i>Aeromonas hydrophila</i> 4AK4 harboring genes <i>phaAB</i>	87.4	n.a	n.a	Ji <i>et al.</i> (2008)
85	3	12	Recombinant <i>Aeromonas hydrophila</i> 4AK4 harboring genes <i>phaAB</i>	87.5	52.4	n.a	Ji <i>et al.</i> (2009)
85	5	10	Recombinant <i>Aeromonas hydrophila</i> 4AK4 harboring genes <i>phaAB</i>	n.a	n.a	n.a	Liang <i>et al.</i> (2008)
82	7	11	Recombinant <i>Aeromonas hydrophila</i> 4AK4, with <i>phaPCJ</i> operon	160	79.0	2.03	Ye <i>et al.</i> (2010)
71	18	11	Recombinant <i>Aeromonas hydrophila</i> 4AK4, with <i>phaPCJ</i> operon	184	85.1	2.16	Ye <i>et al.</i> (2010)
57	20	23	Recombinant <i>Aeromonas hydrophila</i> 4AK4, with <i>phaPCJ</i> or <i>phaAB</i>	75	40.9	2.09	Zhang <i>et al.</i> (2009)
48	24	28	Recombinant <i>Aeromonas hydrophila</i> 4AK4, with <i>phaPCJ</i> or <i>phaAB</i>	94.2	45.1	1.71	Zhang <i>et al.</i> (2009)

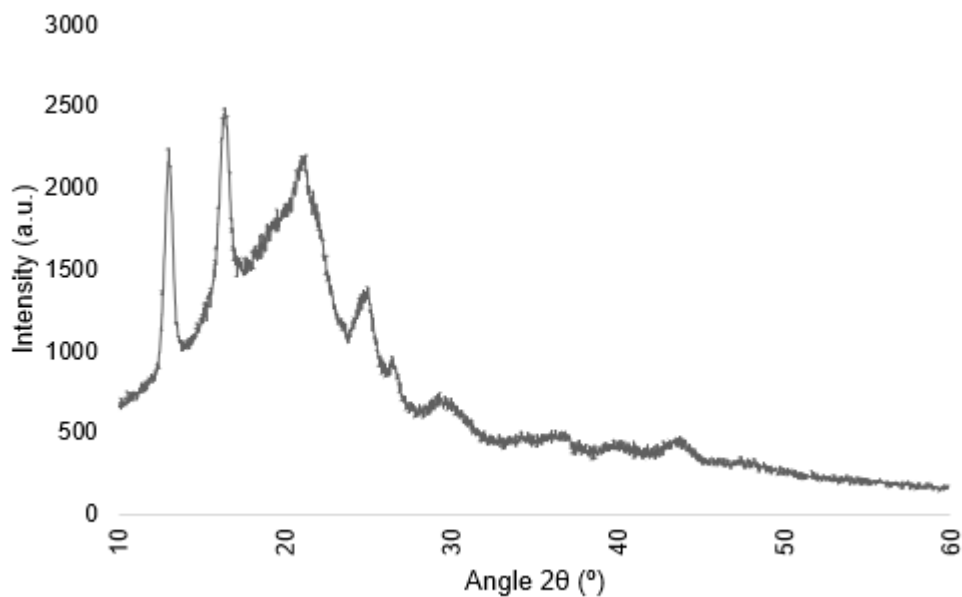
### 2.3.1.2 Molecular Mass Distribution

SEC analysis (Figure A in appendices) of the extracted scl-mcl-PHA revealed an average molecular weight ( $M_w$ ) of  $22.08 \times 10^4$  Da and a polydispersity index (PDI) of 4.1 (Table 2.3). The  $M_w$  obtained in this work is amongst the range of average molecular weight for mcl-PHAs ( $6.0 - 41.2 \times 10^4$  Da) (Rai, Keshavarz, Roether, Boccaccini, & Roy, 2011) and also for PHAs ( $2.0 - 5.0 \times 10^5$  Da). However, it is lower than those observed in the literature ( $30.3 - 184 \times 10^4$  Da) (Table 2.3). Similarly, with PDI value, that is included in the average range for mcl-PHAs (1.6 – 4.4) (Rai *et al.*, 2011), but is higher than the values found in the literature for a similar terpolyester (1.71 – 2.16) (Table 2.3), suggesting non-uniformity of the scl-mcl-PHA. These differences in molecular weight and polymer dispersion between P(HBHVHHx) terpolyesters could be explained by numerous reasons, such as the synthesizing microorganism, the inoculum, medium composition, fermentation conditions, downstream processing methods and even the cell's stage of growth upon harvesting (Rai *et al.*, 2011; Sudesh *et al.*, 2000). Additionally, the monomeric proportions in this PHA could also influence the resulting molecular weight (Zhila & Shishatskaya, 2018).

### 2.3.1.3 X-Ray Diffraction

In order to structurally characterize this polymer, XRD analysis was performed. The diffractogram (Figure 2.3) revealed peaks and humps superposed to those found for crystalline and amorphous polymers, at approximately  $2\theta = 14^\circ$  and  $17^\circ$  and  $2\theta = 20^\circ$  regions, respectively (Dufresne, Kellerhals, & Witholt, 1999). In addition, Ye *et al.* (2010) reported a similar diffractogram for P(HBHVHHx) (7 – 18 wt% of 3HV and 11 wt% of 3HHx). Analysis of the crystalline peaks resulted in a crystallinity fraction of around 26 % ( $X_c$ ). The crystalline fraction (26 %) of this terpolyester renders a balance between semi-crystalline and amorphous behaviour, which can be further supported by the 51 wt% of 3HB that imparts the crystalline peaks and the incorporation of 18 wt% of 3HV and 31 wt% of 3HHx that significantly reduces the degree of crystallinity of the terpolymer (Bhubalan *et al.*, 2008). However, the semi-crystallinity observed, despite the high non-crystallizable 3HHx content (31 wt%), can be associated with the co-crystallization of 3HB and 3HV (Ye *et al.*, 2010).





**Figure 2.3.** P(HBVHx) polymer (raw) diffractogram

#### 2.3.1.4 Thermal Properties

TGA was used to study the thermal stability of the terpolyester (Figure B in appendices). The curve obtained revealed a fast one-step decomposition of this polymer. This curve was stable until 240 °C, suffering a major weight loss ( $\Delta m \approx 81\%$ ) with maximum degradation rate at 290 °C and a char yield of approximately 17.9 % at 500 °C. The degradation rate at 5 % weight loss ( $T_{deg}$ ) was determined, revealing a higher value (267 °C) than those found in the literature (227 – 261 °C), thus this P(HBVHx) possesses a high thermal stability (Table 2.4).

To study the pre-melting behaviour, DSC analysis was performed. Cold crystallization was not detected during the cycle process of the DSC study, supporting the fact that this terpolyester is a random copolymer (H. Zhang *et al.*, 2009).  $T_g$  of this P(HBVHx) revealed to be below room temperature (-2.6 °C), and lower than the values of other PHAs such as PHB, P(HBV) and P(HBHx) found in the literature (Table 2.4). The decrease in  $T_g$  values is associated with elastomeric behaviour at room temperature (W. Zhao & Chen, 2007).  $T_m$  value (145 °C) and especially enthalpy of melting ( $\Delta H_m$ ) (4.3 J/g) of this terpolyester were lower than other similar P(HBVHx), PHB and P(HBV) found in the literature, which could be associated with the higher content of 3HHx in the polymer, since the incorporation of this monomer with 3HB domains disturbs the possibility of crystallization processes associated with 3HB (W. Zhao & Chen, 2007).

**Table 2.4.** Thermal properties of the P(HBHVHHx) extracted in this study, compared to other PHAs found in the literature. (n.a – data not available; n.d – not detected)

Composition (wt%)			$\Delta H_m$ (J/g)	$T_m$ (° C)	$T_g$ (° C)	$T_{deg}$ (° C)	Reference
3HB	3HV	3HHx					
51	18	31	4.3	145	-2.6	267	This study
83	4	13	28.4	113.2	-1.3	255	Hu <i>et al.</i> (2009)
57	20	23	n.a	n.d	-12.5	258	Zhang <i>et al.</i> (2009)
48	24	28	n.a	54.2	-5.1	250	
84	3	13	29.8	114	-2.2	258	Zhao and Chen (2007)
89	3	8	33.2	148	-1.2	261	
95	5	0	n.a	170	2.3	232	Zhang <i>et al.</i> (2009)
88	0	12	n.a	96	-1.2	242	
75	25	0	26	176	n.a	n.a	Esmail (2019)
100	0	0	97	162	-1.2	227	Zhao and Chen (2007)

### 2.3.2 FucoPol

As previously mentioned, the fucose-rich EPS (FucoPol) used in this work was composed of 35 wt% of fucose, 31 wt% of glucose, 24 wt% of galactose and 10 mol% of glucuronic acid. Additionally, the average molecular weight of the polymer was  $4.4 \times 10^6$  Da, with a polydispersity index of 1.9 (Concórdio-Reis *et al.*, 2020).

## 2.4 Conclusions

The P(HBVHHx) extracted in this study was composed of an interesting monomeric proportion (51 wt% of 3HB, 18 wt% of HV and 31 wt% of HHx), with low crystallinity fraction (26 %), low melting temperature (145 ° C) and enthalpy of fusion (4.3 J/g) and high degradation temperature (267 ° C), making this semi-crystalline scl-mcl-PHAs thermally stable, with elastomeric potential.

FucoPol, as a fucose-rich EPS, has some interesting properties that could improve emulsion stability and film forming ability. Also, as mentioned before, studies revealed other biological properties that would be advantageous in the context of this work, such as biocompatibility, hydrophilicity and capability for promoting cell migration and adhesion.

The attained characterization of the extracted terpolyester P(HBVHHx) revealed good physico-chemical properties, suitable for scaffold production intended for skin tissue engineering, which will be explored in the next chapters.





**Chapter Three – Production and characterization of biopolymer-based scaffolds**

---

## 3.1 Introduction

### 3.1.1 Scaffold-based techniques

Scaffold-based tissue engineering has emerged in the mid 1980's, upon the idea of creating scaffolds that could support cells with compatible physical and chemical properties (Dutta, Dey, Dutta, & Basu, 2017). To design a reconstructed tissue, one of the most important aspects to consider is the porosity, that should properly mimic the *in vivo* counterpart (Jensen & Teng, 2020). Additionally, other factors such as the chemical composition of the material, mechanical and degradation properties and the addition of biological components that could improve the bioactivity of the scaffold, should be taken into consideration upon the process of designing a scaffold. Besides selection of the material, fabrication technique plays an important role in this process, since the material processability, ease of handling and complexity of the method are also crucial for the creation of the desired scaffold (Dutta *et al.*, 2017). Several methods have been developed to produce porous scaffolds and amongst the most commonly used are solvent-casting particulate leaching (SCPL) (Esmail, 2019), freeze-drying, thermal-induced phase separation (TIPS), electrospinning (Esmail, 2019) and 3D printing (Eltom, Zhong, & Muhammad, 2019; Jensen & Teng, 2020).

SCPL technique allows forming structures with high porosities (50 – 90 %), through mixing a polymer solution with water-soluble salt particles and casting into a scaffold mould. Then, the solvent is removed by evaporation and the salt particles are leached out of the matrix by submerging in water. This method allows control over the pore size, however the pore interconnectivity is limited (Eltom *et al.*, 2019; Zhu & Che, 2013). Freeze-drying is another method, also known as lyophilization, based on the sublimation of the solvent. A polymer solution is obtained, by dissolving the polymer in appropriate solvent, then poured into a mould and cooled under freezing point, resulting in a solid solvent that later is subjected to sublimation. This results in a porous scaffold with numerous interconnected pores, however the mechanical integrity is limited (Ambekar & Kandasubramanian, 2019; Eltom *et al.*, 2019). TIPS is based in the quenching of the polymer solution under the freezing point of the solvent, resulting in a phase separation composed of a polymer-rich phase that solidifies and a polymer-poor phase that crystallizes, producing a porous structure when the solvent is removed by freeze-drying. This technique allows for tunable mechanical properties, however can only be applied to thermoplastic polymers (Eltom *et al.*, 2019; R. Hokmabad *et al.*, 2017).

Electrospinning is a printing method that is based in the use of an electric field for controlling the formation and deposition of polymer fibers onto a substrate. A high voltage is applied to the polymer solution, creating a charge imbalance that results in a stream of liquid polymer (Taylor cone) that travels to the target, evaporating the solvent in the process. The nanofibrous scaffold obtained has highly interconnected pores, however the thickness achievable is limited (Ambekar & Kandasubramanian, 2019; Jensen & Teng, 2020).

Finally, a continuously evolving technique for the production of 3D tissue scaffolds that copiously mimic the target native structure – 3D printing, is based in the production of a 3D structure with the help of computer aid design (CAD) files. One of the methods used for this rapid prototyping technology is bioprinting, which consists in the layer-by-layer deposition of the selected constituents of a 3D object. This technology allows for nanoscale-controlled pore structure, however expensive (Ambekar & Kandasubramanian, 2019; R. Hokmabad *et al.*, 2017). Table 3.1 includes a comparison between the mentioned methods, with their advantages and limitations.

**Table 3.1.** Commonly used methods to produce porous scaffolds, with their advantages and limitations. Adapted with permission from Ambekar *et al.* (2019), Eltom *et al.* (2019) and Teng *et al.* (2020).

Method	Advantages	Limitations
<b>SCPL</b>	<ul style="list-style-type: none"> <li>○ Simple method</li> <li>○ Controlled porosity and pore size</li> <li>○ Inexpensive</li> </ul>	<ul style="list-style-type: none"> <li>○ Possibility of residual leaching agent</li> <li>○ Limited pore interconnectivity</li> </ul>
<b>Freeze-drying</b>	<ul style="list-style-type: none"> <li>○ Highly interconnected pores</li> <li>○ Controllable pore size</li> </ul>	<ul style="list-style-type: none"> <li>○ Small pore size</li> <li>○ Limited mechanical integrity</li> </ul>
<b>TIPS</b>	<ul style="list-style-type: none"> <li>○ Simple equipment</li> <li>○ Tailorable mechanical properties</li> </ul>	<ul style="list-style-type: none"> <li>○ Only used for thermoplastics</li> </ul>
<b>Electrospinning</b>	<ul style="list-style-type: none"> <li>○ Continuous process</li> <li>○ Highly interconnected pores</li> <li>○ Good surface area to volume ratio</li> <li>○ Random and oriented fibers possible</li> </ul>	<ul style="list-style-type: none"> <li>○ Limited scaffold thickness</li> <li>○ Complexity of different variables</li> </ul>
<b>3D printing</b>	<ul style="list-style-type: none"> <li>○ Controlled quality</li> <li>○ Controlled pore structure, shape accuracy and complexity</li> </ul>	<ul style="list-style-type: none"> <li>○ Expensive</li> <li>○ Limited filament resolution</li> </ul>

### 3.1.2 Emulsion Templating

Emulsion templating is a promising alternative for the fabrication of scaffolds with high porosities (up to 99 %) and high interconnected pores. This method is based in two steps: (i) the preparation of an emulsion, normally composed of two immiscible liquids, where the internal phase (dispersed phase) is dispersed in the continuous phase (external phase); (ii) the solidification of the external phase of the emulsion, where droplets of the internal phase behave like templates, leaving behind a highly porous structure upon their removal. Besides the high porosity and interconnectivity, another advantage of this method is the tailoring of the porosity by changing the internal phase volume. This method combines ease of production with simple equipment necessary and excellent results. However, when a surfactant is added to achieve high stability of the emulsion, this step can turn the technique quite expensive due to the surfactant cost and to the removal process necessary after the solidification (Aldemir Dikici & Claeysens, 2020; T. Zhang, Sanguramath, Israel, & Silverstein, 2019). This method has been used to develop scaffolds for tissue engineering over the last decade. Ruiz *et al.* (2011) produced P(HBV) 3D porous scaffolds by emulsion templating with surfactant, using the solvent evaporation method. Barbetta *et al.* (2005) successfully developed highly porous and interconnected gelatin-methacrylate (GMA) scaffolds, with the addition of NaCl and dimethyl sulfoxide (DMSO) in the emulsions in order to increase void and interconnectivity diameters. Luo *et al.* (2015) developed highly porous PVA hydrogels by surfactant-free CO<sub>2</sub>-in-water emulsion templating, that were tested with fibroblasts and revealed a good proliferation and penetration into the hydrogels. Table 3.2 comprises some examples of emulsion templated scaffolds for tissue engineering.

Additionally, Esmail (2019) recently developed scaffolds intended for skin tissue engineering, with mcl-PHA, PHB and P(HBV), obtaining good results with emulsion templating method for the PHB and P(HBV) scaffolds. Their mechanical properties were acceptable for the intended application, there was interconnectivity between the pores and water uptake ability.



**Table 3.2.** Examples of emulsion templated scaffolds.

<b>Material/Method</b>	<b>Properties</b>	<b>Reference</b>
<b>P(HBV), emulsion templating with solvent evaporation</b>	<ul style="list-style-type: none"> <li>○ Pore size between 3 – 7 <math>\mu\text{m}</math></li> <li>○ Suitable for applications that require flexibility of the scaffold</li> <li>○ With surfactant</li> </ul>	Ruiz <i>et al.</i> (2011)
<b>GMA, emulsion templated</b>	<ul style="list-style-type: none"> <li>○ Addition of DMSO (toxic for cells)</li> <li>○ Excellent pore size and interconnectivity</li> <li>○ With surfactant</li> </ul>	Barbetta <i>et al.</i> (2005)
<b>PVA, CO<sub>2</sub>-in-water emulsion templating</b>	<ul style="list-style-type: none"> <li>○ Pore size between 5 – 21 <math>\mu\text{m}</math></li> <li>○ Surfactant free</li> </ul>	Luo <i>et al.</i> (2015)
<b>PHB, emulsion templating with solvent evaporation</b>	<ul style="list-style-type: none"> <li>○ Maximum porosity approximately 52 %</li> <li>○ With surfactant</li> </ul>	Bergstrand <i>et al.</i> (2012)
<b>PHB and P(HBV), emulsion templating with solvent evaporation</b>	<ul style="list-style-type: none"> <li>○ Pore size between 1 – 7 <math>\mu\text{m}</math></li> <li>○ Interconnectivity, water uptake ability, acceptable mechanical properties</li> <li>○ Surfactant free</li> </ul>	Esmail, (2019)

As mentioned, most emulsion templating techniques with the purpose of developing highly porous and interconnected scaffolds use surfactants to stabilize the emulsion system, which is inherently unstable due to the contacts formed between continuous and dispersed phases, composed of two immiscible liquids. These surfactants stabilize the emulsion through formation of a film in the interface between both phases, that surrounds the droplets of the internal phase, decreasing the interfacial tension and increasing the interfacial viscosity (Akbari & Nour, 2018). Some of the most widely used surfactants in emulsion templating for porous polymers are triblock copolymers (such as polyethyleneoxide (PEO) and polypropyleneoxide (PPO)), high hydrophile-lipophile balance (HLB) number surfactants such as Triton X-405 and sorbitan monooleate (commercial name – Span 80) (Kimmins & Cameron, 2011).

These surfactants are mainly synthetic and some of them have important disadvantages, carrying negative ambiental impacts, being non-biodegradable, with intrinsic toxicity and induction of irritant reactions on the human skin (Bouyer, Mekhloufi, Rosilio, Grossiord, & Agnely, 2012) Therefore, the introduction of natural molecules as surfactants for this purpose represents a significant breakthrough, especially for biomedical applications.

Polysaccharides are one example of natural molecules introduced as biosurfactants, taking advantage of emulsifying and stabilizing properties inherent to some of them. Carrier *et al.* (2011) suggested that the bacterial polysaccharide dextran could be used as a stabilizer in water-in-chloroform emulsion, by hydrophobic modification that enabled a good solubility in organic solvents, however the resulting emulsions suffered Ostwald ripening and coalescence of the droplets in the internal phase due to ageing process. Anarjan and Tan (2013) also studied the application of two polysaccharides, gum Arabic and xanthan gum, as emulsifiers for chloroform-in-water emulsions, revealing weaker physical and chemical stability when compared to other emulsifiers. More recently, López-Ortega *et al.* (2019) studied the emulsifying ability of a novel EPS produced by the haloarchaea *Haloferax mucosum* (DSM 27191) that has a protein content of 10 %, which revealed to be capable to stabilize water-in-chloroform emulsions as with other nonpolar solvents such as *n*-hexane.

The incorporation of FucoPol in the method of emulsion templating can be associated with an expected improvement of some parameters, such as the stability of the emulsion prepared, the consequent interconnectivity obtained and additionally with a possible improvement in cell proliferation upon culture. All of this is due to FucoPol ability to stabilize emulsions and also act as an emulsifier (Freitas *et al.*, 2013, 2011), with the added advantage of the biocompatibility and bioactivity (Concórdio-Reis *et al.*, 2020) properties of this EPS. So, in this perspective, FucoPol could act simultaneously as a surfactant in an emulsion templating method and as a blend for improvement of bioactivity of the resulting scaffold intended for tissue engineering.

### 3.1.3 Desired scaffold specifications

Scaffolds designed for tissue engineering and cell culture applications should correspond to some important characteristics, either biological, chemical, physical or mechanical.

Biocompatibility is an important feature that need to be present whenever a living organism is concerned. A biomaterial that, together with the cells, constitute whole or part of a living structure should not induce any undesirable toxic reactions to the surrounding tissues/cells, either the material itself or degradation products (Dutta *et al.*, 2017; Eltom *et al.*, 2019). Additionally, some cellular events can only occur if the surrounding environment is appropriate, such as cell growth, replication and differentiation. With most of synthetic biomaterials, these events are dependent on the addition of some naturally-derived molecules (e.g. RGD sequence, composed of arginine, glycine and aspartate) that hold the capability of signalling to trigger them (Dutta *et al.*, 2017).

Mechanical properties that match with the ECM of the tissue in question are a key parameter to be taken into account upon fabrication of the scaffold. These properties, such as mechanical strength, elasticity and stiffness, are related to the structure of the scaffold (porosity, interconnectivity, microstructure) as well as with the intrinsic material properties. Cells can have different behaviours depending on mechanical control mechanisms, for instance, in soft tissues the Young modulus (stiffness) falls between 0.4 and 350 MPa, being this the ideal range of values in scaffolds designed for soft tissue engineering/cell culture (Aldemir Dikici & Claeysens, 2020; Dutta *et al.*, 2017).

The arrangement of cells inside the scaffold and their interconnectivity with each other are dependent on the porosity and the interconnectivity between pores of the structure designed, allowing for cell mobility and communication, which in turn lead to the required cell density and physiological response associated (Dutta *et al.*, 2017; Duval *et al.*, 2017). Furthermore, the thickness of the scaffold is also crucial for exchange of gases, nutrients and production/degradation molecules. For this reason, approximately 200  $\mu\text{m}$  are considered to be appropriate for the thickness of the scaffold (Knight *et al.*, 2011).

## **3.2 Materials and Methods**

### **3.2.1 Scaffolds fabrication**

#### **3.2.1.1 Non-porous scaffolds**

Non-porous P(HBVHHx) (9.5 % (w/v)) scaffolds were prepared by dissolving the polymer in chloroform (Honeywell). The homogeneous solution was obtained by overnight oil bath, at 70 ° C, with continuous stirring. The solution was transferred into a 10 cm diameter Petri dish and placed in a desiccator on a fume hood, at room temperature, until complete solvent evaporation.

#### **3.2.1.2 Porous scaffolds by water emulsion**

P(HBVHHx) porous scaffolds were obtained by preparing emulsions with the chloroform solution and deionized water. To obtain the P(HBVHHx)-CHCl<sub>3</sub> solution, two methods were used: the same method described in 3.2.1.1. for some of the scaffolds and for the second method the polymer was dissolved and stirred using a heating plate. After cooling, 1 mL of deionized water was added to the solution and then shaken manually and with a magnetic stirrer until an emulsion formed, with no visible phase separation. The resulting emulsion was then transferred to 5 or 10 cm Petri dishes and left in the fume hood inside a desiccator, at room temperature, until complete solvent (water and chloroform) evaporation. The tested concentrations of the P(HBVHHx)-CHCl<sub>3</sub> solution were: 3.33 % (w/v), 5 % (w/v), 6.67 % (w/v) and 9.5 % (w/v).

#### **3.2.1.3 Porous scaffolds by aqueous FucoPol-solution emulsion**

P(HBVHHx)-FucoPol scaffolds were obtained using the same method described in 3.2.1.2., adding FucoPol dissolved in deionized water on the emulsion step. The concentration of P(HBVHHx) used was 6.7 % (w/v), 8 % (w/v) and 9.5 % (w/v) and for the FucoPol aqueous solution three concentrations were tested: 0.1 % (w/v), 0.5 % (w/v) and 1 % (w/v).

#### **3.2.1.4 Porous scaffolds by water emulsion and FucoPol coating**

To obtain P(HBVHHx)-water emulsion scaffolds the same method presented in 3.2.1.2. was performed. After complete solvent evaporation, the scaffolds obtained were coated with a FucoPol solution, prepared with deionized water at two concentrations: 1.5 % (w/v) and 2 % (w/v). To homogeneously coat the scaffolds, they were immersed in the FucoPol solution in a Schott, and placed in the autoclave for 20 minutes, at 120 ° C and 1 bar. After cooling, the scaffolds were transferred to Petri dishes and left in the fume hood at room temperature until complete solvent evaporation.

## 3.2.2 Scaffolds characterization

### 3.2.2.1 Morphology

Macroscopic characteristics such as color, texture and homogeneity were assessed. The thickness of the scaffolds was measured using a micrometer (Elcometer, England).

Scanning Electron Microscopy (SEM), to assess scaffolds structure, was performed in a bench scanning electron microscope (TM3030 Plus +Quantax 70, Hitachi, Japan) with an acceleration voltage of 15 kV. In order to prevent entrainment of the polymer structure, samples of the selected scaffolds were frozen with liquid nitrogen and broken to obtain smaller pieces with a representative cross section. For each sample, images of the surface, cross section and back (for some) of the scaffold were obtained. To analyse the images and obtain an estimate of the pore size, an image processing program (ImageJ) was used.

### 3.2.2.2 Thermal Properties and XRD

When applicable, the same methods described in 2.2.2.2. and 2.2.2.3. (Chapter Two), respectively, were performed.

### 3.2.2.3 Swelling in Water

Porous samples with 10 mm × 10 mm of the scaffolds were cut and immersed in 15 mL of deionized water at 30 ° C overnight. The weight and thickness of these samples were measured before and after immersion in order to assess the swelling. Three replicates of each sample were tested.

### 3.2.2.4 Porosity

Porosity was determined by two distinct methods. The first was a gravimetric method, by measuring the difference in density of a non-porous film and a porous scaffold. The densities of both were determined, with samples of the same dimensions, from a ratio of mass to volume. These values were used to calculate the porosity of the porous scaffolds, using equation (1) (Yadav, Pal, Nandan, & Srivastava, 2019).

$$P (\%) = \frac{(\rho_{NP} - \rho_P)}{\rho_{NP}} \times 100 \quad (1)$$

The second method was experimental, based on the occupied volume of a non-solvent of the polymer, after immersion. Porous samples with 10 mm × 10 mm of the scaffolds were cut and immersed in 15 mL of absolute ethanol (Fisher Chemical) during 5 min at room temperature. The weight and thickness of these samples were measured before and immediately after immersion for assessment of porosity (P), using the equation (2). Parameters used: ρ (density) of absolute ethanol (0.789 g/cm<sup>3</sup>), W<sub>1</sub> (weight of the scaffold before immersion), W<sub>2</sub> (weight of the scaffold after immersion), V (volume of the scaffold) (Kumar, Lakshmanan, Biswas, Nair, & Jayakumar, 2012).

$$P = \frac{W_2 - W_1}{\rho \times V} \quad (2)$$

### 3.2.2.5 Mechanical Properties

The P(HBVHHx) scaffolds were cut into rectangular-shaped test pieces (~50 × 15 mm). Tensile tests were performed using a texture analyser (Food Technology Corporation, England), operated with a tensile rate of 100 mm/min until break, using a load cell of 50 N, under ambient conditions, resulting in a stress-strain curve. Young Modulus (MPa) was determined as the initial slope of the curve, tensile strength (MPa) was taken at the highest point of the curve just before break and strain at break (%) as the ratio of the elongation of the test piece at rupture point by its initial length. For each P(HBVHHx) scaffold, four replicas were tested to obtain the determinations mentioned.

## 3.3 Results and Discussion

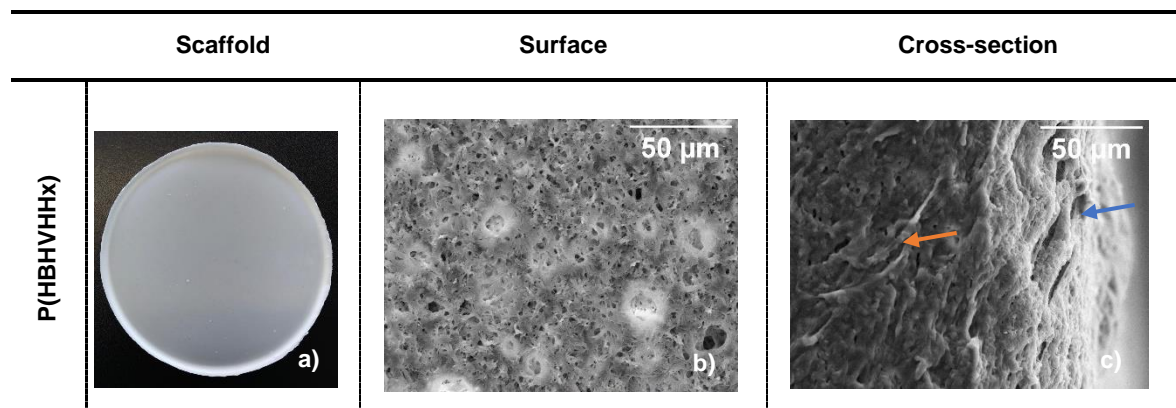
### 3.3.1 Non-porous film by solvent evaporation

To achieve non-porous film of this polymer, the solution-casting/solvent evaporation method was applied, allowing for the study of the behaviour and properties of the film.

#### 3.3.1.1 Morphology

The non-porous film obtained (Figure 3.1, a) was white, opaque and macroscopically homogeneous. Also, it had approximately 208  $\mu\text{m}$  of thickness and a flexible behaviour.

To further study the morphology, SEM analysis of the surface and cross-section of this P(HBHVHHx) film was performed, revealing a high surface roughness and some degree of porosity (Figure 3.1, b and c), which is consistent with other P(HBHVHHx) studies in the literature (Y. Ji *et al.*, 2008; L. Wang *et al.*, 2010). However, for the cross section, the film suffered entrainment on the surface that was cut, becoming more difficult to assess the morphology. Nonetheless, the surface roughness and irregularity can also be seen on the micrograph of the cross-section.



**Figure 3.1.** Non-porous scaffold images; Macroscopic (a); Surface (b) and cross-section (c) obtained by SEM analysis, with amplification of 1000x. Blue arrow indicates the surface roughness; Orange arrow pointing to entrainment of the cross section.

### 3.3.1.2 Thermal properties and XRD

The non-porous film was thermally and structurally studied in order to evaluate if the process of scaffold production affects the material properties (Table 3.3).

DSC analysis revealed two melting peaks for the non-porous film, a  $T_{m1}$  of 144 ° C and a  $T_{m2}$  of 159 ° C, with corresponding melting enthalpy of 1.9 J/g ( $\Delta H_{m1}$ ) and 5.8 J/g ( $\Delta H_{m2}$ ). The glass transition temperature for this film (-3.8 ° C) showed little decrease when compared with the raw polymer (-2.6 ° C). The thermal stability of the casted film suffered a slight decrease, as can be concluded by the decrease in the degradation temperature (260 ° C) when compared with the raw polymer (267 ° C). XRD analysis showed a degree of crystallinity for the processed polymer (25 %) similar to the raw polymer (26 %).

The melting behaviour of this terpolyester can be associated with a process of partial melting-lamellar thickening-remelting, due to chain sliding and reorganization before complete destruction of the crystal structure, which is also associated with a strong hydrogen bond between the monomers and neighbouring chains. This supports the appearance of the second melting peak and the decrease in the degradation temperature for the processed polymer into a thin film (Ye *et al.*, 2010). This process allows for the high thermal stability observed for this polymer. Additionally, the degree of crystallinity decreased very slightly, but not significantly (from 26 % to 25 %).

**Table 3.3.** Comparison of thermal properties and crystallinity between raw P(HBHVHHx) and the non-porous film produced with that polymer. (n.d – not detected)

P(HBHVHHx)	$\Delta H_{m1}$ (J/g)	$T_{m1}$ (° C)	$\Delta H_{m2}$ (J/g)	$T_{m2}$ (° C)	$T_g$ (° C)	$T_{deg}$ (° C)	$X_c$ (%)
Raw	4.3	145	n.d	n.d	-2.6	267	26
Non-porous film	1.9	144	5.8	159	-3.8	260	25



### 3.3.1.3 Mechanical properties

In tissue engineering and 3D cell cultures, the appropriate mechanical properties of the scaffolds employed are of paramount importance. In order to have a baseline for this terpolyester, a texture analyser was used to perform a tensile test on the non-porous film, determining parameters such as Young Modulus, tensile strength at break and elongation at break from the stress-strain curve obtained (Table 3.4).

The attained results show the singular mechanical properties of this terpolyester, with a Young Modulus of 0.8 MPa, a tensile strength of 5 MPa and a elongation at break of 237 %. These findings mean that the P(HBHVHHx) non-porous film needs 5 MPa of applied tension to break, after 237 % of elongation from the original length, resulting in an elastic modulus of 0.8 MPa, which reflects the elasticity of this polymer. When compared with the non-porous film of P(HBHVHHx) produced by Hu *et al.* (2009), the latter has a much higher Young Modulus, which can be associated with less elasticity of the polymer, due to the monomeric composition with low contents of 3HV (4 wt%) and 3HHx (13 wt%). Following this logic, the increase in 3HV and 3HHx content decreases the mechanical strength (decrease in tensile strength) and increases the flexibility of the resulting terpolymer, becoming more ductile (W. Zhao & Chen, 2007). This can be further supported by the comparison with the P(HBHVHHx) film (55 wt% of 3HB, 26 wt% of 3HV and 19 wt% of 3HHx) produced by Zhang *et al.* (2009), which reveals a decrease in Young Modulus (2 MPa) due to higher content of 3HV, but lower proportion of mcl-HA 3HHx impairs the elongation at break (133 %).

Additionally, according to Dikici *et al.* (2020) the Young modulus for soft tissues ranges between 0.4 and 350 MPa, which includes the value obtained in this work for the non-porous film.

**Table 3.4.** Comparison of mechanical properties between the non-porous film obtained in this work and others found in the literature.

Film Sample	Composition (wt%)			Young Modulus (MPa)	Tensile strength (MPa)	Elongation at break (%)	Reference
	3HB	3HV	3HHx				
P(HBHVHHx), non-porous	51	18	31	0.8	5	237	This study
P(HBHVHHx), non-porous	89	3	8	285	5	264	Hu <i>et al.</i> (2009)
P(HBHVHHx), non-porous	55	26	19	2	0.3	133	Zhang <i>et al.</i> (2009)

### 3.3.2 Porous scaffolds by water emulsion templating

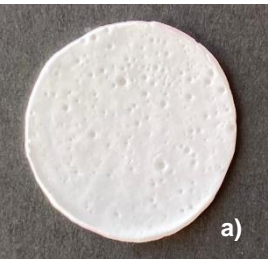
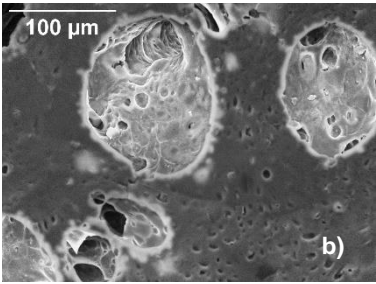
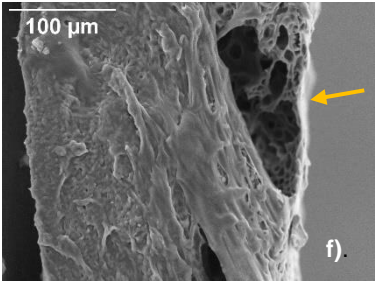
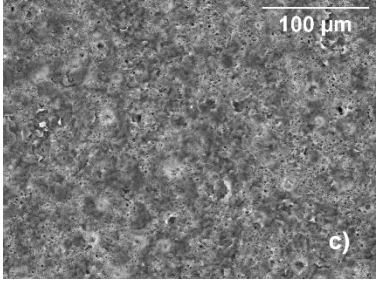
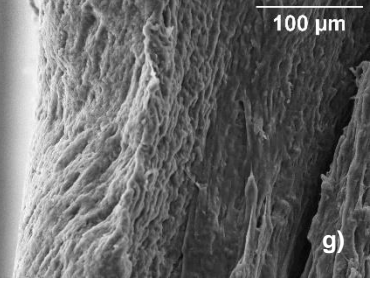
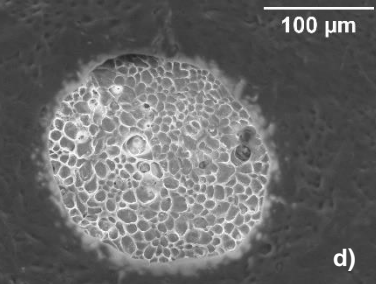
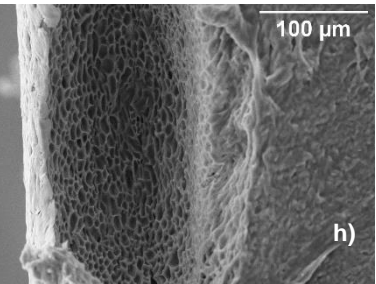
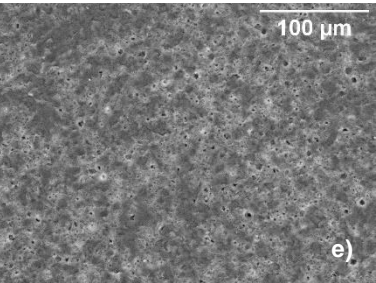
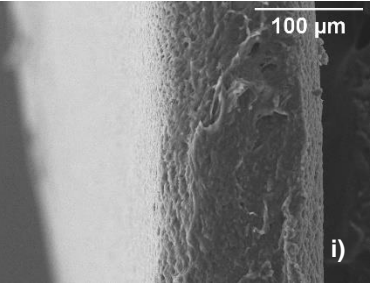
Porous scaffolds were achieved through the emulsion templating method, where the continuous phase had 9.5 % (w/v), 6.67 % (w/v), 5 % (w/v) and 3.33 % (w/v) of P(HBHVHHx) and the dispersed phase was composed of deionized water.

#### 3.3.2.1 Morphology

For the first concentration (9.5 % (w/v)), the scaffold obtained had 10 cm of diameter, approximately 241  $\mu\text{m}$  of thickness, was macroscopically compact and homogeneous, with some visible irregularities that later revealed to be macropores. Figure 3.2 a) illustrates a scaffold with 15 mm of diameter obtained from the original one (10 cm). Furthermore, the flexible behaviour observed for the non-porous film was maintained. The SEM analysis revealed macropores that were macroscopically perceptible with a diameter of approximately 100  $\mu\text{m}$ , and throughout the surface, there were micropores (Figure 3.2, b and f). Additionally, the pores seemed to be interconnected through tunnel-like structures. The cross-section was impaired by the entrainment of the polymer referred in the section 3.3.2.1. However, as depicted in Figure 3.2 f), there is an area of the cross-section (in another plane of the micrograph) that did not suffer entrainment, allowing to see the porous structure of the scaffold.

For lower polymer concentrations, the scaffolds showed no porous structure (6.67 % (w/v) and 3.33 % (w/v)) or presented a porous surface but with non-homogeneous cross-section (5 % (w/v)), as can be seen in Figure 3.2 (c – e, g – f). The SEM images of the surface of 6.67 % (w/v) and 3.33 % (w/v) scaffolds actually revealed a similar morphology to the non-porous film (Section 3.3.1.1, Figure 3.1). These findings can be related to the instability of the emulsion during the solvent evaporation process that took up to 72h. Additionally, the thickness of the scaffolds ranged from approximately 162 to 400  $\mu\text{m}$ , which could influence their properties, such as lower mechanical strength for the thinner one and impairment of the exchange of gases, nutrients and other degradation molecules for the thicker one.

The scaffold chosen to be further characterized was the one with 9.5 % (w/v) of P(HBHVHHx), due to morphologic features discussed above.

	Scaffold	Surface	Cross-section
P(HBVHHx) 9.5 % (w/v)	 a)	 b)	 f)
P(HBVHHx) 6.67 % (w/v)		 c)	 g)
P(HBVHHx) 5 % (w/v)		 d)	 h)
P(HBVHHx) 3.3 % (w/v)		 e)	 i)

**Figure 3.2.** Images of porous scaffold by water emulsion templating; Macroscopic (a); Surface (b,c,d and e) and cross-section (f,g,h and i) obtained by SEM analysis, with amplification of 500x. Yellow arrow indicates area of the cross-section that did not suffer entrainment.

### 3.3.2.2 Thermal properties and XRD

Similarly to the previous section, the structural and thermal properties of this porous scaffold were evaluated in order to assess if the different processing methods of the polymer would affect them (Table 3.5). DSC revealed two melting peaks, in accordance with the non-porous film, and their values ( $T_{m1}$  of 145 °C and  $T_{m2}$  of 160 °C) were very similar to the ones found for the non-porous ( $T_{m1}$  of 144 °C and  $T_{m2}$  of 159 °C). However, the melting enthalpy decreased for both  $\Delta H_{m1}$  (from 1.9 to 0.93 J/g) and  $\Delta H_{m2}$  (from 5.8 to 2.53 J/g) when compared to the non-porous film. Interestingly, the opposite occurred for the glass transition temperature (-12.7 °C), degradation temperature (274 °C) and degree of crystallinity (27 %), all showing an increase in their values. These findings can be related to the previously discussed process of partial melting-lamellar thickening-remelting that occurs upon heating of this terpolyester, with the addition of water-emulsion processing that possibly could affect the size and organization of the crystalline structure (Ye *et al.*, 2010). The  $T_g$ , however, suffered a considerable increase, which could be related to the fact that different equipment were used to determine this parameter: one for the raw sample and non-porous film of P(HBHVHHx), and other for the water emulsion templated scaffold (as described in section 2.2.2.4).

**Table 3.5.** Comparison of thermal properties and crystallinity between raw P(HBHVHHx), non-porous film and water emulsion templated porous scaffold produced with that polymer. (n.d – not detected)

P(HBHVHHx)	$\Delta H_{m1}$ (J/g)	$T_{m1}$ (° C)	$\Delta H_{m2}$ (J/g)	$T_{m2}$ (° C)	$T_g$ (° C)	$T_{deg}$ (° C)	$X_c$ (%)
Raw	4.3	145	n.d	n.d	-2.6	267	26
Non-porous	1.9	144	5.8	159	-3.8	260	25
Water emulsion templated	0.93	145	2.53	160	-12.7	274	27

### 3.3.2.3 Porosity

The gravimetical assessment of this porous scaffold, revealed a rather low percentual porosity of about 17 %. This value is drastically low when compared to the value obtained through the experimental method, which revealed a porosity of approximately 92 %. The results from both of these methods could have suffered from a high error, the first due to very low weight of the samples and the second due to the immediate weighting of the samples after immersion in ethanol, that could have resulted in weighting droplets of ethanol on the surface of the samples, increasing the porosity value. Therefore, this results are inconclusive and should be further validated/confirmed.

### 3.3.2.4 Swelling in water

Swelling in water determined for the water emulsion templated scaffold revealed a water uptake of approximately 14 %. This value shows that the porous scaffold has some capacity for swelling in water, however, the hydrophobic nature of P(HBHVHHx) does not allow for the higher water uptake observed in other scaffolds produced for 3D cell culture found in the literature and discussed below (section 3.3.3.4).

### 3.3.2.5 Mechanical properties

The water emulsion templated scaffold with 9.5 % (w/v) of P(HBHVHHx) was also subjected to mechanical characterization, evaluating the Young Modulus, tensile strength and elongation at break (Table 3.6). The interpretation of the stress-strain curve revealed a decrease in mechanical properties in general for the water emulsion templated porous scaffold, which reinforces the fact that polymer processing affects the final properties of the scaffolds. Upon comparison of the non-porous film and the water emulsion porous scaffold, the Young Modulus decreased from 0.8 to 0.6 MPa, the tensile strength also decreased from 5 to 3.6 MPa and the elongation at break suffered a steep decrease from 237 to 56 %. The most significant alteration, for the intended application of this scaffold, is the elongation at break, which reflects the loss of flexibility associated with the porous structure.

**Table 3.6.** Comparison of mechanical properties between the non-porous film and water emulsion templated porous scaffold obtained in this work.

Scaffold	Young Modulus (MPa)	Tensile strength (MPa)	Elongation at break (%)	Reference
P(HBHVHHx), non-porous	0.8	5	237	This study
P(HBHVHHx), porous by water emulsion	0.6	3.6	56	This study

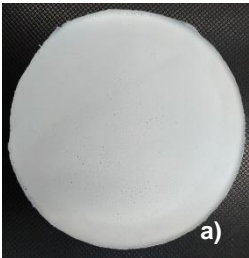
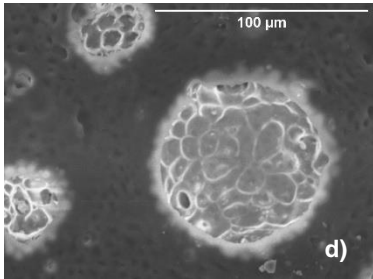
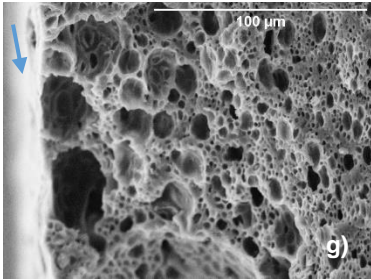
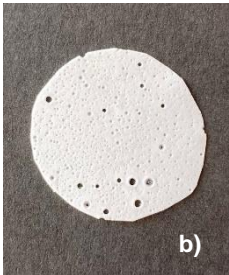
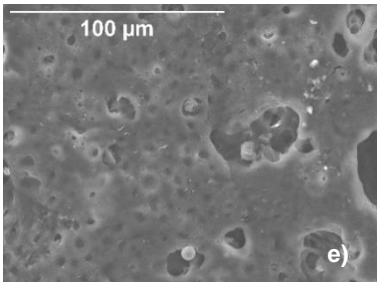
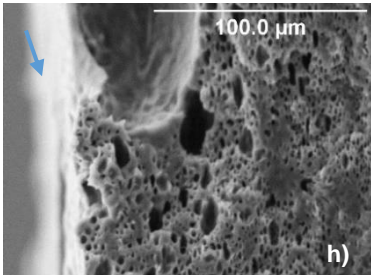

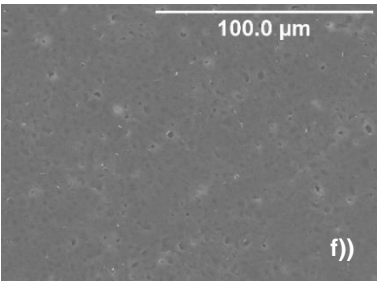
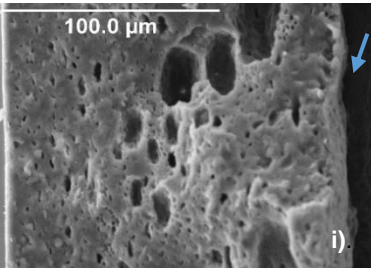
### 3.3.3 Porous scaffolds by FucoPol-water emulsion templating

For this method, porous scaffolds were achieved through the emulsion templating method. Three concentrations of the P(HBHVHHx) solution were tested (6.67, 8.0 and 9.5 % (w/v)), with 0.1 % (w/v) of the FucoPol solution, in order to determine which continuous phase concentration would result in a more stable emulsion. The three emulsions were left at room temperature for 72h and the emulsion that revealed to be more stable (less phase separation) was the one with 6.67 % (w/v) of P(HBHVHHx). Therefore, the porous scaffolds were developed through the emulsion templating method where the continuous phase had 6.67 % (w/v) of P(HBHVHHx) and several aqueous FucoPol solutions (0.1, 0.5 and 1 % (w/v)) were tested as the dispersed phase.

#### 3.3.3.1 Morphology

Macroscopically, the scaffolds presented distinct characteristics. For the lowest concentration of FucoPol (0.1 % (w/v)), the surface was compact, homogeneous, white and opaque, with the same flexibility observed earlier and thickness of approximately 159  $\mu\text{m}$ . The scaffold with 0.5 % (w/v) of FucoPol was much thinner (117  $\mu\text{m}$ ), presented macroscopically visible holes on the surface, revealing to be non-homogeneous, however the white colour and flexibility were maintained. With 1 % (w/v) of FucoPol, the scaffold had an intermediate thickness (145  $\mu\text{m}$ ), was compact, homogeneous, white and opaque, similarly maintaining the flexible behaviour (Figure 3.3; a, b and c). SEM analysis further supported the macroscopic findings. The scaffold with 0.1 % (w/v) of FucoPol presented a porous surface and cross-section, with some interconnected pores (Figure 3.3, d and g). However, the diameter of the pores was not homogeneous, decreasing in size along the thickness of the scaffold, which could also be related to the stability of the emulsion during the solvent evaporation step. The increase in concentration of FucoPol lead to an evident decrease in porosity and pore volume, depicted in the images of cross-section (Figure 3.3, h and i).

Furthermore, the viscosity and adhesive property of FucoPol seemed to influence the emulsion stability. This lead to a coalescence of the internal phase for a concentration of 0.5 % (w/v), resulting in macroscopic holes and bigger pores on the surface (Figure 3.3; b, e and h), and to an almost total loss of porosity on the surface for a concentration of 1 % (w/v) (Figure 3.3; f and i). Additionally, these images appeared to have a blurred effect on the limits of the pores, which could also be associated with the FucoPol. Nonetheless, the presence of FucoPol in this emulsion can be associated with an improvement on the porosity and interconnection of the pores when compared to the scaffolds produced by water emulsion, supporting the possibility of emulsion stabilization provided by this exopolysaccharide at low concentrations. The scaffold chosen to be further characterized was the one with 0.1 % (w/v) of FucoPol, due to morphologic features discussed above.

	Scaffold	Surface	Cross-section
P(HBHVHHx) – FucoPol 0.1 %			
P(HBHVHHx) – FucoPol 0.5 %			
P(HBHVHHx) – FucoPol 1 %			

**Figure 3.3.** Images of porous scaffold by FucoPol-water emulsion templating; Macroscopic (a,b,c); Surface (d,e,f) and cross-section (g,h,i) obtained by SEM analysis, with amplification of 1000x. Blue arrows indicate the surface of the scaffold.

### 3.3.3.2 Thermal properties and XRD

The porous scaffold produced by emulsion templating with 0.1 % (w/v) of FucoPol was structural and thermally characterized to assess possible processing influence on these properties (Table 3.7).

Thermal properties and degree of crystallinity of this scaffold revealed to be very similar to those found for the water emulsion templated one.  $T_{m1}$  (149 °C) and  $T_{m2}$  (162 °C) revealed a very slight increase, whereas  $\Delta H_{m1}$  (1.33 J/g) and  $\Delta H_{m2}$  (1.91 J/g) showed very little deviation in their values. Degree of crystallinity (26 %) was the same of the raw polymer and had a non-significant variation when compared with the other scaffolds. Both  $T_g$  (-10 °C) and  $T_{deg}$  (270 °C) presented lower values that again could be related with the thermal behaviour of this terpolyester upon processing. However, the decrease in  $T_g$  value compared to the one obtained for the water emulsion scaffold (-12.7 °C) could also be related to the thickness (159  $\mu\text{m}$ ) of this scaffold, revealing that  $T_g$  value decreases with the decrease in thickness of the sample analysed (Keddie, Jones, & Cory, 1994).

**Table 3.7.** Comparison of thermal properties and crystallinity between raw P(HBHVHHx), non-porous film, water emulsion templated and FucoPol-water emulsion templated porous scaffolds produced with that polymer. (n.d – not detected)

P(HBHVHHx)	$\Delta H_{m1}$ (J/g)	$T_{m1}$ (°C)	$\Delta H_{m2}$ (J/g)	$T_{m2}$ (°C)	$T_g$ (°C)	$T_{deg}$ (°C)	$X_c$ (%)
Raw	4.3	145	n.d.	n.d.	-2.6	267	26
Non-porous	1.9	144	5.8	159	-3.8	260	25
Water emulsion templated	0.93	145	2.53	160	-12.7	274	27
FucoPol 0.1 % (w/v) emulsion templated	1.33	149	1.91	162	-10	270	26



### 3.3.3.3 Porosity

For the FucoPol-water emulsion templated porous scaffold the gravimetric method resulted in a porosity of 24 % and the experimental method proved again to be discordant, with a porosity value of 94 %. When compared to the water emulsion templated scaffold (section 3.3.2.1), this one has demonstrated a superior porosity upon SEM analysis of the cross-sections. These findings are in agreement with the relative porosity found, being this value higher for the FucoPol-water emulsion templated scaffold with both methods used for this determination. Therefore, the incorporation of FucoPol in the aqueous phase of the emulsion resulted in an improvement of the porosity for this scaffold, when compared to the one without. However, this porosity and interconnection of the pores could be much improved. This could be done by increasing the viscosity of the continuous phase of the emulsion, or by increasing the volume of the internal phase (Aldemir Dikici & Claeysens, 2020), without compromising the mechanical properties achieved with these scaffolds and that will be further discussed below.

### 3.3.3.4 Swelling in water

The swelling in water of FucoPol-water emulsion templated scaffold (13 %) revealed to be similar to the water emulsion templated one (14 %). Despite the incorporation of the EPS in the P(HBVHx) porous scaffold composition, there were no significant changes in the water uptake capacity, although there were improvements in the morphology and mechanical properties.

As mentioned earlier, the capacity of water uptake attained for these emulsion templated scaffolds (with and without the incorporation of FucoPol) were lower than the values found in the literature for porous/fibrous scaffolds produced for skin tissue engineering. Bergstrand *et al.* (2012) reported up to 75 % of water uptake for emulsion templated PHB scaffolds with lithium sulphate in their composition. Lei *et al.* (2014) produced P(HBV)/SF (50:50 (w/w)) nanofibrous porous scaffolds that revealed a water uptake of approximately 42 %. These differences can be correlated to the porosity, interconnectivity of the pores and hydrophilicity of the different scaffold material and, additionally, the introduction of electrolytes can increase the water uptake capacity, as seen with the PHB/Li<sub>2</sub>SO<sub>4</sub> scaffolds.

### 3.3.3.5 Mechanical properties

FucoPol-water emulsion templated scaffold, with 0.1 % (w/v) of FucoPol solution, was subjected to mechanical test, revealing a stress-strain curve similar to the obtained for the water emulsion porous scaffold. The Young Modulus attained for this scaffold (0.85 MPa) was slightly higher than the values for the non-porous (0.8 MPa) and for the porous by water emulsion (0.6 MPa), which can correlate to a decrease in elasticity (52 % of elongation at break) but an increase in mechanical strength (tensile strength of 4.4 MPa), when compared to the porous by water emulsion. This is especially relevant considering that this scaffold was thinner (159  $\mu\text{m}$ ) and with a higher porosity as seen in the SEM micrographs depicted above. Therefore, the FucoPol incorporation in the P(HBHVHHx) scaffold can be associated with an improvement in mechanical strength. Furthermore, mechanical strength of the scaffold is a fundamental property when cell culture is intended, supporting the cell ingrowth, mobility and functionalization by maintaining the shape and microstructure of the scaffold (X. Wang *et al.*, 2012). Considering the tensile strength reported for native human dermis (1.03 to 3.10 MPa) (Gennisson *et al.*, 2004), the slightly higher value obtained for this scaffold possibly allow the support of the cell activities without contraction. When compared to other porous scaffolds produced through emulsion templating for tissue engineering applications found in the literature (Table 3.8), the Young Modulus obtained in this study (0.6 – 0.8 MPa) was lower than the one determined for fibrin and collagen/fibrin porous scaffolds (1 – 2 MPa) (Lim, Potter, Cui, & Dye, 2018), but higher than the values of silk fibroin porous scaffolds (0.23 – 0.36 MPa) (Wen, Yao, Chen, & Shao, 2018).

**Table 3.8.** Comparison of mechanical properties between the non-porous film, water emulsion templated and FucoPol-water emulsion templated porous scaffolds obtained in this work and others found in the literature; (n.a – data not available)

Scaffold	Young Modulus (MPa)	Tensile strength (MPa)	Elongation at break (%)	Reference
P(HBHVHHx), non-porous	0.8	5	237	This study
P(HBHVHHx), porous by water emulsion	0.6	3.6	56	This study
P(HBHVHHx)/FucoPol, porous by FucoPol-water emulsion	0.85	4.4	52	This study
Collagen/Fibrin, porous by oil-in-water emulsion	1 - 2	12 - 16	n.a	Lim <i>et al.</i> (2018)
Fibrin, porous by oil-in-water emulsion	1 - 2	4 - 5	n.a	
Silk fibroin, porous by oil-in-water emulsion/freezing	0.23 – 0.36	n.a	n.a	Wen <i>et al.</i> (2018)

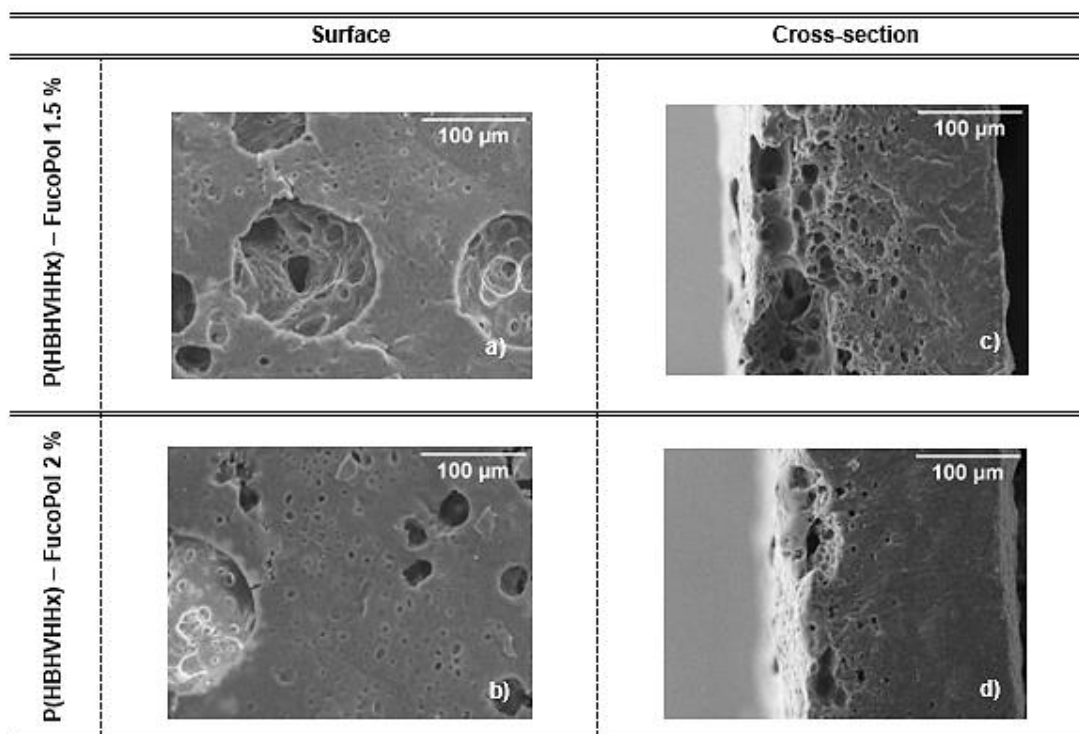


### 3.3.4 Porous scaffolds by water emulsion templating and FucoPol coating

The coating of the water-emulsion templated scaffolds (with 9.5 % (w/v) of P(HBHVHHx)) was tested for 1.5 and 2 % (w/v) of FucoPol solutions, in order to assess their morphology and later test their performance on cell culture with HDFn. The concentration of P(HBHVHHx) (9.5 % (w/v)) chosen for the water emulsion templated scaffold was based on the results discussed in section 3.3.2. The higher concentrations (1.5 and 2 % (w/v)) of the FucoPol solution were chosen in order to assess if an increase in FucoPol concentration would affect the cell response upon culturing, such as adherence, proliferation and differentiation.

#### 3.3.4.1 Morphology

Macroscopically, these scaffolds were compact, smooth, white, opaque and after solvent evaporation they adhered to the surface of the Petri dish, probably due to the adhesive properties of FucoPol. The flexibility decreased and the thickness increased slightly with the high concentration of FucoPol, the one with 1.5 % (w/v) had 253  $\mu\text{m}$  and the other with 2 % (w/v) had 256  $\mu\text{m}$ , being this relevant when compared to the water-emulsion templated scaffold (section 3.3.2.1), since it was the same scaffold that was used for these coatings.



**Figure 3.4.** Images of porous scaffolds by water emulsion templating and FucoPol coating; Surface (a, b) and cross-section (c, d) obtained by SEM analysis, with amplification of 500x.

The SEM analysis revealed that the superficial porosity was kept (Figure 3.4, a-b), although at a smaller degree. The cross-section showed that the porosity was present up to half the thickness of the scaffold for the 1.5 % (w/v) (Figure 3.4, c) and up to one third for the 2 % (w/v) (Figure 3.4, d) of FucoPol coating. These findings can be related to the high concentrations of FucoPol, considering that the same scaffold was used for both coatings, the reduction in porosity for the latter possibly is associated with the filling of the pores with FucoPol.

### 3.4 Conclusions

All the scaffolds obtained have in their composition P(HBHVHHx) as the main constituent of their structure. Deionized water was only used for emulsification with the polymer solution, being evaporated afterwards. Subsequently, FucoPol was dissolved in deionized water to form a more viscous solution for the emulsification with P(HBHVHHx), being this exopolysaccharide incorporated in the structure of the scaffold obtained after solvent evaporation. The method of coating the porous scaffold with a concentrated FucoPol solution resulted in the filling of the pores with this EPS, which could be advantageous for cell adherence but revealed to be detrimental for the porosity of the scaffold.

Overall, P(HBHVHHx) non-porous film showed very promising mechanical properties, such as Young Modulus, tensile strength and elongation at break with values of 0.8 MPa, 5 MPa and 237 %, respectively. The porous scaffolds, as would be expected, showed a steep reduction in elasticity (elongation at break of 56 % for the water emulsion scaffold and 52 % for the FucoPol-water emulsion templated scaffold), due to the introduction of porosity. However, the mechanical strength (tensile strength) and ductility (low Young Modulus) were kept at acceptable values for the intended application, especially the scaffold with 0.1% of FucoPol (4.4 and 0.85 MPa, respectively). Additionally, the high thermal stability of the polymer was maintained after polymer processing, as well as the pre-melting behaviour and crystallinity fraction, revealing that the processing of the polymer into porous scaffolds does not alter significantly the thermal and physical properties of the resulting structure. Moreover, the attained porosity and inferred low interconnectivity, due to insufficient water uptake capacity, of the porous scaffolds were sub-optimal. Nonetheless, both porous scaffolds were further studied in order to assess their bioactivity with HDFn.





**Chapter Four – Biopolymer-based scaffolds for reconstructed human dermis**

---



## 4.1 Introduction

Tissue engineering and 3D cell culturing for reconstitution of tissues require certain characteristics of the biomaterial chosen for the development of the construct. PHAs have increasingly gathered interest in this field due to their biodegradability, biocompatibility, non-cytotoxicity, tunable physico-chemical and mechanical properties, as well as reported bioactive functions. The natural occurrence of HA oligomers, such as 3HB, in the blood stream of humans and animals further improves the biocompatibility and non-cytotoxicity of these biopolyesters, making them promising candidates for biotechnological applications (Koller, 2018; Muneer *et al.*, 2020). Additionally, one of these PHAs achieved a major landmark in the medical field upon approval by Food and Drug Administration (FDA) of P(3HB) as a biomaterial for use in resorbable sutures (Grigore *et al.*, 2019). Another PHA terpolyester – P(HBHVHHx), has received attention in this field, due to its improved thermal stability, mechanical properties and biocompatibility (Hu *et al.*, 2009; Ye *et al.*, 2010). Moreover, this terpolyester has been associated to skin-tissue engineering, being a promising biomaterial to this application (Y. Ji *et al.*, 2008). Therefore, the application of P(HBHVHHx) porous scaffolds for reconstruction of human dermis seems to be a promising development for skin tissue engineering as well for 3D cell culturing *in vitro*.

### 4.1.1 Desired Dermal Construct Specifications

Upon seeding of HDFn on the scaffold intended for dermal reconstitution, a sequence of events normally occurs in order to achieve a viable dermis-analogue. This sequence of events starts with the seeding of the cells in a scaffold that had previously been embedded with HDFn medium, promoting the adhesion of these cells to the surface of the scaffold. Next, additional medium is supplied in order to immerse the construct, allowing the cells to receive the required nutrients and oxygen. The following expected steps recapitulate the order of events that would proceed in a neo-tissue formation scenario. If the biological, physical, chemical and mechanical properties of the scaffold are appropriate, along with the diffusion of nutrients to the cells, they should be able to proliferate and migrate throughout the structure, producing and organizing ECM components homogeneously, forming a viable neo-dermis (Ng, Khor, & Hutmacher, 2004).

## 4.2 Materials and Methods

### 4.2.1 Dermal Construct

#### 4.2.1.1 Fibroblasts Defrosting and Subculture

A cryovial of neonatal human dermal fibroblasts (HDFn) (Gibco™, #COO45C) with a volume of 1.5 mL and an average concentration of  $10^5$  cells/mL, was transferred from liquid nitrogen to a 37 ° C water bath. To neutralize the freezing solution containing dimethyl sulfoxide (DMSO) (SIGMA-ALDRICH, #D2650), 500 µL of warmed HDFn culture medium (IMDM, Glutamax™, Thermofisher, #31980030) 10 % Fetal Bovine Serum (FBS S, Life Technologies, #A3160802), 1 % PenStrep (Penicilin-Streptomycin, 10.000 U/mL, Gibco™, #15140-122) and 500 µL of cell suspension were added alternately to a 15 mL falcon, until all the cell suspension was in the falcon. This cell suspension was inoculated by distribution in a T-75 culture flask and incubated at 37 ° C with a 5 % CO<sub>2</sub>/95 % air, humidified cell culture incubator. The culture medium was changed once a week.

To perform a subculture, the T-75 flask was examined by microscopy in order to check for possible contaminations. Then the culture medium was discarded from the flask and 5 mL of PBS 1x was added, mixed and removed to wash the remnant of culture medium. 5 mL of trypsin-EDTA solution was added, rocked to ensure coverage of all the cells and incubated at 37 ° C for 2 min, optimizing the action of trypsin and releasing at least 90 % of the cells from the flask. To block the action of the trypsin, 10 mL of HDFn culture medium was added, transferring the resulting cell suspension to a 50 mL falcon. This suspension was then centrifuged (5 min, 2500 rpm), the supernatant discarded and the pellet resuspended with 400 µL of culture medium. To determine the concentration, 5 µL of the cell suspension were diluted in 95 µL of Tripan Blue and this dilution was used to count the cells in a haemocytometer. After this determination, the concentration was adjusted by diluting with cell culture medium, seeding a new culture vessel with a concentration of  $4.0 \times 10^3$  cells/cm<sup>2</sup> and incubating at 37 ° C with a 5 % CO<sub>2</sub>/95 % air atmosphere, humidified cell incubator.

#### 4.2.1.2 Cell Seeding and Dermal Construct

To perform the dermal constructs, porous P(HBHVHHx) scaffolds obtained by water emulsion, FucoPol-water emulsion/P(HBHVHHx) and P(HBHVHHx) porous by water emulsion/FucoPol coating were cut into circles with 15 mm in diameter, fitted in commercial inserts placed in a 6-well plate and sterilized under a 22-watt UV lamp for 15 min. To impregnate the scaffolds with cell culture medium each well was filled with 9 mL of IMDM and incubated at 37 ° C until needed.

After subculture and with a confluency of ~90 %, the cells (HDFn) are ready for seeding. The medium was discarded and the same procedure of subculture was performed until the cell counting. The final volume of the cell suspension was determined in order to allow for 100  $\mu$ L of this suspension for seeding each scaffold with a concentration of  $10 \times 10^6$  cells/mL. After seeding the scaffolds were incubated at 37 ° C with 5 % CO<sub>2</sub>/95 % air, in a humidified cell culture incubator for 1h and 30 min allowing for the cells to infiltrate through the thickness of the scaffold. 9 mL of IMDM supplemented with ascorbic acid (100  $\mu$ g/mL) were added to each well, submerging the scaffolds, and incubated for 8 days at 37 ° C with the same atmosphere mentioned earlier. The dermal culture medium (IMDM Glutamax, 10 % Fetal Bovine Serum (FBS), 1 % PenStrep, 0.01 % ascorbic acid) was changed every 48 h. For the fourteen-day long assay, the same procedure described above was performed.

## **4.2.2 Histological Processing**

### **4.2.2.1 Paraffin embedded sections**

The dermal constructs obtained from the eight-day assays were preserved with 10 % formalin for 24h and sent to IGC (*Instituto Gulbenkian de Ciênci*a) for histological processing. Each dermal construct was embedded in liquid paraffin, after the paraffin solidification the result are paraffin blocks that can be sectioned. From this sectioning (3  $\mu$ m of thickness) the histological slides were obtained. For better morphological evaluation, these slides were stained with haematoxylin and eosin, allowing microscopic observation.

### **4.2.2.2 Cryo-sections**

The dermal constructs obtained from the fourteen-day assays were preserved with 10 % formalin for 24h and immersed in a cryoprotective aqueous solution of 30 % sucrose before they were sent to IGC for histological processing. Each dermal construct was embedded in O.C.T.<sup>TM</sup> compound (Tissue Tek, Sakura), frozen in liquid nitrogen and sectioned (8  $\mu$ m of thickness). The slides obtained were stained with haematoxylin and eosin for morphological assessment.

## **4.2.3 Microscopic evaluation**

In order to assess the cells morphology in the dermal constructs, these histological slides were observed in a Zeiss Axio Imager 2.

## 4.3 Results and Discussion

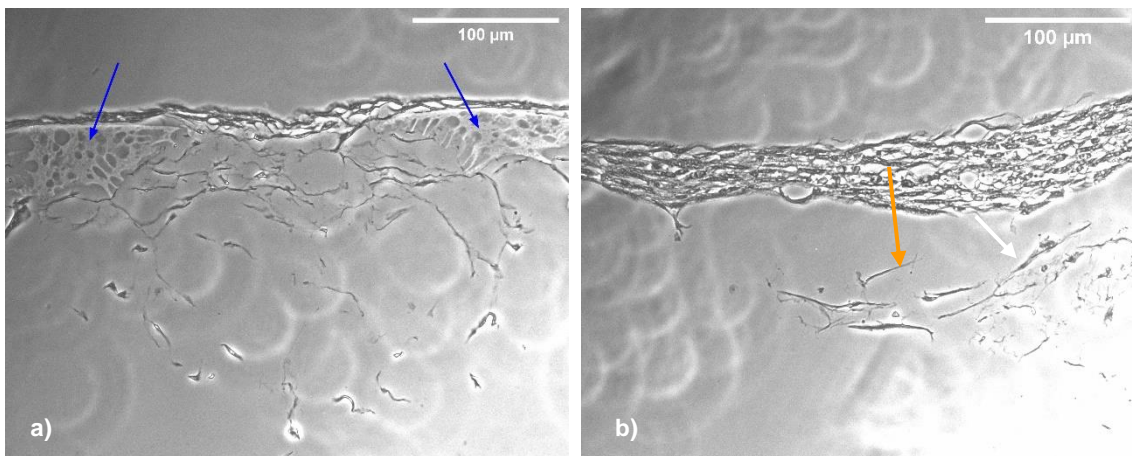
After sectioning and staining, the slides were microscopically assessed with a magnification of 400 $\times$ . The images are presented in a scale of greys due to the nature of the microscope used.

### 4.3.1 Eight-day assays

The fragmentation or detachment of the scaffold were a common finding throughout all the sections observed. This phenomena could be explained by the plasticization of the scaffold after the histological processing, that could be related to the utilization of xylene for prolonged intervals, since this aromatic hydrocarbon has been associated to this effect on other polymers (Stuart, 1997). The entrainment of this terpolymer has already been observed in this work when samples were cut for SEM analysis, therefore, this could have happened during sectioning with the microtome (slice thickness of 3  $\mu\text{m}$ ).

#### 4.3.1.1 Non-porous film and porous scaffold by water emulsion templating

The non-porous film, after histological processing, was not detectable in the slides. This may have happened due to difficulties in histological processing of samples, since the scaffold proved to be challenging to section, especially because in this assay the sections were made with only 3  $\mu\text{m}$  of thickness, as this was the normal protocol for similar samples in IGC.



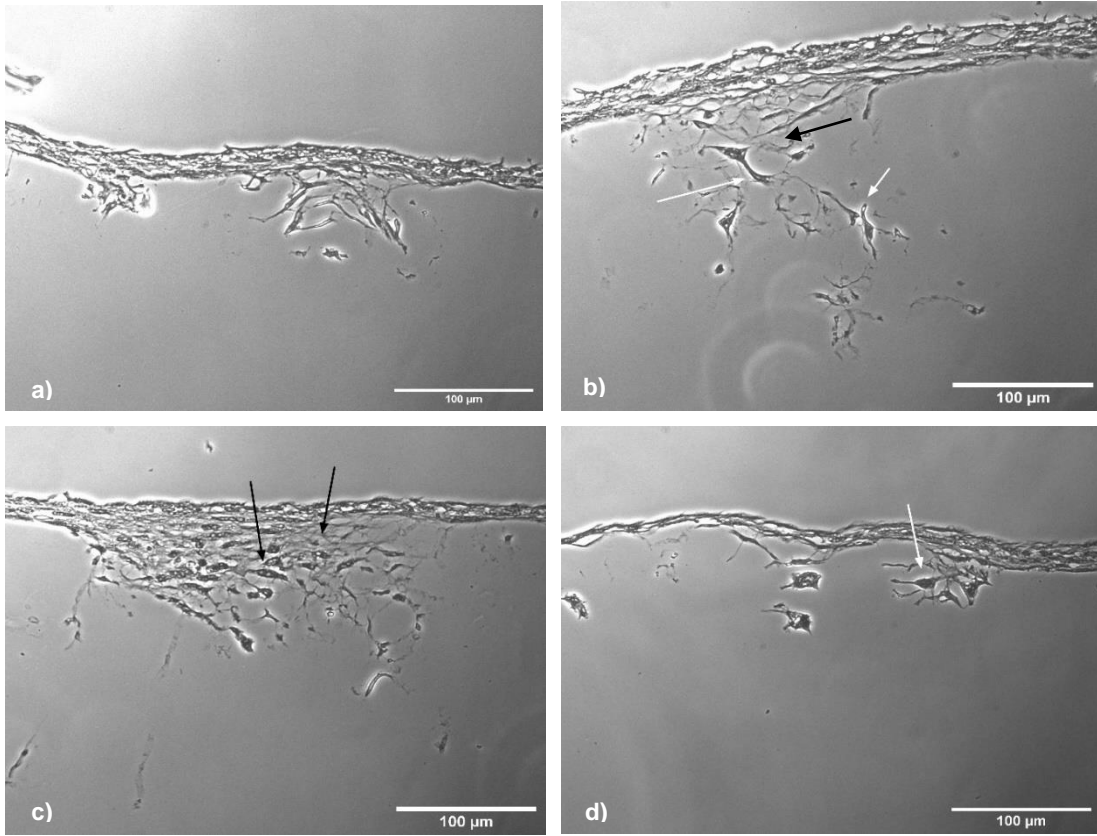
**Figure 4.1.** Microscopic images of the eight-day dermal constructs with porous scaffolds by water emulsion templating. Amplification of 400 $\times$ . Blue arrows indicate the scaffold. Orange arrow indicate interconnected pores. White arrow indicates spindle-like shape of fibroblasts.

For the porous water emulsified scaffold the sections were clearly visible, some of them showing pieces of the fragmented scaffold (Figure 4.1, a; blue arrows). Throughout all the sections a layer of fibroblasts (FBs) on the surface of the scaffold was observed, being thinner on areas where pores were available for infiltration (Figure 4.1, a). In some areas the presence of interconnected pores (Figure 4.1, b; orange arrows) could be inferred, since there was no connection between those cells in the middle of the section and the cells on the surface layer, meaning that they reached that area through interconnected pores. The morphology of the FBs after eight days of culture is consistent with an active and proliferating state of these cells. The flattened shape (spindle-like shape) with pseudopods extending lengthwise (Figure 4.1, b; white arrows), responsible for their motility and differentiation, is a characteristic response to microenvironmental cues such as ECM stiffness (H. Liu *et al.*, 2020).

#### 4.3.1.2 FucoPol-water emulsion templating porous scaffolds

For this dermal construct assay, the chosen concentrations of the FucoPol solution to produce the FucoPol-water emulsion templated scaffolds were 0.1 and 0.25 % (w/v). This choice was made considering that the best morphological features were observed for the first concentration, and the 0.25 % (w/v) was the chosen value between 0.1 and 0.5 % (w/v) in order to see if a slightly higher concentration would have positive effects on cell growth without compromising the structural and morphological aspects of the scaffold.

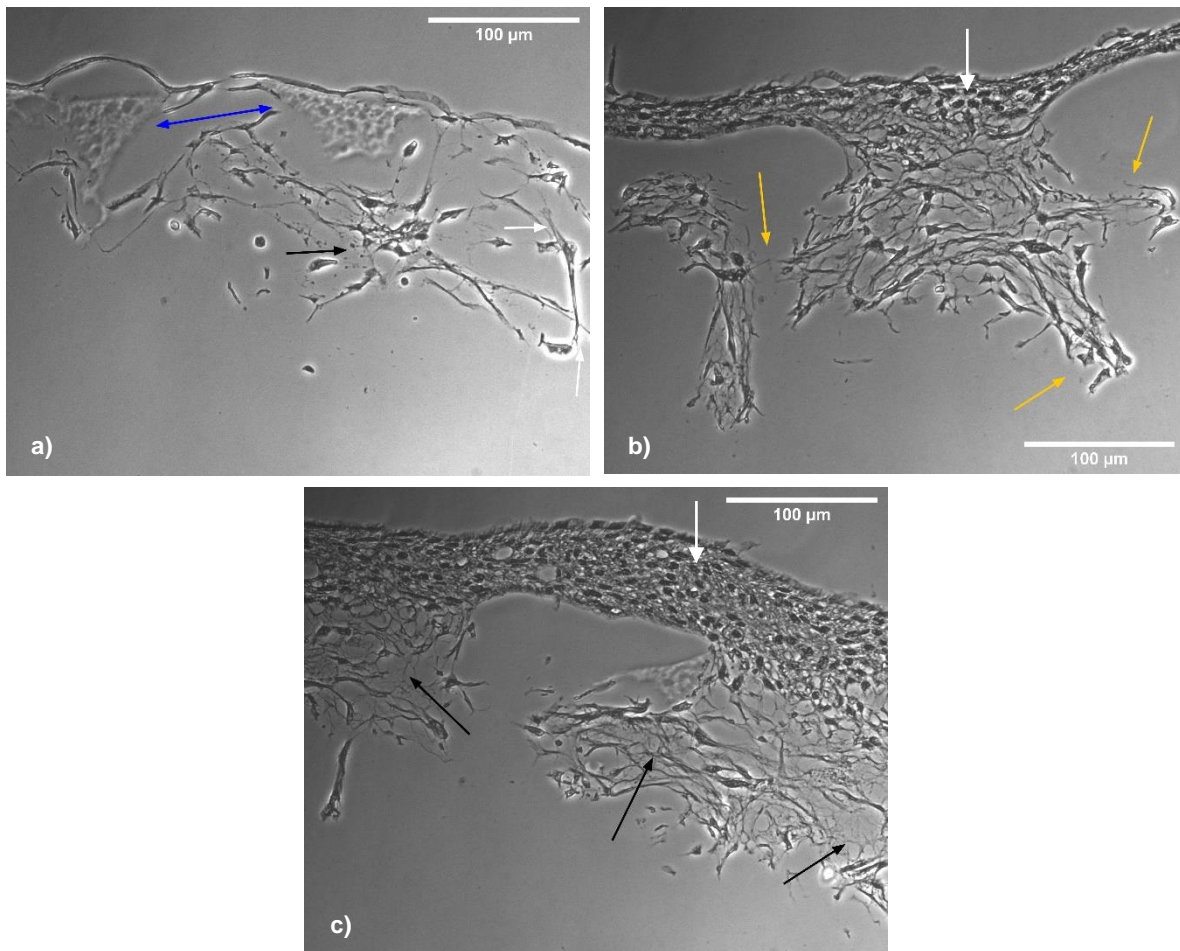
For both these scaffolds there were improvements in cell density within the available pores of the constructs (Figure 4.2), which could be associated to the presence of FucoPol. The spindle-like shape of FBs is again observed (Figure 4.2, white arrows), indicating that they were active and proliferating within this microenvironment. Additionally, for both concentrations, there were signs of possible ECM deposition by the proliferating FBs, as can be seen in images b) and c) of Figure 4.2 (black arrows). Throughout the sections observed the migration of FBs was scarce, due to low interconnectivity of the pores in these scaffolds.



**Figure 4.2.** Microscopic images of the eight-day dermal constructs with porous scaffolds by FucoPol-water emulsion templating; a), b) 0.1 % (w/v) of FucoPol; c), d) 0.25 % (w/v) of FucoPol. Amplification of 400x. White arrow indicates spindle-like shape of FBs. Black arrows indicate possible inclusions and/or ECM deposition.

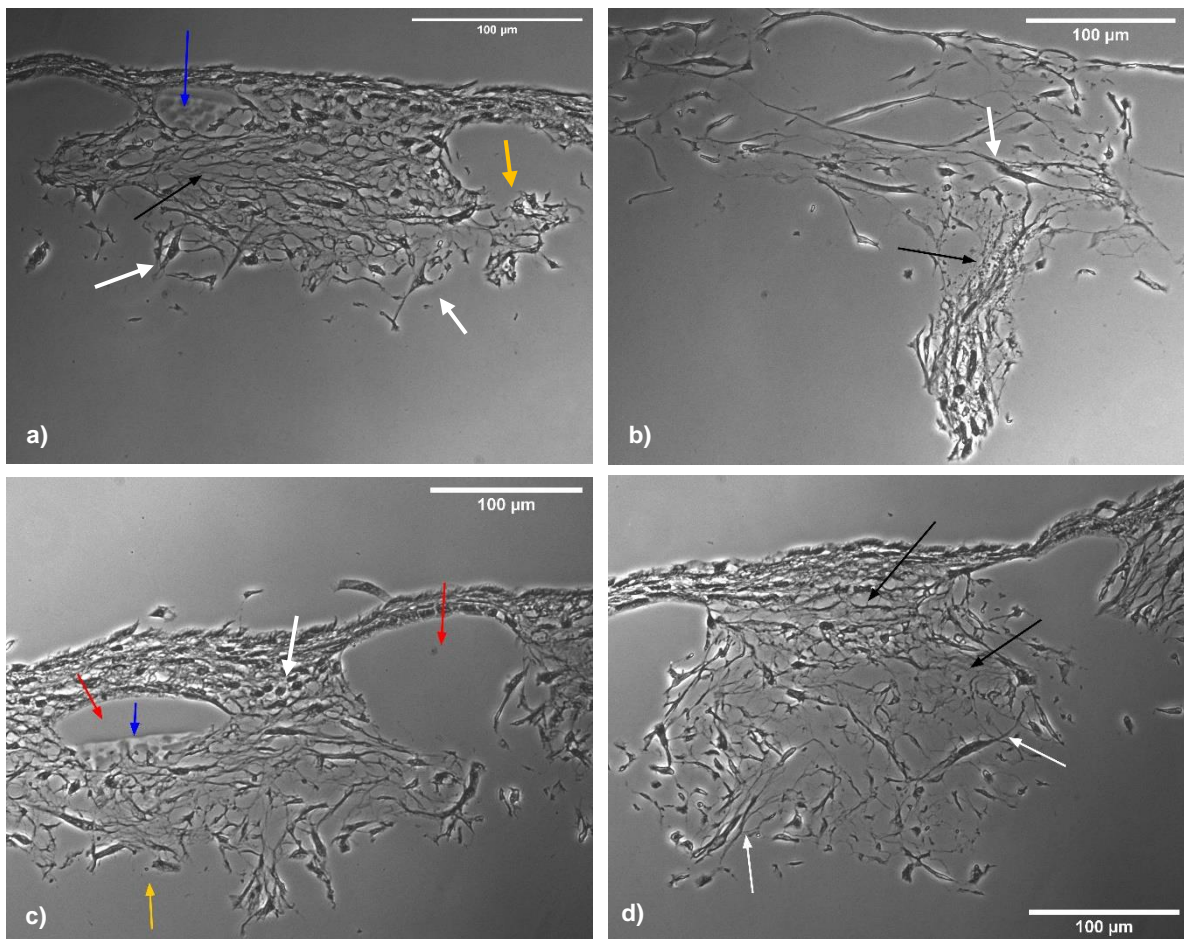
#### 4.3.1.3 FucoPol-coated water emulsion templated scaffolds

For this FucoPol coated (2 % (w/v)) scaffold the increment on cell density is clearly visible, especially in images b) and c) of Figure 4.3. The FBs were able to migrate through the available interconnected pores (Figure 4.3, b; orange arrows), their spindle-like shape (Figure 4.3; a, b and c; white arrows) is again present, so as the possibly ECM secretions (Figure 4.3; a, c; black arrows). The fragmented scaffold pieces can be seen in Figure 4.3, image a) (blue arrow). Despite the increased cell density, the lack of sufficient pores and interconnectivity of this scaffold impairs the FBs migration, leading to a layered accumulation of round-shaped FBs (Figure 4.3; b, c; vertical white arrows) on the surface of the scaffold.



**Figure 4.3.** Microscopic images of the eight-day dermal constructs with porous scaffolds by water emulsion templating with 2 % (w/v) FucoPol coating; Amplification of 400x. White arrow indicates spindle-like shape, or round shape FBs. Black arrows indicate possible inclusions and/or ECM deposition. Blue arrow shows fragmented scaffold. Orange arrow indicating interconnected pores.

Similarly, the cell density observed for the 1.5 % (w/v) FucoPol-coated porous scaffold (Figure 4.4; a,c and d) was greater than for the water emulsion templated, and even greater than the 2 % (w/v) FucoPol-coated construct. The possible ECM production and secretion by the active FBs can also be identified as filament-like and/or dotted, light-grey depositions (Figure 4.4; black arrows) between cells. Moreover, the extent of infiltration revealed to be superior, with more FB migration through the thickness of the scaffold (Figure 4.3). This also correlates with less round-shaped FBs on the surface and a prevalence of spindle-like FBs (Figure 4.4; white arrows), due to increased interconnected pores available (Figure 4.4; a, c; orange arrows), despite the presence of some visible closed pores (Figure 4.4; c; red arrows). These findings are consistent with the morphological features discussed previously (chapter two – section 3.3.4).



**Figure 4.4.** Microscopic images of the eight-day dermal constructs with porous scaffolds by water emulsion templating with 1.5 % (w/v) FucoPol coating; Amplification of 400x. White arrow indicates spindle-like shape, or round shape FBs. Black arrows indicate possible inclusions and/or ECM deposition. Blue arrow shows fragmented scaffold. Orange arrow indicate interconnected pores. Red arrows indicate non-interconnected pores.



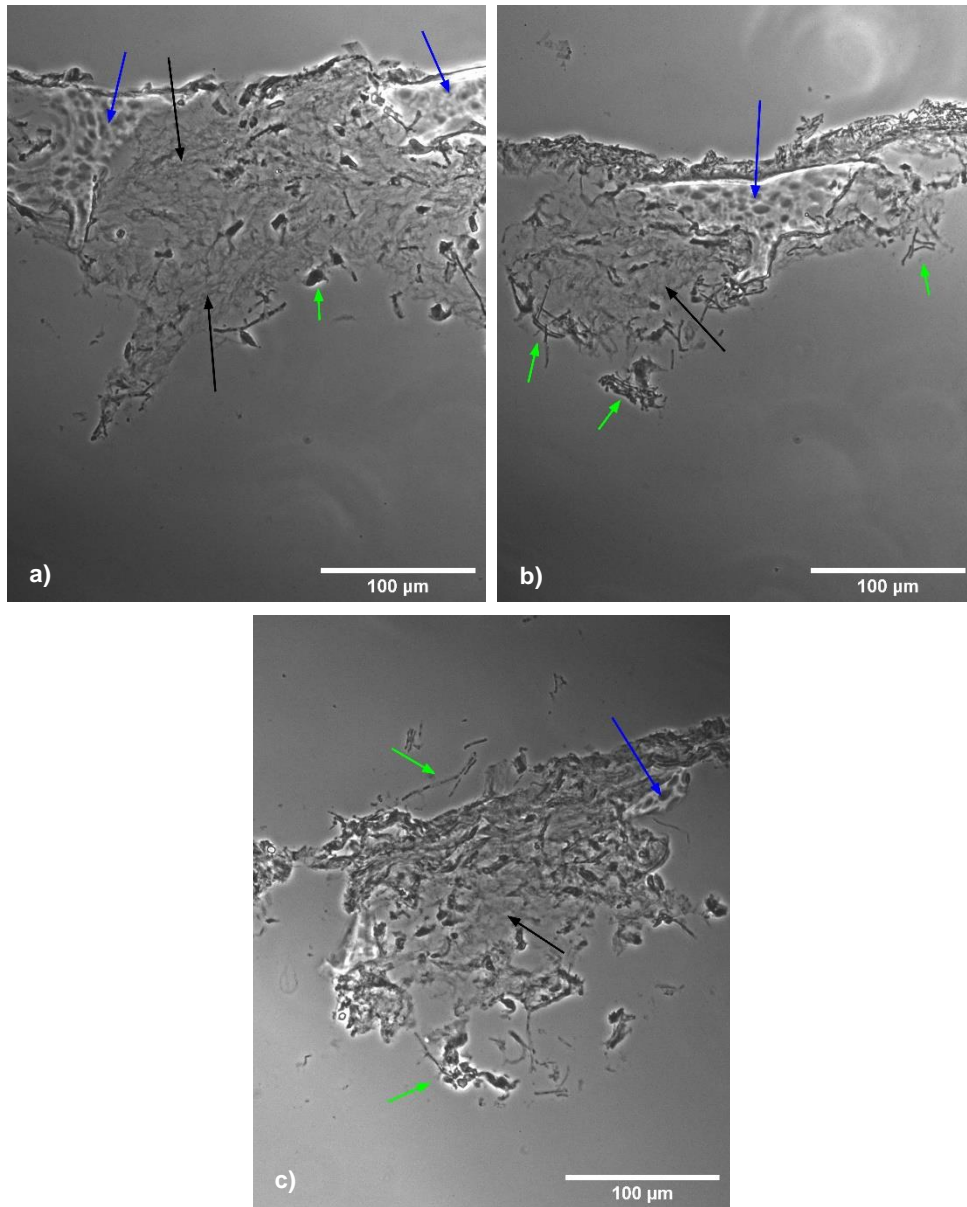
### 4.3.2 Fourteen-day assay

For this extended period of dermal construct assay, the histological processing protocol was changed in an attempt to surpass the difficulties observed with the latter protocol, namely the detachment and/or the fragmentation of the scaffold during sectioning of the embedded constructs. The sectioning was performed with a higher thickness (8  $\mu\text{m}$ ), which allowed for the observation of the whole construct (Figure 4.6; a,b; blue arrows), however, the fragmentation of the scaffold still occurred (Figure 4.5; blue arrows). Additionally, in spite of the cryoprotective sucrose solution in which the constructs were immersed, the liquid nitrogen affected the viability and consequently the morphology of the FBs, thereby cellular debris has been observed throughout all sections.

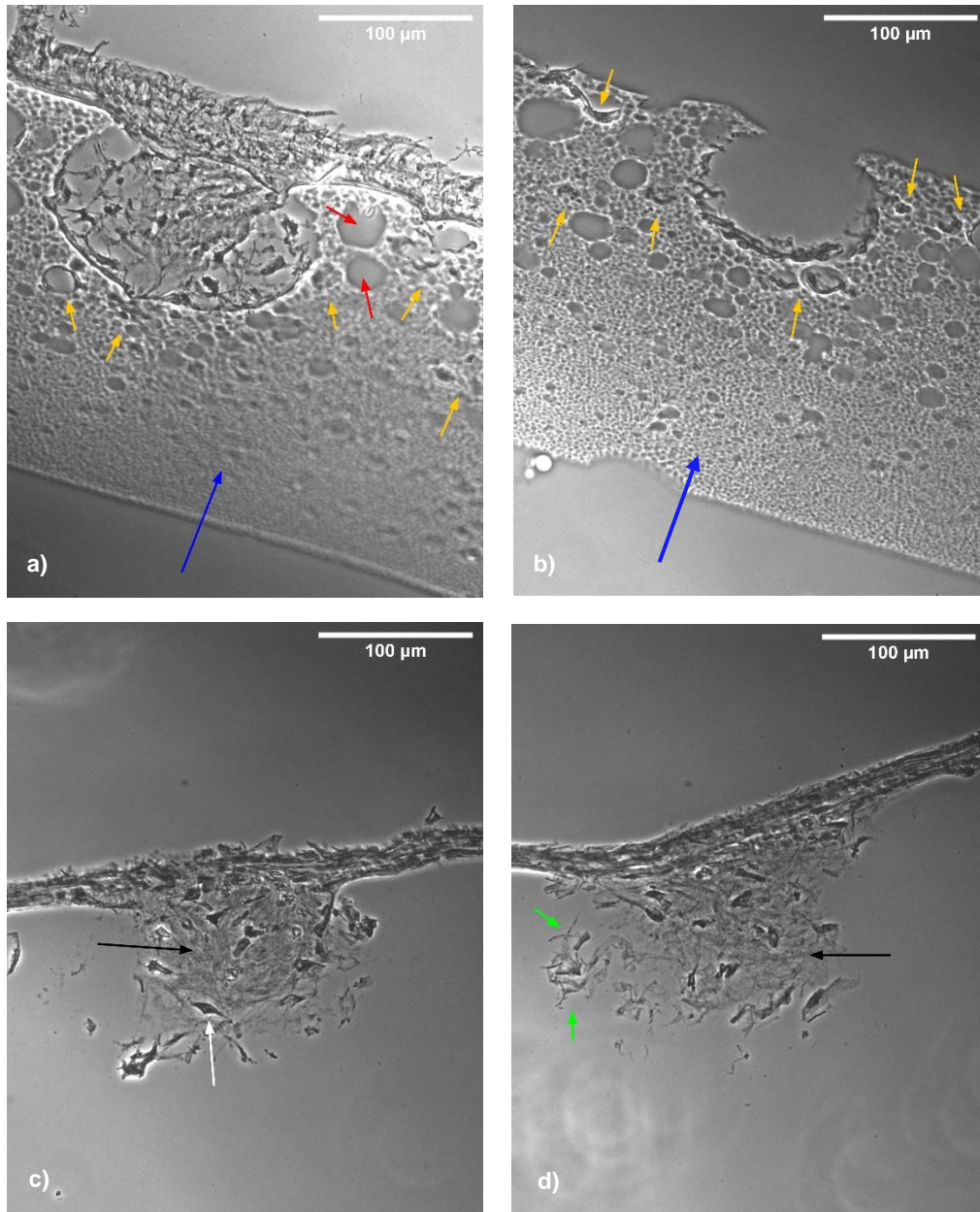
#### 4.3.2.1 Water emulsion templated and FucoPol-water emulsion templated porous scaffolds

The fourteen-day long dermal constructs obtained were processed with a different protocol, as mentioned above, resulting in distinct morphological aspects. The cell density observed in the sections (Figure 4.5 and 4.6) proved to be difficult to assess, due to the scattered cellular debris (Figure 4.5 and 4.6; green arrows) present in both scaffolds. However, in some areas the spindle-like shape of the FBs (Figure 4.6, c; white arrow) was still perceptible. This indicated that the cells were eventually active and proliferating during culture, in addition, there were visible depositions of expressed ECM components (Figure 4.5 and 4.6, black arrows) in all sections.

Both scaffolds still suffered fragmentation, which can be seen in Figure 4.5, images a) and b) (blue arrows). Nonetheless, the major finding in these sections can be seen in Figure 4.6, images a) and b) (blue arrows) and represents the whole cross-section of the construct. This indicates that the thickness (8  $\mu\text{m}$ ) chosen for this histological processing allowed for the preservation of the whole scaffold, at least in that section. Additionally, the observation of these sections showed that the detachment and fragmentation of the scaffold might have carried cells that were lodged inside (Figure 4.6, b; orange arrows). In these same sections there were some interconnected pores (Figure 4.6; a, b; orange arrows) that allowed the migration of the FBs through some extent of the scaffold thickness. However, the presence of closed pores (Figure 4.6; a, b; red arrows) - or with a small diameter - did not allow for the migration of cells across the entire scaffold.



**Figure 4.5.** Microscopic images of the fourteen-day dermal constructs with porous scaffolds by water emulsion templating. Amplification of 400x. Black arrows indicate possible inclusions and/or ECM deposition. Blue arrow shows fragmented scaffold. Green arrows indicate cellular debris.



**Figure 4.6.** Microscopic images of the fourteen-day dermal constructs with porous scaffolds by FucoPol-water emulsion templating (0.1 % (w/v) of FucoPol). Amplification of 400x. Black arrows indicate possible inclusions and/or ECM deposition. Blue arrow shows whole scaffold. Green arrows indicate cellular debris. Orange arrows indicate interconnected pores and cells lodged inside. Red arrows indicate non-interconnected pores.

## 4.4 Conclusions

Dermal construct assays were performed with HDFn in order to assess if the P(HBVHx) porous scaffolds would stimulate biological responses in these cells, promoting neo-dermis formation.

All porous scaffolds tested revealed FBs adherence and proliferation. The extent of proliferation and migration proved to be dependent on pore size and availability, as well as on their interconnectivity. The addition of increased FucoPol concentration improved the biological responses, especially the organized neo-tissue formation.

Therefore, the produced P(HBVHx) porous scaffolds have demonstrated to be suitable for dermis reconstitution, with an improvement seen on the scaffolds with incorporated FucoPol, proving not to be cytotoxic by allowing the adherence and proliferation of cells, with the limiting factor being the geometry of the pores that did not allow full invasion of the scaffold.





## **Chapter Five – Conclusions and Future Perspectives**

---

## 5.1 Conclusions and Future Perspectives

In this work, the P(HBHVHHx) extracted from a MMC biomass revealed to be composed of an interesting monomeric proportion when compared to similar terpolyesters in the literature. The characterization of this P(HBHVHHx) showed its high thermal stability and elastomeric potential, being a semi-crystalline scl-mcl-PHA. In addition, with the promising properties of FucoPol, namely emulsion stabilizing ability and biological activity, these biomaterials gathered the potential to produce a naturally-derived porous scaffold for skin tissue engineering.

A non-porous film of this terpolyester was produced, and its elastomeric nature was demonstrated, achieving very promising mechanical properties, with good mechanical strength and stiffness, but especially impressing elongation at break. The first approach to develop the porous scaffold, with water emulsion templating, revealed to be effective in introducing porosity to the otherwise densely packed structure of the non-porous film. This porosity decreased the elasticity of the scaffold, which was expected. Similarly, the FucoPol-water (0.1 % (w/v)) emulsion templated scaffold showed decreased elasticity, however, the achieved porosity was higher and the mechanical strength and stiffness were kept at adequate values for skin tissue engineering. Nevertheless, the coating method with high concentration of FucoPol revealed to be detrimental for the morphology of the scaffold, decreasing the porosity. Additionally, the porosity and interconnectivity obtained were not optimal, indicating that the emulsions were not stable for long enough, which could be addressed by various approaches, namely increasing the internal phase volume, increasing the viscosity of the external phase, accelerate the solvent evaporation period, or a combination of these. The increase in the porosity tends to impair the mechanical properties, therefore this adjustment should be well balanced.

The dermal constructs developed with these porous scaffolds demonstrated their suitability for skin tissue engineering, especially the culturing of FBs. All the scaffolds supported cell adherence and proliferation, with a clear improvement in cell density and organized deposition of ECM components for the scaffolds with FucoPol incorporated. However, the full invasion of the cells through the scaffold was limited by the pore geometry, which further supports the need to adjust the porosity and interconnectivity mentioned above. In addition, the biological response of the FBs is greatly influenced by microenvironmental cues within the scaffold, namely the scaffold stiffness, which revealed to be adequate in the scaffolds tested. Therefore, the improvement of the scaffold porosity should be performed without significantly impairing the mechanical properties. Besides the optimization of the emulsion method, another technique that could be studied with this combination of P(HBHVHHx)/FucoPol is electrospinning, with the possibility to improve or maintain the mechanical properties and achieve a higher porosity.

Upon achievement of a fully proliferated neo-dermis, immunohistochemical studies should be performed in order to evaluate the expression of ECM components, assessing if the results recapitulate the expression levels found in its natural counterpart. Additionally, tests that evaluate the matrix contraction over time should also be performed to ensure that the porous scaffold can effectively support the mechanical forces inherent to neo-dermis formation. Afterwards, human keratinocytes should be cultured on this neo-dermis at air-liquid interface, achieving a 3D human skin model.







## References



- Ahvenainen, P., Kontro, I., & Svedström, K. (2016). Comparison of sample crystallinity determination methods by X-ray diffraction for challenging cellulose I materials. *Cellulose*, 23(2), 1073–1086.
- Akbari, S., & Nour, A. H. (2018). Emulsion types, stability mechanisms and rheology: A review. *International Journal of Innovative Research and Scientific Studies*, 1(1), 14–21.
- Albuquerque, M. G. E., Torres, C. A. V., & Reis, M. A. M. (2010). Polyhydroxyalkanoate (PHA) production by a mixed microbial culture using sugar molasses: Effect of the influent substrate concentration on culture selection. *Water Research*, 44(11), 3419–3433.
- Aldemir Dikici, B., & Claeysens, F. (2020). Basic Principles of Emulsion Templating and Its Use as an Emerging Manufacturing Method of Tissue Engineering Scaffolds. *Frontiers in Bioengineering and Biotechnology*, 8(August).
- Ali, N., Hosseini, M., Vainio, S., Taïeb, A., Cario-André, M., & Rezvani, H. R. (2015). Skin equivalents: Skin from reconstructions as models to study skin development and diseases. *British Journal of Dermatology*, 173(2), 391–403.
- Aljuraifani, A. A., Berekaa, M. M., & Ghazwani, A. A. (2018). Bacterial biopolymer (polyhydroxyalkanoate) production from low-cost sustainable sources. *MicrobiologyOpen*, 8(6), 1–7.
- Ambekar, R. S., & Kandasubramanian, B. (2019). Progress in the Advancement of Porous Biopolymer Scaffold: Tissue Engineering Application. *Industrial and Engineering Chemistry Research*, 58(16), 6163–6194. review-article
- Anarjan, N., & Ping Tan, C. (2013). Physico-chemical stability of astaxanthin nanodispersions prepared with polysaccharides as stabilizing agents. *International Journal of Food Sciences and Nutrition*, 64(6), 744–748.
- Anjum, A., Zuber, M., Zia, K. M., Noreen, A., Anjum, M. N., & Tabasum, S. (2016). Microbial production of polyhydroxyalkanoates (PHAs) and its copolymers: A review of recent advancements. *International Journal of Biological Macromolecules*, 89, 161–174.
- Antoni, D., Burckel, H., Josset, E., & Noel, G. (2015). Three-dimensional cell culture: A breakthrough *in vivo*. *International Journal of Molecular Sciences*, 16(3), 5517–5527.
- Barbetta, A., Dentini, M., Zannoni, E. M., & De Stefano, M. E. (2005). Tailoring the porosity and morphology of gelatin-methacrylate polyHIPE scaffolds for tissue engineering applications. *Langmuir*, 21(26), 12333–12341.
- Bell, E., Ivarsson, B., & Merrill, C. (1979). Production of a tissue-like structure by contraction of collagen lattices by human fibroblasts of different proliferative potential *in vitro*. *Proceedings of the National Academy of Sciences of the United States of America*, 76(3), 1274–1278.
- Bergstrand, A., Andersson, H., Cramby, J., Sott, K., & Larsson, A. (2012). Preparation of Porous Poly(3-Hydroxybutyrate) Films by Water-Droplet Templating. *Journal of Biomaterials and Nanobiotechnology*, 03(04), 431–439.

- Bhubalan, K., Lee, W. H., Loo, C. Y., Yamamoto, T., Tsuge, T., Doi, Y., & Sudesh, K. (2008). Controlled biosynthesis and characterization of poly(3-hydroxybutyrate-co-3-hydroxyvalerate-co-3-hydroxyhexanoate) from mixtures of palm kernel oil and 3HV-precursors. *Polymer Degradation and Stability*, 93(1), 17–23.
- Bian, Y. Z., Wang, Y., Aibaidoula, G., Chen, G. Q., & Wu, Q. (2009). Evaluation of poly(3-hydroxybutyrate-co-3-hydroxyhexanoate) conduits for peripheral nerve regeneration. *Biomaterials*, 30(2), 217–225.
- Bouyer, E., Mekhloufi, G., Rosilio, V., Grossiord, J. L., & Agnely, F. (2012). Proteins, polysaccharides, and their complexes used as stabilizers for emulsions: Alternatives to synthetic surfactants in the pharmaceutical field? *International Journal of Pharmaceutics*, 436(1–2), 359–378.
- Carrier, O., Covis, R., Marie, E., & Durand, A. (2011). Inverse emulsions stabilized by a hydrophobically modified polysaccharide. *Carbohydrate Polymers*, 84(1), 599–604.
- Chai, Q., Jiao, Y., & Yu, X. (2017). Hydrogels for Biomedical Applications: Their Characteristics and the Mechanisms behind Them. *Gels*, 3(1), 6.
- Chandrasekaran, A. R., Venugopal, J., Sundarrajan, S., & Ramakrishna, S. (2011). Fabrication of a nanofibrous scaffold with improved bioactivity for culture of human dermal fibroblasts for skin regeneration. *Biomedical Materials*, 6(1).
- Chen, S., He, Z., Xu, G., & Xiao, X. (2016). Fabrication of nanofibrous tubular scaffolds for bone tissue engineering. *Materials Letters*, 182, 289–293.
- Concórdio-Reis, P., Pereira, C. V., Batista, M. P., Sevrin, C., Grandfils, C., Marques, A. C., Fortunato, E., Gaspar, F.B., Matias, A.A., Freitas, F., Reis, M. A. M. (2020). Silver nanocomposites based on the bacterial fucose-rich polysaccharide secreted by *Enterobacter* A47 for wound dressing applications: Synthesis, characterization and *in vitro* bioactivity. *International Journal of Biological Macromolecules*, 163, 959–969.
- Constantinides, C., Basnett, P., Lukasiewicz, B., Carnicer, R., Swider, E., Majid, Q. A., Srinivas, M., Carr, C., Roy, I. (2018). *In Vivo* Tracking and 1H/19F Magnetic Resonance Imaging of Biodegradable Polyhydroxyalkanoate/Polycaprolactone Blend Scaffolds Seeded with Labeled Cardiac Stem Cells. *ACS Applied Materials and Interfaces*, 10(30), 25056–25068.
- Cruickshank, C. N., Cooper, J. R., & Hooper, C. (1960). The cultivation of cells from adult epidermis. *The Journal of Investigative Dermatology*, 34(5), 339–342.
- Cruz, M. V., Freitas, F., Paiva, A., Mano, F., Dionísio, M., Ramos, A. M., & Reis, M. A. M. (2016). Valorization of fatty acids-containing wastes and byproducts into short- and medium-chain length polyhydroxyalkanoates. *New Biotechnology*, 33(1), 206–215.
- Degli Esposti, M., Chiellini, F., Bondioli, F., Morselli, D., & Fabbri, P. (2019). Highly porous PHB-based bioactive scaffolds for bone tissue engineering by *in situ* synthesis of hydroxyapatite. *Materials Science and Engineering C*, 100(February), 286–296.

- Derr, K., Zou, J., Luo, K., Song, M. J., Sittampalam, G. S., Zhou, C., Michael, S., Ferrer, M., Derr, P. (2019). Fully Three-Dimensional Bioprinted Skin Equivalent Constructs with Validated Morphology and Barrier Function. *Tissue Engineering - Part C: Methods*, 25(6), 334–343.
- Dufresne, A., Kellerhals, M. B., & Witholt, B. (1999). Transcrystallization in Mcl-PHAs/cellulose whiskers composites. *Macromolecules*, 32(22), 7396–7401.
- Dutta, R. C., Dey, M., Dutta, A. K., & Basu, B. (2017). Competent processing techniques for scaffolds in tissue engineering. *Biotechnology Advances*, 35(2), 240–250.
- Duval, K., Grover, H., Han, L. H., Mou, Y., Pegoraro, A. F., Fredberg, J., & Chen, Z. (2017). Modeling physiological events in 2D vs. 3D cell culture. *Physiology*, 32(4), 266–277.
- Elmowafy, E., Abdal-Hay, A., Skouras, A., Tiboni, M., Casettari, L., & Guarino, V. (2019). Polyhydroxyalkanoate (PHA): Applications in drug delivery and tissue engineering. *Expert Review of Medical Devices*, 16(6), 467–482.
- Eltom, A., Zhong, G., & Muhammad, A. (2019). Scaffold Techniques and Designs in Tissue Engineering Functions and Purposes: A Review. *Advances in Materials Science and Engineering*, 2019.
- Esmail, A. (2019). Biopolymeric substrates for reconstructed dermis development, (September).
- Ferreira, A. R. V., Torres, C. A. V., Freitas, F., Reis, M. A. M., Alves, V. D., & Coelho, I. M. (2014). Biodegradable films produced from the bacterial polysaccharide FucoPol. *International Journal of Biological Macromolecules*, 71, 111–116.
- Ferreira, A. R. V., Torres, C. A. V., Freitas, F., Sevrin, C., Grandfils, C., Reis, M. A. M., Alves, V. D., Coelho, I. M. (2016). Development and characterization of bilayer films of FucoPol and chitosan. *Carbohydrate Polymers*, 147, 8–15.
- Ferreira, S. S., Passos, C. P., Madureira, P., Vilanova, M., & Coimbra, M. A. (2015). Structure-function relationships of immunostimulatory polysaccharides: A review. *Carbohydrate Polymers*, 132, 378–396.
- Fontoura, J. C., Viezzer, C., dos Santos, F. G., Ligabue, R. A., Weinlich, R., Puga, R. D., Antonow, D., Severino, P., Bonorino, C. (2019). Comparison of 2D and 3D cell culture models for cell growth, gene expression and drug resistance. *Materials Science and Engineering C*, 107, 110264.
- Freitas, F., Alves, V. D., Gouveia, A. R., Pinheiro, C., Torres, C. A. V., Grandfils, C., & Reis, M. A. M. (2013). Controlled production of exopolysaccharides from *Enterobacter* A47 as a function of carbon source with demonstration of their film and emulsifying abilities. *Applied Biochemistry and Biotechnology*, 172(2), 641–657.
- Freitas, F., Alves, V. D., & Reis, M. A. M. (2011). Advances in bacterial exopolysaccharides: From production to biotechnological applications. *Trends in Biotechnology*, 29(8), 388–398.
- Freitas, F., Alves, V. D., Torres, C. A. V., Cruz, M., Sousa, I., Melo, M. J., Ramos, A.M., Reis, M. A.

- M. (2010). Fucose-containing exopolysaccharide produced by the newly isolated *Enterobacter* strain A47 DSM 23139. *Carbohydrate Polymers*, 83(1), 159–165.
- Gautam, S., Chou, C. F., Dinda, A. K., Potdar, P. D., & Mishra, N. C. (2014). Surface modification of nanofibrous polycaprolactone/gelatin composite scaffold by collagen type I grafting for skin tissue engineering. *Materials Science and Engineering C*, 34(1), 402–409.
- Gennisson, J. L., Baldeweck, T., Tanter, M., Catheline, S., Fink, M., Sandrin, L., Cornillon, C., Querleux, B. (2004). Assessment of elastic parameters of human skin using dynamic elastography. *IEEE Transactions on Ultrasonics, Ferroelectrics, and Frequency Control*, 51(8), 980–989.
- Grigore, M. E., Grigorescu, R. M., Iancu, L., Ion, R. M., Zaharia, C., & Andrei, E. R. (2019). Methods of synthesis, properties and biomedical applications of polyhydroxyalkanoates: a review. *Journal of Biomaterials Science, Polymer Edition*, 30(9), 695–712.
- Guerreiro, B. M., Freitas, F., Lima, J. C., Silva, J. C., Dionísio, M., & Reis, M. A. M. (2020). Demonstration of the cryoprotective properties of the fucose-containing polysaccharide FucoPol. *Carbohydrate Polymers*, 245(May), 116500.
- Haldar, S., Sharma, A., Gupta, S., Chauhan, S., Roy, P., & Lahiri, D. (2019). Bioengineered smart trilayer skin tissue substitute for efficient deep wound healing. *Materials Science and Engineering C*, 105(April), 110140.
- Han, F., Dong, Y., Su, Z., Yin, R., Song, A., & Li, S. (2014). Preparation, characteristics and assessment of a novel gelatin-chitosan sponge scaffold as skin tissue engineering material. *International Journal of Pharmaceutics*, 476(1), 124–133.
- Hoarau-Véchet, J., Rafii, A., Touboul, C., & Pasquier, J. (2018). Halfway between 2D and animal models: Are 3D cultures the ideal tool to study cancer-microenvironment interactions? *International Journal of Molecular Sciences*, 19(1).
- Hu, Y. J., Wei, X., Zhao, W., Liu, Y. S., & Chen, G. Q. (2009). Biocompatibility of poly(3-hydroxybutyrate-co-3-hydroxyvalerate-co-3-hydroxyhexanoate) with bone marrow mesenchymal stem cells. *Acta Biomaterialia*, 5(4), 1115–1125.
- Jensen, C., & Teng, Y. (2020). Is It Time to Start Transitioning From 2D to 3D Cell Culture? *Frontiers in Molecular Biosciences*, 7(March), 1–15.
- Ji, G. Z., Wei, X., & Chen, G. Q. (2009). Growth of human umbilical cord Wharton's jelly-derived mesenchymal stem cells on the terpolyester poly(3-hydroxybutyrate-co-3-hydroxyvalerate-co-3-hydroxyhexanoate). *Journal of Biomaterials Science, Polymer Edition*, 20(3), 325–339.
- Ji, Y., Li, X. T., & Chen, G. Q. (2008). Interactions between a poly(3-hydroxybutyrate-co-3-hydroxyvalerate-co-3-hydroxyhexanoate) terpolyester and human keratinocytes. *Biomaterials*, 29(28), 3807–3814.
- Keddie, J. L., Jones, R. A. L., & Cory, R. A. (1994). Size-dependent depression of the glass transition

- temperature in polymer films. *Epl*, 27(1), 59–64.
- Khan, T., Date, A., Chawda, H., & Patel, K. (2019). Polysaccharides as potential anticancer agents—A review of their progress. *Carbohydrate Polymers*, 210(January), 412–428.
- Khanna, S., & Srivastava, A. K. (2005). Recent advances in microbial polyhydroxyalkanoates. *Process Biochemistry*, 40(2), 607–619.
- Kimmins, S. D., & Cameron, N. R. (2011). Functional porous polymers by emulsion templating: Recent advances. *Advanced Functional Materials*, 21(2), 211–225.
- Kinikoglu, B. (2017). A Comparison of Scaffold-free and Scaffold-based Reconstructed Human Skin Models as Alternatives to Animal Use. *ATLA Alternatives to Laboratory Animals*, 45(6), 309–316.
- Knight, E., Murray, B., Carnachan, R., & Przyborski, S. (2011). Alvetex®: Polystyrene Scaffold Technology for Routine Three Dimensional Cell Culture. *3D Cell Culture: Methods and Protocols, Methods in Molecular Biology*, 695, 323–340.
- Knight, E., & Przyborski, S. (2014). Advances in 3D cell culture technologies enabling tissue-like structures to be created *in vitro*. *Journal of Anatomy*, 227(6), 746–756.
- Koller, M. (2018). Biodegradable and biocompatible polyhydroxy-alkanoates (PHA): Auspicious microbial macromolecules for pharmaceutical and therapeutic applications. *Molecules*, 23(2).
- Kumar, P. T. S., Lakshmanan, V. K., Biswas, R., Nair, S. V., & Jayakumar, R. (2012). Synthesis and biological evaluation of chitin hydrogel/nano ZnO composite bandage as antibacterial wound dressing. *Journal of Biomedical Nanotechnology*, 8(6), 891–900.
- Langhans, S. A. (2018). Three-dimensional *in vitro* cell culture models in drug discovery and drug repositioning. *Frontiers in Pharmacology*, 9(JAN), 1–14.
- Lanigan, S. ., & Zaidi, Z. (2010). Dermatology in Clinical Practice. In *Dermatology in Clinical Practice* (pp. 1–15).
- Lee, S. Y. (1995). Review Bacterial Polyhydroxyalkanoates. *Biotechnology and Bioengineering*, 49, 1–14.
- Lei, C., Zhu, H., Li, J., Feng, X., & Chen, J. (2014). Preparation and Characterization of Polyhydroxybutyrate-co-hydroxyvalerate/Silk Fibroin Nanofibrous Scaffolds for Skin Tissue Engineering. *Polymer Engineering and Science*, 908–916.
- Lemoigne, M. (1926). Products of dehydration and of polymerization of  $\beta$ -hydroxybutyric acid. *Bull Soc Chem Biol*, 8, 770–782.
- Levine, A. C., Heberlig, G. W., & Nomura, C. T. (2016). Use of thiol-ene click chemistry to modify mechanical and thermal properties of polyhydroxyalkanoates (PHAs). *International Journal of Biological Macromolecules*, 83, 358–365.
- Liang, Y. S., Zhao, W., & Chen, G. Q. (2008). Study on the biocompatibility of novel terpolyester poly(3-hydroxybutyrate-co-3-hydroxyvalerate-co-3-hydroxyhexanoate). *Journal of Biomedical*

*Materials Research - Part A*, 87(2), 441–449.

- Lim, X., Potter, M., Cui, Z., & Dye, J. F. (2018). Manufacture and characterisation of EmDerm—novel hierarchically structured bio-active scaffolds for tissue regeneration. *Journal of Materials Science: Materials in Medicine*, 29(6).
- Liu, H., Wu, M., Jia, Y., Niu, L., Huang, G., & Xu, F. (2020). Control of fibroblast shape in sequentially formed 3D hybrid hydrogels regulates cellular responses to microenvironmental cues. *NPG Asia Materials*, 12(1).
- Liu, Q., Tian, S., Zhao, C., Chen, X., Lei, I., Wang, Z., & Ma, P. X. (2015). Porous nanofibrous poly(l-lactic acid) scaffolds supporting cardiovascular progenitor cells for cardiac tissue engineering. *Acta Biomaterialia*, 26, 105–114.
- López-Ortega, M. A., Rodríguez-Hernández, A. I., Camacho-Ruiz, R. M., Córdova, J., López-Cuellar, M. del R., Chavarría-Hernández, N., & González-García, Y. (2019). Physicochemical characterization and emulsifying properties of a novel exopolysaccharide produced by haloarchaeon *Haloferax mucosum*. *International Journal of Biological Macromolecules*, 142, 152–162.
- Lou, T., Leung, M., Wang, X., Chang, J. Y. F., Tsao, C. T., Sham, J. G. C., Edmonson, D., Zhang, M. (2014). Bi-layer scaffold of chitosan/PCL-nanofibrous mat and PLLA-microporous disc for skin tissue engineering. *Journal of Biomedical Nanotechnology*, 10(6), 1105–1113.
- Lu, B., Wang, T., Li, Z., Dai, F., Lv, L., Tang, F., Yu, K., Liu, J., Lan, G. (2016). Healing of skin wounds with a chitosan-gelatin sponge loaded with tannins and platelet-rich plasma. *International Journal of Biological Macromolecules*, 82, 884–891.
- Luo, W., Zhang, S., Li, P., Xu, R., Zhang, Y., Liang, L., Wood, C.D., Lu, Q., Tan, B. (2015). Surfactant-free CO<sub>2</sub>-in-water emulsion-templated poly (vinyl alcohol) (PVA) hydrogels. *Polymer*, 61, 183–191.
- Matsumine, H., Fujimaki, H., Takagi, M., Mori, S., Iwata, T., Shimizu, M., & Takeuchi, M. (2019). Full-thickness skin reconstruction with basic fibroblast growth factor-impregnated collagen-gelatin sponge. *Regenerative Therapy*, 11, 81–87.
- Medawar, P. B. (1948). The cultivation of adult mammalian skin epithelium *in vitro*. *The Quarterly Journal of Microscopical Science*, 89(6), 187–196.
- Moulin, V., Castilloux, G., Jean, A., Garrel, D. R., Auger, F. A., & Germain, L. (1996). *In vitro* models to study wound healing fibroblasts. *Burns*, 22(5), 359–362.
- Muneer, F., Rasul, I., Azeem, F., Siddique, M. H., Zubair, M., & Nadeem, H. (2020). Microbial Polyhydroxyalkanoates (PHAs): Efficient Replacement of Synthetic Polymers. *Journal of Polymers and the Environment*, 28(9), 2301–2323.
- Neumann, A. J., Quinn, T., & Bryant, S. J. (2016). Nondestructive evaluation of a new hydrolytically degradable and photo-clickable PEG hydrogel for cartilage tissue engineering. *Acta*



- Biomaterialia*, 39, 1–11.
- Ng, K. W., Khor, H. L., & Hutmacher, D. W. (2004). *In vitro* characterization of natural and synthetic dermal matrices cultured with human dermal fibroblasts. *Biomaterials*, 25(14), 2807–2818.
- Niehues, H., Bouwstra, J. A., El Ghalbzouri, A., Brandner, J. M., Zeeuwen, P. L. J. M., & van den Bogaard, E. H. (2018). 3D skin models for 3R research: The potential of 3D reconstructed skin models to study skin barrier function. *Experimental Dermatology*, 27(5), 501–511.
- Nikolova, M. P., & Chavali, M. S. (2019). Recent advances in biomaterials for 3D scaffolds: A review. *Bioactive Materials*, 4(August), 271–292.
- Pellevoisin, C., Videau, C., Briotet, D., Grégoire, C., Tornier, C., Alonso, A., Rigaudeau, A.S., Bouez, C., Seyler, N. (2018). SkinEthic™ RHE for *in vitro* evaluation of skin irritation of medical device extracts. *Toxicology in Vitro*, 50(January), 418–425.
- Pereira, J. R., Araújo, D., Marques, A. C., Neves, L. A., Grandfils, C., Sevrin, C., Alves, V.D., Fortunato, E., Reis, M.A.M., Freitas, F. (2019). Demonstration of the adhesive properties of the medium-chain-length polyhydroxyalkanoate produced by *Pseudomonas chlororaphis* subsp. *aurantiaca* from glycerol. *International Journal of Biological Macromolecules*, 122, 1144–1151.
- Péterszegi, G., Fodil-Bourahla, I., Robert, A. M., & Robert, L. (2003). Pharmacological properties of fucose. Applications in age-related modifications of connective tissues. *Biomedicine and Pharmacotherapy*, 57(5–6), 240–245.
- Polonchuk, L., Chabria, M., Badi, L., Hoflack, J. C., Figtree, G., Davies, M. J., & Gentile, C. (2017). Cardiac spheroids as promising *in vitro* models to study the human heart microenvironment. *Scientific Reports*, 7, 1–12.
- R. Hokmabad, V., Davaran, S., Ramazani, A., & Salehi, R. (2017). Design and fabrication of porous biodegradable scaffolds: a strategy for tissue engineering. *Journal of Biomaterials Science, Polymer Edition*, 28(16), 1797–1825.
- Rai, R., Keshavarz, T., Roether, J. A., Boccaccini, A. R., & Roy, I. (2011). Medium chain length polyhydroxyalkanoates, promising new biomedical materials for the future. *Materials Science and Engineering R: Reports*, 72(3), 29–47.
- Randall, M. J., Jüngel, A., Rimann, M., & Wuertz-Kozak, K. (2018a). Advances in the biofabrication of 3D skin *in vitro*: Healthy and pathological models. *Frontiers in Bioengineering and Biotechnology*, 6(154).
- Remya, K. R., Chandran, S., Mani, S., John, A., & Ramesh, P. (2018). Hybrid Polycaprolactone/Polyethylene oxide scaffolds with tunable fiber surface morphology, improved hydrophilicity and biodegradability for bone tissue engineering applications. *Journal of Biomaterials Science, Polymer Edition*, 29(12), 1444–1462.
- Rheinwald, J. G., & Green, H. (1975). Serial Cultivation of Strains of Human Epidermal Keratinocytes: the Formation of Keratinizing Colonies from Single Cells. *Cell*, 6(3), 331–343.

- Rodriguez-Contreras, A. (2019). Recent Advances in the Use of Polyhydroxyalkanoates in Biomedicine. *Bioengineering*, 6(82), 1–14.
- Ruiz, I., Hermida, É. B., & Baldessari, A. (2011). Fabrication and characterization of porous PHBV scaffolds for tissue engineering. *Journal of Physics: Conference Series*, 332(1), 1–10.
- Santos, A. R., Ferreira, B. M. P., Duek, E. A. R., Dolder, H., Wada, R. S., & Wada, M. L. F. (2004). Differentiation Pattern of Vero Cells Cultured on Poly(L-Lactic Acid)/Poly(Hydroxybutyrate-co-Hydroxyvalerate) Blends. *Artificial Organs*, 28(4), 381–389.
- Sedlacek, P., Slaninova, E., Koller, M., Nebesarova, J., Marova, I., Krzyzanek, V., & Obruca, S. (2018). PHA granules help bacterial cells to preserve cell integrity when exposed to sudden osmotic imbalances. *New Biotechnology*, 49, 129–136.
- Shafei, S., Foughi, J., Stevens, L., Wong, C. S., Zabihi, O., & Naebe, M. (2016). Electroactive nanostructured scaffold produced by controlled deposition of PPy on electrospun PCL fibres. *Research on Chemical Intermediates*, 43(2), 1235–1251.
- Sharif, S., Ai, J., Azami, M., Verdi, J., Atlasi, M. A., Shirian, S., & Samadikuchaksaraei, A. (2017). Collagen-coated nano-electrospun PCL seeded with human endometrial stem cells for skin tissue engineering applications. *Journal of Biomedical Materials Research - Part B Applied Biomaterials*, 106(4), 1578–1586.
- Shi, L. (2016). Bioactivities, Isolation and Purification Methods of Polysaccharides from Natural Products: A review. *International Journal of Biological Macromolecules*, 92, 37–48.
- Shishatskaya, E. I., & Volova, T. G. (2004). A comparative investigation of biodegradable polyhydroxyalkanoate films as matrices for *in vitro* cell cultures. *Journal of Materials Science: Materials in Medicine*, 15(8), 915–923.
- Shishatskaya, Ekaterina I., Nikolaeva, E. D., Vinogradova, O. N., & Volova, T. G. (2016). Experimental wound dressings of degradable PHA for skin defect repair. *Journal of Materials Science: Materials in Medicine*, 27(165), 1–16.
- Sobhanian, P., Khorram, M., Hashemi, S. S., & Mohammadi, A. (2019). Development of nanofibrous collagen-grafted poly (vinyl alcohol)/gelatin/alginate scaffolds as potential skin substitute. *International Journal of Biological Macromolecules*, 130, 977–987.
- Sridhar, S., Venugopal, J. R., & Ramakrishna, S. (2015). Improved regeneration potential of fibroblasts using ascorbic acid-blended nanofibrous scaffolds. *Journal of Biomedical Materials Research - Part A*, 103(11), 3431–3440.
- Stuart, B. H. (1997). Scratch Friction Studies of Polycarbonate. *Polymer Testing*, 16(5), 517–522.
- Sudesh, K., Abe, H., & Doi, Y. (2000). Synthesis, structure and properties of polyhydroxyalkanoates: Biological polyesters. *Progress in Polymer Science (Oxford)*, 25(10), 1503–1555.
- Suhail, S., Sardashti, N., Jaiswal, D., Rudraiah, S., Misra, M., & Kumbar, S. G. (2019). Engineered Skin Tissue Equivalents for Product Evaluation and Therapeutic Applications. *Biotechnology*

*Journal*, 14(7).

- Teimouri, A., Yeung, P., & Agu, R. (2019). 2D vs. 3D Cell Culture Models for *In Vitro* Topical (Dermatological) Medication Testing. *Cell Culture*, 3–20.
- Torres, C. A. V., Marques, R., Antunes, S., Alves, V. D., Sousa, I., Ramos, A. M., Oliveira, R., Freitas, F., Reis, M. A. M. (2011). Kinetics of production and characterization of the fucose-containing exopolysaccharide from *Enterobacter* A47. *Journal of Biotechnology*, 156(4), 261–267.
- Torres, F. G., Troncoso, O. P., Pisani, A., Gatto, F., & Bardi, G. (2019). Natural polysaccharide nanomaterials: An overview of their immunological properties. *International Journal of Molecular Sciences*, 20(20), 1–22.
- Vidal, S. E. L., Tamamoto, K. A., Nguyen, H., Abbott, R. D., Cairns, D. M., & Kaplan, D. L. (2018). 3D biomaterial matrix to support long term, full thickness, immuno-competent human skin equivalents with nervous system components. *Biomaterials*, 198, 194–203.
- Wallen, L. L., & Rohwedder, W. K. (1974). Poly-P-hydroxyalkanoate from Activated Sludge. *Environmental Science and Technology*, 8(6), 576–579.
- Wang, L., Wang, Z. H., Shen, C. Y., You, M. L., Xiao, J. F., & Chen, G. Q. (2010). Differentiation of human bone marrow mesenchymal stem cells grown in terpolyesters of 3-hydroxyalkanoates scaffolds into nerve cells. *Biomaterials*, 31(7), 1691–1698.
- Wang, S., Sun, C., Guan, S., Li, W., Xu, J., Ge, D., Zhuang, M., Liu, T., Ma, X. (2017). Chitosan/gelatin porous scaffolds assembled with conductive poly(3,4-ethylenedioxythiophene) nanoparticles for neural tissue engineering. *Journal of Materials Chemistry B*, 5(24), 4774–4788.
- Wang, X., Li, Q., Hu, X., Ma, L., You, C., Zheng, Y., Sun, H., Han, C., Gao, C. (2012). Fabrication and characterization of poly(l-lactide-co-glycolide) knitted mesh-reinforced collagen-chitosan hybrid scaffolds for dermal tissue engineering. *Journal of the Mechanical Behavior of Biomedical Materials*, 8, 204–215.
- Wang, X., Wu, P., Hu, X., You, C., Guo, R., Shi, H., Guo, S., Zhou, H., Yu, C., Zhang, Y., Han, C. (2016). Polyurethane membrane/knitted mesh-reinforced collagen-chitosan bilayer dermal substitute for the repair of full-thickness skin defects via a two-step procedure. *Journal of the Mechanical Behavior of Biomedical Materials*, 56, 120–133.
- Wang, X., You, C., Hu, X., Zheng, Y., Li, Q., Feng, Z., Sun, H., Gao, C., Han, C. (2013). The roles of knitted mesh-reinforced collagen-chitosan hybrid scaffold in the one-step repair of full-thickness skin defects in rats. *Acta Biomaterialia*, 9(8), 7822–7832.
- Wang, Y. W., Yang, F., Wu, Q., Cheng, Y. C., Yu, P. H. F., Chen, J., & Chen, G. Q. (2005). Effect of composition of poly(3-hydroxybutyrate-co-3-hydroxyhexanoate) on growth of fibroblast and osteoblast. *Biomaterials*, 26(7), 755–761.
- Wen, J., Yao, J., Chen, X., & Shao, Z. (2018). Silk Fibroin Acts as a Self-Emulsifier to Prepare Hierarchically Porous Silk Fibroin Scaffolds through Emulsion-Ice Dual Templates. *ACS*

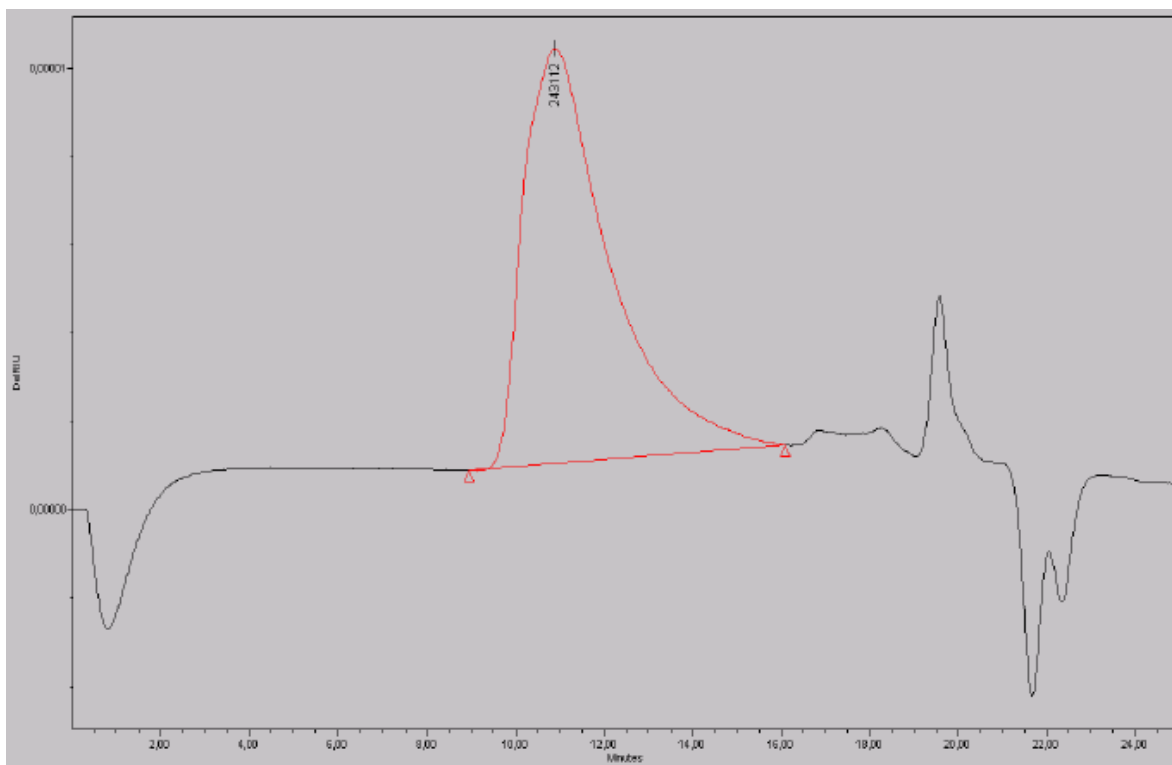
- Omega*, 3(3), 3396–3405. <https://doi.org/10.1021/acsomega.7b01874>
- Wheeler, C. E., Canby, C. M., & Cawley, E. P. (1957). Long-term tissue culture of epithelial-like cells from human skin. *The Journal of Investigative Dermatology*, 29(5), 383–392.
- Yadav, A., Pal, J., Nandan, B., & Srivastava, R. K. (2019). Macroporous scaffolds of cross-linked Poly( $\epsilon$ -caprolactone) via high internal phase emulsion templating. *Polymer*, 176, 66–73.
- Yang, Y., Zhu, X., Cui, W., Li, X., & Jin, Y. (2009). Electrospun composite mats of poly[(D, L)lactide-co-glycolide] and collagen with high porosity as potential scaffolds for skin tissue engineering. *Macromolecular Materials and Engineering*, 294(9), 611–619.
- Ye, H. M., Wang, Z., Wang, H. H., Chen, G. Q., & Xu, J. (2010). Different thermal behaviors of microbial polyesters poly(3-hydroxybutyrate-co-3-hydroxyvalerate-co-3-hydroxyhexanoate) and poly(3-hydroxybutyrate-co-3-hydroxyhexanoate). *Polymer*, 51(25), 6037–6046.
- Yu, Y., Shen, M., Song, Q., & Xie, J. (2017). Biological activities and pharmaceutical applications of polysaccharide from natural resources: A review. *Carbohydrate Polymers*, 183(235), 91–101.
- Zhang, H., Ma, L., Wang, Z., & Chen, G. (2009). Biosynthesis and Characterization of 3-Hydroxyalkanoate Terpolyesters With Adjustable Properties by *Aeromonas hydrophila*. *Biotechnology and Bioengineering*, 104(3), 582–589.
- Zhang, Heng, Xia, J. Y., Pang, X. L., Zhao, M., Wang, B. Q., Yang, L. L., Wan, H.S., Wu, J.B., Fu, S. Z. (2017). Magnetic nanoparticle-loaded electrospun polymeric nanofibers for tissue engineering. *Materials Science and Engineering C*, 73, 537–543.
- Zhang, T., Sanguramath, R. A., Israel, S., & Silverstein, M. S. (2019). Emulsion Templating: Porous Polymers and beyond. *Macromolecules*, 52(15), 5445–5479.
- Zhang, Y. S., & Khademhosseini, A. (2017). Advances in engineering hydrogels. *Science*, 356(6337).
- Zhao, K., Deng, Y., Chen, J. C., & Chen, G. Q. (2003). Polyhydroxyalkanoate (PHA) scaffolds with good mechanical properties and biocompatibility. *Biomaterials*, 24(6), 1041–1045.
- Zhao, W., & Chen, G. Q. (2007). Production and characterization of terpolyester poly(3-hydroxybutyrate-co-3-hydroxyvalerate-co-3-hydroxyhexanoate) by recombinant *Aeromonas hydrophila* 4AK4 harboring genes *phaAB*. *Process Biochemistry*, 42(9), 1342–1347.
- Zhila, N., & Shishatskaya, E. (2018). Properties of PHA bi-, ter-, and quarter-polymers containing 4-hydroxybutyrate monomer units. *International Journal of Biological Macromolecules*, 111, 1019–1026.
- Zhu, N., & Che, X. (2013). Biofabrication of Tissue Scaffolds. *Advances in Biomaterials Science and Biomedical Applications*, 315–328.



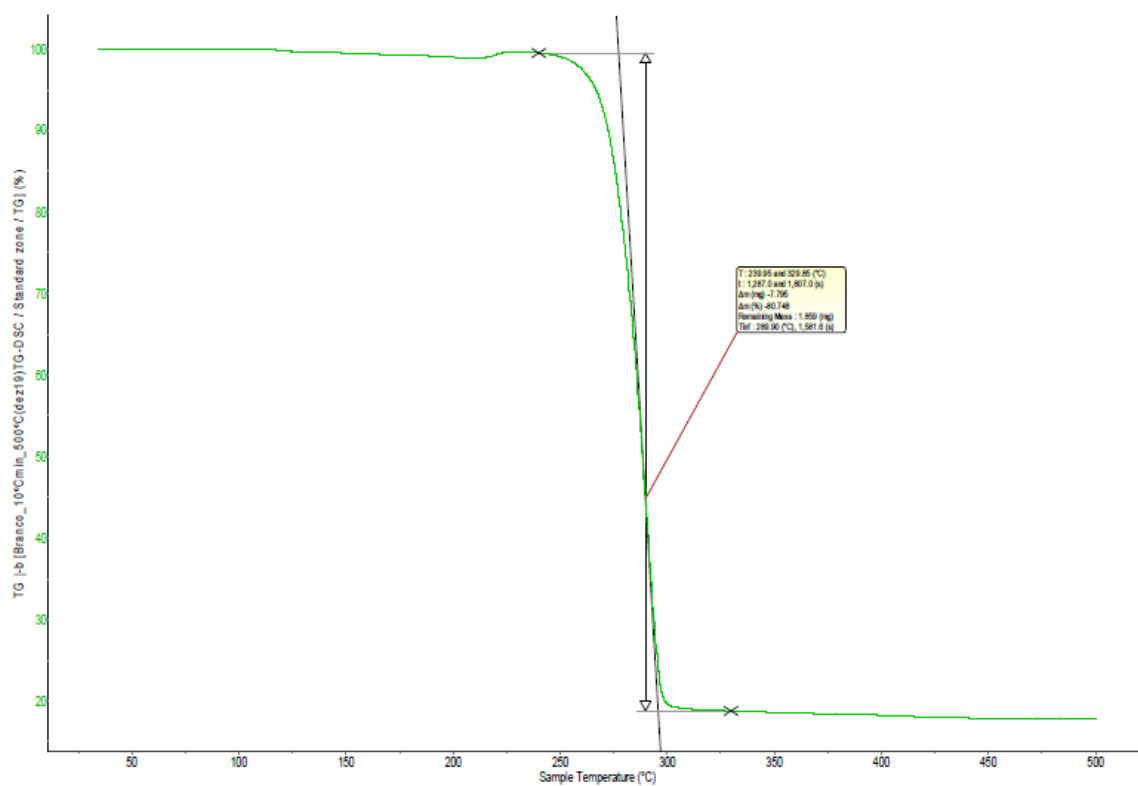


## **Appendices**

---



**Figure A.** SEC analysis of the extracted P(HBVHx).



**Figure B.** TGA curve of the extracted P(HBVHx).